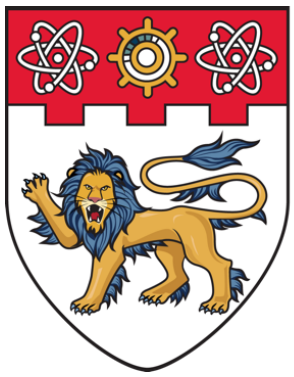

NANYANG TECHNOLOGICAL UNIVERSITY
SINGAPORE

Plant Conformable Electrode for Mimosa Soft Robotics

CAI LINGFENG

SCHOOL OF MATERIALS SCIENCE AND ENGINEERING

2020

Plant Conformable Electrode for Mimosa Soft Robotics

CAI LINGFENG

SCHOOL OF MATERIALS SCIENCE AND ENGINEERING

A thesis submitted to the Nanyang Technological University
in partial fulfilment of the requirement for the degree of
Master of Engineering

2020

Statement of Originality

I hereby certify that the work embodied in this thesis is the result of original research, is free of plagiarised materials, and has not been submitted for a higher degree to any other University or Institution.

16 Nov 2020

. . . . . .

Date

. . . . . .

Cai Lingfeng

Supervisor Declaration Statement

I have reviewed the content and presentation style of this thesis and declare it is free of plagiarism and of sufficient grammatical clarity to be examined. To the best of my knowledge, the research and writing are those of the candidate except as acknowledged in the Author Attribution Statement. I confirm that the investigations were conducted in accord with the ethics policies and integrity standards of Nanyang Technological University and that the research data are presented honestly and without prejudice.

17 Nov 2020

. . . . . .

Date

. . . . . .

Chen Xiaodong

Authorship Attribution Statement

This thesis **does not** contain any materials from papers published in peer-reviewed journals or from papers accepted at conferences in which I am listed as an author.

16 Nov 2020
. . . . . .
Date

. . . . . .
Cai Lingfeng

Abstract

Soft robots with high degree of compliance can easily deform to delicate task settings and unstructured environments, realizing more adaptive and comfort interfaces for human-machine and human-environment. Since soft robots are made with materials with moduli similar to soft biological matters and capable of autonomous movements, scientists have been seeking insights from the nature due the excellent structural and functional capabilities. Most of the design inspiration for soft robots come from animals, such as cephalopod mollusks, because they have no rigid body structure and yet, they can perform sophisticated tasks and move around swiftly. However, very limited studies on plant-based soft robots are present, because as compared to animals, plants do not possess mobility and fast interactions with environmental changes. Nevertheless, there are still some plants demonstrating fast movements, such as insectivorous flytrap trapping down small bugs and "shy" mimosa folding its leaves upon touch. The mechanisms behind these fast movements in plants could also generate new design concepts for soft robots.

In previous signal measuring works, invasive Ag/AgCl metal wires were inserted into mimosa to conduct intracellular measurements, which led to problems such as wounding to the plant. To solve this problem, in this work, we deployed an extracellular measurement on mimosa by fabricating a conformable electrode that could detect the action potentials in mimosa and apply a voltage to trigger the petiole bending. The plant conformable electrode based on PDMS substrate that consists of a layer of conductive Au thin film formed by thermal evaporation and a layer of hydrogel formed by photopolymerization as the adhesion layer between the electrode and the *mimosa pudica* surface. PDMS provides most of the stretchability for the entire electrode. Since the Au thin film cannot be directly attached to the plant surface, hydrogel is added as the adhesion. The as-synthsized electrodes demonstrated excellent comfortability and adhesiveness on various plant surfaces, due to the stretchable PDMS

substrate and hydrogel. The adhesive strength of electrode can maintain at 1.0 N/m for 9 days in ambient condition. In addition, the sandwiched Au thin layer contributed to good electrical conductivity of the entire electrode, which allowed us to successfully detect the electrical signal from mechanical simulation of mimosa pudica. The action potential signal detected using the plant conformable electrodes was comparable to those reported in previous research. Furthermore, we also successfully triggered the mechanical movement in *mimosa* by electrostimulation using these electrodes. The electrodes reported in this work can serve as a universal method for other plant signals detection and electrostimulation in the future.

Lay Summary

Our world is undergoing rapid aging due to better quality of life and medical technology. The ever-increasing elderly population place a heavy burden on healthcare system. Yet, the declining birthrate in many developed countries make the situation worse, as fewer healthcare workers will be available in the future. Hence, introduction of robots in healthcare systems seem to be an inevitable option.

Unlike automation in manufacturing sectors that only requires simple and repetitive work, providing precise care services to the elderly is much complicated, which requires the robots to be highly intelligent and responsive to the specific needs. In particular, there will be many human-machine interactions, it is important to design a robot using soft materials to prevent injuring humans. Hence, a new field of robots named soft robot, which is defined as robot made from highly compliant materials, is introduced. As compared to the industrial robots working on assembly lines, soft robots are more adaptive to delicate task by deformation and generate reactive forces to “sense” human interactions. Many of the soft robots designed were inspired by soft-bodied creatures, such as octopus, which has no hard body structure but demonstrating remarkable mobility and dexterity.

However, very limited studies on plant-based soft robots are present. Traditionally, plants are deemed as static and impercipient, as compared to animals. However, there are some plants which show animal-like movements, such as insectivorous flytrap and “shy” mimosa. By studying the mechanisms behind these fast movements in plants, new insights for soft robotics could be applied on creating new soft robots.

Take mimosa as an example. It is very well known for its leaves closing upon physical touch. The leaf folding can also be achieved by applying a small voltage. In previous research, scientists have used thin metal wire and pierced through the Mimosa for electrical stimulation, which had some side effects such as damaging to the

plant. Hence, in this work, we proposed the plant conformable electrode, which is a non-invasive stretchable electrode that could measure and stimulate the Mimosa.

The conformable plant electrode is a polymeric based, non-toxic and conductive electrode, which is capable of measuring the electrical signal generated by the mimosa plant upon mechanical stimulation, such as touching. Also, we could use this electrode to apply a small voltage to excite the mimosa to bend its branch. Ultimately, by studying the mechanism behind the leaf folding movements of mimosa, we would be able to apply this mechanism to fabricate a soft robot mimicking the grasping action of human hands. In addition, the importance of this electrode is that its application is not limited to Mimosa, but also other plants that use electrical signals to coordinate their physiological functions. Therefore, more plant physical behaviors could be studied, offering more ideas for soft robotic designs.

Acknowledgements

I would like to thank my supervisor Prof. Chen Xiaodong, for the valuable teaching and advising for the past one year. The project progress would not be possible without the patient and helpful guidance with Prof. Chen. I very much want to give my sincerest gratitude to Prof. Chen for allowing me to convert from a Ph.D degree to a M.Eng degree. His understanding and supports play the most important role in completing my Master degree within one year.

My gratitude also goes to my mentor, Mr. Li Wenlong for his consistent guidance and helps for the generation of ideas, various experiment set-ups and result discussions. The progress of my thesis work would never be this fast without his patience and willingness.

I would also like to thank my lab seniors for their help in my lab experiments and their experiences on experimental procedures for the past one year.

Table of Contents

Abstract ..... *i*

Lay Summary ..... *iii*

Acknowledgements ..... *v*

Table of Contents ..... *vii*

Figure Captions ..... *xi*

Abbreviations ..... *xv*

Chapter 1 Introduction *1*

1.1 Background 2

1.2 Hypothesis/Problem 4

1.3 Objective and Scope 4

1.4 Expected Outcomes and Challenges 5

References 5

Chapter 2 Literature Review *7*

2.1 Soft Robotics 8

2.1.1 Actuation System 9

2.1.2 Materials 12

2.1.3 Bioinspiration in Soft Robots Designs 14

2.2 Plant Intelligence 18

2.2.1 Plant Electrophysiology 20

2.2.2 Electrical Signals in Plants 22
2.2.2.1 Action Potentials (APs) 23
2.2.2.2 Variation Potentials (VPs) 24
2.2.2.3 Physiological Effects of Electrical Signals 25
2.3 Traditional Signal Measurement Techniques 26
2.3.1 Extracellular Potential Measurement 26
2.3.2 Intracellular Potential Measurement 28
2.4 Mimosa Pudica 30
2.5 Plant Applications in Materials and Devices 35
2.5.1 Plant Applications in Smart Fabrics 35
2.5.2 Plant Applications in Morphing and Actuation System 38
2.5.3 Plant Applications in Flexible Devices 40
2.6 Stretchable Electrodes Design 42
2.6.1 Structure-based Stretchable Electrodes 44
2.6.1.1 Wavy structures 44
2.6.1.2 Serpentine Structures 45
2.6.1.3 Nanomesh 46
2.6.1.4 Microcracks 48
2.6.2 Novel Stretchable Electrode Materials 49
2.6.2.1 Liquid Metal 49
2.6.2.2 Ionic Conductor 50
2.6.2.3 Conducting Polymer 51
2.6.3 Composite Stretchable Electrode 52
2.6.3.1 Bilayer Composites 52
2.6.3.2 Printable Elastic Electrodes 53
References 56

Chapter 3 Experimental Methodology 65

3.1 Rationale of Selection 66
3.2 Synthesis of Electrodes 67
3.2.1 Fluorination of the Silicon Wafers 67

3.2.2 Preparation of PDMS Substrates 68
3.2.3 Vacuum Deposition of Conducting Layers 68
3.2.4 Hydrogel Precursor Preparation 69
3.2.5 Oxygen Plasma Etching 69
3.2.6 Hydrogel Grafting on the Plasma-etched Substrates 70
3.3 Characterization Techniques 71
3.3.1 Optical Microscope 71
3.3.2 Adhesion Strength on Plant Surface 71
3.3.3 Interfacial Adhesion Strength of Plant Conformable Electrodes 72
3.3.4 Effect of Plant Conformable Electrodes on Plant Leaves 73
3.3.5 Stretchability of Plant Conformable Electrodes 74
3.3.6 Interfacial Impedance Measurements of Plant Conformable Electrodes 75
3.4 *Mimosa Pudica* Electrical Signal Measurements 76
3.4.1 Mechanical Stimulation of *Mimosa Pudica* 77
3.4.2 Electrical Stimulation of *Mimosa Pudica* 77
3.4.3 Smartphone-controllable Platform for *Mimosa* Movements Manipulation 78
References 80

Chapter 4 Results and Discussion ***..... 81***

4.1 Introduction 82
4.2 Results and Discussions 82
4.2.1 Surface Morphology Characterization 82
4.2.2 Adhesion Strength of Conformable Plant Electrodes on Leaves 83
4.2.3 Adhesion Strength between Hydrogel and PDMS Substrates 85
4.2.4 Effect of Plant Conformable Electrodes on Plant Leaves 86
4.2.5 Stretchability of Plant Conformable Electrodes 88
4.2.6 Impedance Measurements of Conformable Plant Electrodes 88
4.2.7 Mechanical Stimulation of *Mimosa Pudica* 89
4.2.8 Electrical Stimulation of *Mimosa Pudica* 90

4.2.9 Smartphone-controllable Platform for *Mimosa* Movements Manipulation 92
References 94

Chapter 5 Future Work ***95***

5.1 Conclusions 96

5.2 Future Work 97

5.2.1 Hydrogel Patterning via Photolithography 97
5.2.2 Electrically-induced Pinnules Folding Movements in *Mimosa* 98
References 100

Figure Captions

Figure 1. Social robots in real life: (a) Betty[18], Copyright © International Psychogeriatric Association 2017 ; (b) Pepper[19], Copyright © SoftBank Robotics Europe; (c) Paro, AIST[20], Copyright © 2015 AMDA – The Society for Post-Acute and Long-Term Care Medicine.
Figure 2. Three categories of soft robots based on actuation system, materials and the design inspiration from nature, respectively.
Figure 3. (a) Resilience of the untethered soft robot in various harsh environments: snowstorm and fire[9], Copyright © 2014, Mary Ann Liebert, Inc.; (b) Images from high-speed cameras of the actuation of a fast pneu-net (fPN) actuator[10], Copyright © 2014 WILEY-VCH Verlag GmbH & Co. KGaA, Weinheim; (c) An uncamouflaged (top) soft robot in an artificial condition and the same robot camouflaged (bottom)[11], Copyright © 2012, American Association for the Advancement of Science.
Figure 4. (a) The OctArm operating in water and on ground[12], Copyright © 2006, IEEE. (b) A tip-to-tip PneuNet holding an egg[14], Copyright © 2011 WILEY-VCH Verlag GmbH & Co. KGaA, Weinheim. (c) A pneumatically driven soft robotic hand gripping a cylinder[13], Copyright © 2016, © SAGE Publications. (d) The PneuArm inflatable manipulator prototype[15], Copyright © 2014 by ASME.
Figure 5. Various material applications in soft robots. (a) A soft-bodied snake robot made by silicone rubber[23], Copyright © 2013 IOP Publishing. (b) A tethered soft robot based on elastomeric material (Ecoflex)[14], Copyright © 2011 John Wiley & Sons. (c) An artificial caterpillar bot with a silicone rubber body and SMA backbones[28], Copyright © 2011 IOP Publishing Ltd. (d) Time series of a SMP stent recovering in water at 52 ℃[30], © 2007 Springer Nature Switzerland AG.
Figure 6. Various octopus-inspired soft robots. (a) Octopus arm-like robot prototype in waster at rest and wrapping human wrist[6], Copyright © Taylor & Francis. (b) OctArm grasping a ball[12], Copyright © 2006, IEEE. (c) A continuum soft arm grasping a pencil[5], Copyright © 2011 IOP Publishing Ltd. (d) Prototype of a flexible hull inflatable robot inspired by octopuses[42], Copyright © 2015 IOP Publishing Ltd. (e) Camouflaging of a soft robot crawling across a rock bed[11], Copyright © 2012, American Association for the Advancement of Science.
Figure 7. Demonstration of several worm-inspired soft robots. (a) A structural comparison between the robot and an inchworm, and schematic display of the robot during locomotion[51], Copyright © 2014 IOP Publishing Ltd. (b) Dissection of an Oligochaeta and prototype designed using micro NiTi coil actuators based on its structural arrangement[7], Copyright © 2013, IEEE. (c) GoBbot, a soft robot with two actuation components: anterior and posterior flexors, which together helped to generate ballistic rolling[28], Copyright © 2011 IOP Publishing Ltd.
Figure 8. Electrical signaling in higher plants. Stimulations such as touch or cold shock (star) triggers calcium ions influx into a living cell, e.g. a mesophyll cell (MC). The membrane potential drops after the depolarization, and an AP is evoked by chloride and potassium efflux. This AP is then transmitted over short distances via plasmodesmal (P) networks and enters the SE/CC-complex in order to be propagated over longer distances. Sieve pores (SP) that have large diameters provide pathways with small resistance for fast electrical signal transmission along the SE plasma membrane and exit the phloem through plasmodesmata to elicit physiological reactions in the surrounding tissue[69], Copyright © Springer-Verlag Berlin Heidelberg 2006.
Figure 9. Three types of electrical signals in plants: action potential (AP), variation potential (VP) and system potential (SP)[77]. AP and VP are two most thoroughly studied electrical signals in plants. For SP, there is still a lack of systematic understanding of this signal, hence it will not be discussed further in this work.
Figure 10. Examples of invasive metal electrodes in *Mimosa pudica*[98], Copyright © 2009 Blackwell Publishing Ltd.
Figure 11. Illustration of a recording setup for surface potential changes measurement of *Arabidopsis* using Ag/AgCl electrode with KCl/agar solution[100], Copyright © 2014, Springer Nature.

Figure 12. Aphid electrode. (a) An aphid inserting stylet into a sieve element on the leaf surface. (b) After separation of aphid from the stylet using laser pulse, the stylet served as a connection between the sieve tube and the microelectrode. An AP was produced by cooling the shoot while a VP was generated from flaming of a leaf[106], Copyright © 2006 John Wiley & Sons Ltd.

Figure 13. General appearance of *Mimosa pudica*. The leaf A is in normal state whereas the leaf B displays the position after excitation[107], Copyright © Cambridge Philosophical Society.

Figure 14. Electrical signals in *Mimosa pudica*. (a) An AP is generated when a pinna tip is touched or cooled by ice and transmitted basipetally within the rhachis at 20-30 mm s^{-1}. The AP is limited to the base of pinna and cannot propagate further. (b) A VP is evoked when the pinna is cut, which has an irregular shape and last for a longer time than AP. In addition, it travels at a lower speed (5-6mm s^{-1}) but is capable of transmitting over the secondary pulvini at the base of pinna, causing the neighboring pinnules to fold and also the falling of the petiole at the primary pulvinus[106], Copyright © John Wiley & Sons Ltd.

Figure 15. Experimental setup for the Charged Capacitor Method in (a) *Dionaea muscipula* Ellis[79] and (b) *Mimosa pudica*[118], Copyright © 2010 Landes Bioscience and © 2008 Elsevier B.V, respectively. A double pole-double throw (DPDT) switch connects a capacitor to one 1.5V battery for charging and to the plant for stimulation.

Figure 16. Lotus-like fabrics with water and dust repelling characteristic[127], Copyright © 2011 Elsevier Ltd.

Figure 17. A sensitive cloth design mimicking the *Mimosa pudica* pulvinus. Reduction of turgor pressure causes a rapid shrinking movement fueled by rearrangement of water and ion influx. A touch sensitive fabric model is designed to mimic pulvinus features[127], Copyright © 2011 Elsevier Ltd.

Figure 18. Schematic illustration of humid sensitive fabric which experience cumulative movements when hygroscopic components below changes, inspired by pinecone's unique actuation responds to surrounding humidity variations[127], Copyright © 2011 Elsevier Ltd.

Figure 19. Different utilization of material anisotropy to obtain desired hygroscopic deformation. (a) Biomorph inspired by pinecones as responsive building skins[145, 146], Copyright © 2012 John Wiley & Sons, Ltd and Copyright © 2015 Elsevier Ltd, respectively. (b) Multi-material modulation capable of helical twisting[142], Copyright © 2013, Springer Nature. (c) Programmable short fiber-reinforced ribbon for complex deformation[144], Copyright © The Royal Society of Chemistry 2014.

Figure 20. Nature-inspired structural materials for pressure sensing. (a) Schematic fabrication process of flexible micro-structured e-skin inspired by rose petals[153], Copyright © The Royal Society of Chemistry 2015. (b) Photograph of a *Spongia officinalis* and schematic demonstration of a porous structured pressure sensor that has a spongy structure of PDMS thin film dielectric layer, and a top view SEM image that reveals the uniform formation of pores in the multilayer configuration[154], © 2016 WILEY-VCH Verlag GmbH & Co. KGaA, Weinheim. (c) A flexible pressure sensor mimicking the leaves movement of *Mimosa pudica*[152], Copyright © 2014 WILEY-VCH Verlag GmbH & Co. KGaA, Weinheim.

Figure 21. A flexible electrode made with a gold/PDMS composite film with strong interlayer adhesion mimicking the plants root system. (a) Illustration of the interlocking nanopile structure combining the "hard" and "soft" materials together. (b) The strain distribution in the film under FEM simulations. (c) Comparison of the adhesive strength of nanopile film to a crack-based stretchable film and a flat non-stretchable film[158], © 2016 WILEY-VCH Verlag GmbH & Co. KGaA, Weinheim.

Figure 22. Stretchable electronic device designs. A schematic illustration of (a) "rigid islands" and (b) "fully stretchable" structure[167], Copyright ©The Royal Society of Chemistry 2019. Stretchable light emitting devices adapting (c) the "rigid islands"[168] and (d) "fully stretchable"[166] approaches, Copyright © 2010, Springer Nature and © 2016, American Association for the Advancement of Science, respectively.

Figure 23. The wavy structure stretchable electrodes. (a) Illustration of the preparation of the electrodes by pre-strained elastomer and the image sequence showing the stretchable electrodes in different strain rate[170], Copyright © 2014 The Authors. Published by WILEY-VCH Verlag GmbH & Co. KGaA, Weinheim. (b) Schematic preparation of metal films on PDMS via thermal expansion[172] and the optical images of the wave pattern formed[171], Copyright © 1998, Springer Nature and © 2003 American Institute of Physics, respectively. (c) A schematic of on-skin electrodes fabricated from plasticized silk protein, synthesized by substrates hydration, and optical images of Au on plasticized

silk at various strain conditions[173], Copyright © 2018 WILEY-VCH Verlag GmbH & Co. KGaA, Weinheim.
Figure 24. Serpentine structured stretchable conductors. (a) Pictures of the original and deformed serpentine structure gold nanowires[178], Copyright © 2004 WILEY-VCH Verlag GmbH & Co. KGaA, Weinheim. (b) Photo of extendible microwire under an optical microscope[174], Copyright © 2010 WILEY-VCH Verlag GmbH & Co. KGaA, Weinheim. (c) The 10x10 RGB LED matrix fabricated using a serpentine structure[179], Copyright © 2015 John Wiley and Sons.
Figure 25. Nanomesh structure electrodes. (a) Schematic showing how the Au nanomesh is obtained: Au is first deposited onto electrospun PVA nanofibers, which are dissolved by water and the Au nanomesh is adhered onto the skin. The Au nanomesh on the human fingertips showed good conformability. An SEM image shows the microscopic structure of the Au nanomesh[180], Copyright © 2017, Springer Nature. (b) A paper replicate of the nanomesh experiencing strain and the SEM images of Au nanomesh/PDMS electrode under different strain conditions[183], Copyright © 2014, Springer Nature.
Figure 26. Microcrack based stretchable electrodes. (a) SEM images of microcrack morphology of Au thin film on PDMS with 0% and 20% strains, respectively[187], Copyright © AIP Publishing. SEM images of microstructures of the gold films (b) with and (c) without nanopiles under 30% tensile strain, respectively[158], Copyright © 2016 WILEY-VCH Verlag GmbH & Co. KGaA, Weinheim. Due to the weak adhesion in the nostretchable film, the crack edge rolled up, but in the nanopile-enhanced film, microcracks propagation are suppressed.
Figure 27. Liquid metals based stretchable electrodes. (a) EGain liquid metals filled into a fluidic channel made of thermoplastic elastomer gel (TPEG) subjected to a 1000% strain to demonstrate ultra-stretchability and elasticity[195], Copyright © The Royal Society of Chemistry 2013. (b) Liquid metals serve as bridges between other metal-based conductors[200], Copyright © 2018 WILEY-VCH Verlag GmbH & Co. KGaA, Weinheim. (c) The excellent tear resistance of liquid metal embedded elastomer (LFEE) is shown by creating a notch stretched to 300% strain and is totally blunted via an autonomous tear elimination mechanism[198], Copyright © 2018 WILEY-VCH Verlag GmbH & Co. KGaA, Weinheim.
Figure 28. Nanowire based bilayer stretchable electrodes. (a) Schematics and AEM images of SWCNTs on PDMS substrates, and (b) picture of the actual device demonstrating good transparency[214], Copyright © 2011, Springer Nature. (c) The flexible SEBS -based sensing array with CNT pattern on a human palm that is conformable and able to detect location of a artificial ladybug with six conductive legs[217], Copyright © 2018, Springer Nature. (d) Images of a polymer light-emitting electrochemical cell (PLEC) based on a patterned AgNW-Polyurethane acrylate composites illuminates under different strain levels[218], Copyright © 2013, Springer Nature.
Figure 29. Printable elastic conductors based on various conductive fillers. (a) SWCNTs[225], Copyright © 2009, Springer Nature. (b) Self-organized Ag flakes[226], Copyright © 2015, Springer Nature. (c) *In situ* Ag NPs formed with Ag flakes[230], Copyright © 2017, Springer Nature.
Figure 30. Large area stretchable electronics fabricated from printable elastic conductors. (a,b) Stretchable transistor matrices[226], Copyright © 2015, Springer Nature. (c,d) Stretchable displays utilizing organic LEDs[225], and micro-LEDs[234], Copyright © 2009, Springer Nature and © 2018 Takao Someya Research Group, respectively. (e) E-textiles with multipoint EMG measurement electrodes and (f) Pressure sensing e-textiles groves[230], Copyright © 2017, Springer Nature.
Figure 31 . Schematic of the PDMS spin coating process.
Figure 32. Schematic illustration of thermal vacuum deposition of the composite electrode.
Figure 33. Schematic illustration of plant conformable electrode.
Figure 34. Illustration of peel test of electrodes on leaves: (a) & (b) schematic of the peeling test; (c)&(d) actual peeling test set-up.
Figure 35. Illustration of the sliding resistance test of the electrodes: (a) front view, (b) side view.
Figure 36. The electrodes attached onto the devil's ivy leaves with numerical markings.
Figure 37. Stretchability test set-up. (a) The sample was clamped and liquid metal was applied on it. (b) Full set-up of the test.
Figure 38. Impedance measurement set-up. Hydrogel was sandwiched between the Au deposited PDMS electrodes with two copper wires connecting to the electrochemical workstation. (a) the static impedance measurement set-up. (b) the dynamic impedance measurement set-up. The stacked electrodes were being stretched by a tensile workstation.

Figure 39. Schematics of mechanical stimulation set-up. (a) Before stimulation; (b) after stimulation.
Figure 40. Schematics of electrical stimulation set-ups. (a) APs induced by voltage applied across ES1 and ES2; (b) Control experiment to observe if APs were induced when voltage was applied across ES2 and ES3.
Figure 41. Schematic of the smartphone-controllable platform that enables inducing physical movements of *mimosa* at designated locations. The platform consists of a smartphone application that could send the command via internet, a Wi-Fi module with General Purpose Input Output (GPIO) that could deliver a 3.3V electrical output to the plant conformable electrodes warped onto the petioles of *mimosa*. (a) The initial set-up. (b) When a "on" command for ES2 is sent from the application via internet, and Wi-Fi module then impose a 3.3V voltage onto the ES2, leading the dropping of the petiole.
Figure 42. Cross-sections of plant conformable electrodes under optical microscope: (a) plant conformable electrodes stuck tightly on leaf; (b) & (c) plant conformable electrodes warped around the *mimosa* stem.
Figure 43. (a) Illustration of the adhesive strength versus displacement diagram; (b) The adhesive strength versus displacement diagram in day 1.
Figure 44. Changes in average adhesive strength of the plant conformable electrodes every 48 hours in ambient conditions.
Figure 45. (a) & (b) The surfaces of the electrodes before and after the test. (c) The adhesive force versus displacement diagram of 4 samples.
Figure 46. Photos of devil's ivy leaf: (a) before the test, (b) during the test and (c) right after the test. (d) & (e) Photos of the electrode on leaf after rains.
Figure 47. (a) Variations of chlorophyll content and (b) nitrogen content.
Figure 48. A plot of resistance variations versus strain for plant conformable electrodes.
Figure 49. (a) Impedance of conformable plant electrodes at 0% and 25% strain conditions. (b) Variations of impedance versus strain at 30Hz for 5 samples.
Figure 50. Mechanical stimulation of *Mimosa pudica*. (a) Upon stimulation, three spikes were detected by the three electrodes, shown as three successive troughs. By zooming in, the time intervals between each AP could be measured, and subsequently, the AP transmission speed was calculated in (b).
Figure 51. Electrostimulation of *mimosa* pudica. Schematic illustration of (a) mimosa in normal state, and (b) after connecting to the battery. (c) Time series of the bending of petiole upon electrostimulation.
Figure 52. Control experiment on electrostimulation. Schematic illustration of (a) mimosa in normal state, and (b) after connecting to the battery.
Figure 53. (a)-(b) Setup of the mimosa controlling platform. (c) Time series of petiole bending controlled by the "mimosa controller" app.
Figure 54. Schematic of patterning process of hydrogel. The UV light would only shine on the unmasked region. The covered regions would not crosslink and subsequently washed away. The patterned hydrogel would replicate the details from the photomask[1], © 2017 by The American Society for Cell Biology.
Figure 55. Illustration of AP detection and stimulation in rachis. The electrodes were wrapped between the tertiary pulvinus (bases of pinnules).
Figure 56. Schematic illustration of three functional layers of new plant conformable electrode. High transparency is achieved by replacing the vacuum deposited gold layer to spin-coated PEDOT: PSS layer.
Figure 57. Schematics of a portable mimosa soft robot with its root soaked in water-rich material to maintain its life form.

Abbreviations

SMP	Shape memory polymers
PDMS	Polydimethylsiloxane
PVC	Polyvinyl chloride
IPMC	Ionic polymer-metal composite or compound
AP	Action potential
VP	Variation potential
MC	Mesophyll cell
SE/CC	Sieve element/companion cells
PA	Phloem parenchyma
V_m	Membrane potential
ECG	Electrocardiograms
EEG	Electrocephalograms
SEM	Scanning electron microscope
FESEM	Field emission scanning electron microscope
BSE	Back scattering electron
SE	Secondary electrons
SW	Slow wave
VS	Voltage spikes
VT	Voltage transients
REA	Rhythmical electrical activity
DPDT	Double pole-double throw
TPEG	Thermoplastic elastomer gel
LFEE	Liquid metal embedded elastomer
AC	Alternate current
DC	Direct current
PET	Polyethylene terephthalate
PUD	Polyurethane nanoparticles
PEO	Poly(ethylene oxide)

PVA	Poly(vinyl alcohol)
AAm	Acrylamide
TMSPMA	3-(tri-methoxysilyl) propyl methacrylate
GOx	Glucose oxidase
APS	Ammonium persulfate
TEMED	N,N,N', N'-tetramethyl ethylenediamine
PEDOT:PSS	Poly(2,3-dihydrothieno-1,4-dioxin)–poly(styrenesulfonate)

Chapter 1 Introduction

Rapidly aging population put a pressure on medical and social care resources. Fortunately, progresses in automation and robotic technology seem to replace human care providers with smarter robots. In this chapter, research background including the statistics of aging and healthcare burden and the concept of soft robotics will be presented. The objectives of this work will be included and the expected outcomes will also be present.

1.1 Background

The world is rapidly aging as human society progresses. The number of people who are currently above 60 years old is estimated to be 800 million, which accounts for 11% of the global population. However, this age group number will skyrocket to 2 billion in 2050, representing 22% of the total population [1]. Although the extent of aging varies largely among different countries and continents, for example, the percentage of Japan's population greater than 65 years old is 28%, but only 6.4% for India [2]. While advanced medical technology and improving nutritional levels enable a longer life expectancy, the increasing burden on healthcare system [3] and shortage of elderly caring personnel [4] becomes a pressing issue for all countries.

Automation is regarded as a promising solution for aging workforce. In the late 1980s, introduction of industrial robots automated many labor-intensive jobs in manufacturing sectors [5]. Automation are not just limited to industry and agriculture. Computer software can be deemed as a form of automation that replaces several tasks by workers in retail, sales and business services. Software and AI-powered technologies are capable of complicated document translation, crafting business proposals and diseases diagnosis[6]. Robots have been deployed in medicine and healthcare. Telerobotic systems are being used to perform long-distance surgery to deliver a more liable outcomes in certain procedures [7-9]. Robotics systems are also capable of lost limb replacement [10], onsite [11] and even home-based therapy without human supervision[12], which can mitigate the problem of shortage in therapists.

In this aging society, demands for elderly such as medical and social care are rising fast. Many efforts have been spent on designing various types of robots as humans' companions to interact physically and provide mental comfort to the elderly[13-15]. Some of the examples are shown in Fig.1. The use of these robots have helped to reduce stress level in elderly people[16, 17].

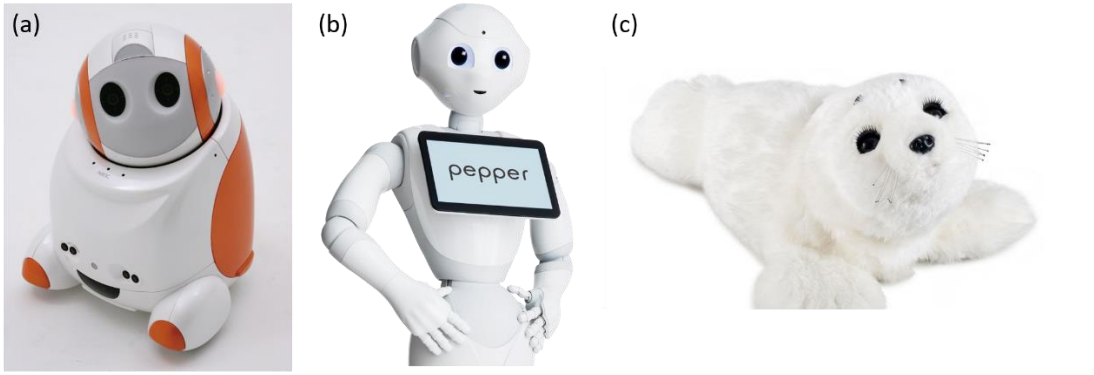

Figure 1. Social robots in real life: (a) Betty[18], Copyright © International Psychogeriatric Association 2017 ; (b) Pepper[19], Copyright © SoftBank Robotics Europe; (c) Paro, AIST[20], Copyright © 2015 AMDA – The Society for Post-Acute and Long-Term Care Medicine.

Most of the social and medical robots are manufactured using plastic and metals as their backbones, which are unsafe for human interaction due to rigid joints and links. Hereby, a concept known as soft robotics, was introduced as a new subfield of robots fabricated from compliant materials, which make them more like living organisms[21]. As compared to the rigid members, soft robots are more flexible[22] and have higher adaptability[23], which are safer to work with humans. The key to achieve that is to develop an actuation system that produces reaction forces to move around and interact with surrounding environments.

Since soft robots have no rigid body structure, most of their design inspirations come from soft-bodied creatures such as cephalopods (octopuses[23, 24]), and arthropods (caterpillars[25]). However, very limited works were considering plants as a source for soft robot designs, as plants are generally deemed as immobile and impercipient. Nevertheless, there are still some plants exhibiting fast movements such as Venus trap[26] and *mimosa pudica*[27] that could provide an alternative design inspiration for soft robotic system. For these plants, electrical signals play an important role in stimulating various physical movements for prey hunting or self-protection. In this work, we would use mimosa pudica as an example, to detect and stimulate such electrical signals by a non-damaging method.

1.2 Hypothesis/Problem

The detection and stimulation electrodes used in previous studies were pierced into the *mimosa* plant, which were invasive in nature and required a resting period of 3-25 hours before any accurate signal detections. There has been no non-invasive detection method reported. Hence, this thesis will describe and validate the fabrication of a conformable plant electrode that is capable of instant detecting the electrical signals evoked upon mechanical stimulation on the *mimosa pudica*, and delivering electrical stimulation to the *mimosa* to trigger the physical movements such as pinnules closing and petiole bending.

1.3 Objective and Scope

The objectives of this thesis are to design and fabricate a conformable electrode that can both detect the electrical signals from the *mimosa pudica* and also to provide electrical stimulation to trigger the physical movements in the *mimosa*. Firstly, the conformable electrode should possess good electrical conductivity to measure the electrical signals accurately. Secondly, the electrode needs to be stretchable since physical movements from *mimosa* will be expected. Lastly, the electrode should have good adhesion on the *mimosa* plant for signal detections. Ultimately, the conformable electrodes are qualified to be used to detect the electrical signals evoked upon mechanical stimulation on the *mimosa pudica* and deliver electrical stimulation to the *Mimosa* to trigger physical movements such as pinnules closing and petiole bending.

Thereby, in order to satisfy the abovementioned requirements, we proposed a three-layer stretchable electrode: the plant conformable electrode based on stretchable PDMS substrate that consists of a layer of conductive Au thin film formed by thermal evaporation and a layer of hydrogel formed by photopolymerization as the adhesion layer between the electrode and the mimosa pudica surface.

This thesis would focus on the synthesis of plant conformable electrode. If necessary, the additives in hydrogels would be studied to increase the adhesiveness and toughness. The mechanical properties would be characterized by a mechanical tester. The electrical properties would be characterized by an electrochemical workstation. The electrical signals received from the electrode would be recorded by a data acquisition system.

1.4 Expected Outcomes and Challenges

Firstly, the fabricated plant conformable electrodes should remain conductive while being stretched to 100% strain. Secondly, the electrodes should stay adhered onto the Mimosa during the test. Thirdly, the electrodes should not cause any negative impact to the health of *mimosa pudica*.

For the plant signal detection, the electrodes should record the induced AP led by the external mechanical stimulation on the *mimosa*. Furthermore, the electrodes should also be able to electrically stimulate the *mimosa* and the corresponding physical movements (petiole bending) should be observed.

Difficulty to set up the signal detection experiment is also anticipated due to the sensitivity of the *mimosa* plant, any light movements could cause the leaves to close. The signal detection and electrostimulation on plants could only be done in daytime due to the nyctinastic property of mimosa: it changes the leaf orientation during darkness, and any mechanical stimulation on it will not result in any response[28].

References

[1] M. A. McEvoy, N. Correll, Science 2015, 347, 1261689.
[2] U. Nations, in *World Population Prospects 2019*, Vol. II, 2019.

[3] F. Pammolli, M. Riccaboni, L. Magazzini, The European Journal of Health Economics 2012, 13, 623.
[4] T. M. Dall, P. D. Gallo, R. Chakrabarti, T. West, A. P. Semilla, M. V. Storm, Health Affairs 2013, 32, 2013.
[5] M. W. Mikell P. Groover, Roger N. Nagel, Nicholas G. Odrey, *Industial Robotics: Technology, Programming, and Applications*, Mcgraw-Hill Inc., 1986.
[6] E. Brynjolfsson, A. McAfee, *The second machine age: Work, progress, and prosperity in a time of brilliant technologies*, W W Norton & Co, New York, NY, US 2014.
[7] P. Kazanzides, G. Fichtinger, G. D. Hager, A. M. Okamura, L. L. Whitcomb, R. H. Taylor, IEEE Robotics & Automation Magazine 2008, 15, 122.
[8] G. Fichtinger, P. Kazanzides, A. Okamura, G. Hager, L. Whitcomb, R. Taylor, IEEE robotics & automation magazine / IEEE Robotics & Automation Society 2008, 15, 94.
[9] G. Hager, A. Okamura, P. Kazanzides, L. Whitcomb, G. Fichtinger, R. Taylor, IEEE robotics & automation magazine / IEEE Robotics & Automation Society 2008, 15, 84.
[10] S. Micera, M. Carrozza, L. Beccai, F. Vecchi, P. Dario, Proceedings of the IEEE 2006, 94, 1752.
[11] E. Guglielmelli, M. Johnson, T. Shibata, Robotics, IEEE Transactions on 2009, 25, 477.
[12] M. J. Matarić, J. Eriksson, D. J. Feil-Seifer, C. J. Winstein, Journal of NeuroEngineering and Rehabilitation 2007, 4, 5.
[13] T. T. Takanori Shibata, Kazuo Tanie, IEEE SMC'99 Conference Proceedings. 1999 IEEE International Conference on Systems, Man, and Cybernetics 1999, 2, 1024.
[14] T. Shibata, K. Inoue, R. Irie, "Emotional robot for intelligent system-artificial emotional creature project", presented at *Proceedings 5th IEEE International Workshop on Robot and Human Communication. RO-MAN'96 TSUKUBA*, 11-14 Nov. 1996, 1996.
[15] C. D. Kidd, W. Taggart, S. Turkle, "A sociable robot to encourage social interaction among the elderly", presented at *Proceedings 2006 IEEE International Conference on Robotics and Automation, 2006. ICRA 2006.*, 15-19 May 2006, 2006.
[16] T. Saito, "Examination of Change of Stress Reaction by Urinary Tests of Elderly before and after Introduction of Mental Commit Robot to an Elderly Institution", 2002.
[17] K. Wada, T. Shibata, T. Saito, K. Tanie, "Analysis of factors that bring mental effects to elderly people in robot assisted activity", presented at *IEEE/RSJ International Conference on Intelligent Robots and Systems*, 30 Sept.-4 Oct. 2002, 2002.
[18] S. M. Loi, A. Bennett, M. Pearce, K. Nguyen, N. T. Lautenschlager, R. Khosla, D. Velakoulis, International Psychogeriatrics 2018, 30, 1075.
[19] S. Robotics.
[20] R. Bemelmans, G. J. Gelderblom, P. Jonker, L. de Witte, Journal of the American Medical Directors Association 2015, 16, 946.
[21] D. Rus, M. T. Tolley, Nature 2015, 521, 467.
[22] A. D. Marchese, R. Tedrake, D. Rus, The International Journal of Robotics Research 2015, 35, 1000.
[23] L. Margheri, C. Laschi, B. Mazzolai, Bioinspiration & Biomimetics 2012, 7, 025004.
[24] M. Calisti, M. Giorelli, G. Levy, B. Mazzolai, B. Hochner, C. Laschi, P. Dario, Bioinspiration & Biomimetics 2011, 6, 036002.
[25] H.-T. Lin, G. G. Leisk, B. Trimmer, Bioinspiration & Biomimetics 2011, 6, 026007.
[26] D. Hodick, A. Sievers, Planta 1988, 174, 8.
[27] J. FROMM, S. LAUTNER, Plant, Cell & Environment 2007, 30, 249.
[28] M. Ueda, S. Yamamura, Tetrahedron 1999, 55, 10937.

Chapter 2 Literature Review

In this chapter, the concept of soft robotics and the relevant progress will be introduced first. Followed by studies on plant intelligence and plant applications in materials and devices. Traditional methods of measuring plant electrical signals will be reviewed. A comprehensive study of mimosa pudica will also be shown, along with reviews on material designs for flexible devices.

2.1 Soft Robotics

The word ‘robot’ usually accompanies with the impression of rigid, clumsy, metallic. Currently, more and more robots are being extensively deployed in manufacturing industries to replace labor-intensive and repetitive works and to increase the operation efficiency, thus reducing the cost of production. However, these robots usually suffer from insufficient adaptability due to the rigid joints and links. Hence, they might lead to potential harm interacting with humans. The common practice is to separate workers and robotic workspaces in factories to minimize safety accidents. Ultimately, the compliance in actuation mechanisms is the solution to real human-robot interactions.

To expand the uses of robots from manufacturing and industrial automation to more adaptive and responsive areas such as healthcare and cooperative human assistants, a new sub-field of robot, namely soft robots, which contain little or no rigid materials was introduced[1-3]. The choice of materials for soft robots must have similar elastic and rheological properties of living organisms, which allow the robots to remain functional even at stretched or compressed states.

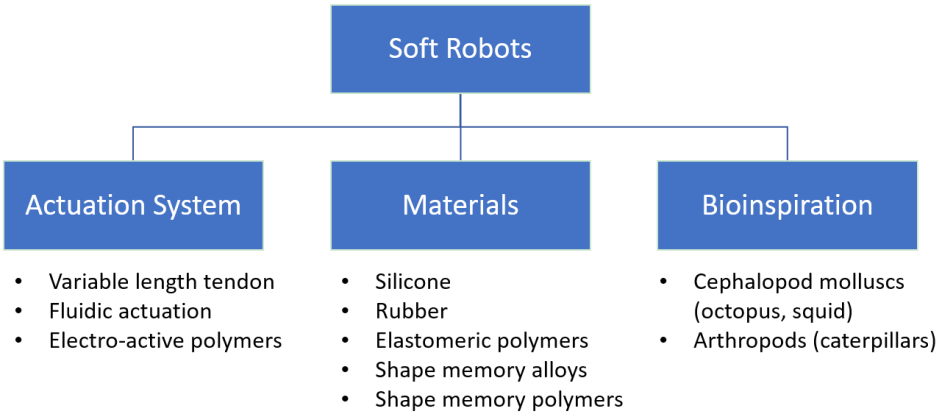

Figure 2. Three categories of soft robots based on actuation system, materials and the design inspiration from nature, respectively.

In general, all soft robots could be categorized into three groups: (1) the actuation systems that provide motion; (s) the materials used to fabricate; (3) the bioinspiration that helps to design. The sequent reviews will be based on these three categories.

2.1.1 Actuation System

Conventionally, rigid motors and other intricate mechanisms that enable rotational and linear actuation in robots. However, soft robots that experience continuous elastic deformation generate motion based on a backbone curve[4]. Hence, flexibility of the soft robots that allow for continuum deformation results in a higher degrees of freedom (DOFs) of motion, whereas traditional ones has less DOFs due to rigid joints and links. In general, actuation systems for soft robots are classified into three groups: variable length tendon, fluidic actuation, and electro-active polymer (EAP)[3].

Variable-length tendons connect the soft segments and control the extent of deformation of the soft segments Unlike the tendons in human bodies that are made of fibrous connective tissues, variable-length tendons in soft robots are fabricated tension cables or shape-memory alloys (SMAs) actuators. A bio-inspired robot arm was fabricated with silicone cable that mimic the crawling of octopus by Dario's group[5]. In another study, Dario et al. used ultrahigh molecular weight polyethylene (UHMWPE) as longitudinal actuators and spiral SMA as transverse actuators to build a similar octopus-like soft robot[6]. A meshworm robot that is capable of peristaltic movement used coiled nickel titanium SMA as its actuation system[7]. Similarly, spiral-shaped SMAs were deployed to build a cater-pillar inspired rolling robot (GoQbot). However, the use of SMAs also creates several problems such as relatively small strain limit in straight shape, low working cycles (heat generated by high current) and low controllability (non-linear behavior). These problems can be tackled respectively by spiral shape design of SMAs, installation of advanced cooling system and use of all-or-none activation techniques[6].

Fluidic actuation is achieved by structural deformation via inner channels inflation of the soft materials[3]. Pneumatic artificial muscle (PAM), or McKibben actuator, is a flexible linear soft actuator in a form of elastomer tubes bundles packed by fiber sleeves[8]. In the later stage, fluidic elastomer actuator (FEA), which is highly flexible and adaptable, became more prevalent. Soft robots using FEA are actuated by the

expansion of pressurized fluid within the embedded channels, and this architecture is later referred as Pneu-Nets (PN). The advantage of PN is that once the soft robots are deformed, little or no energy is needed to preserve the shape. Whitesides's Group has done many studies on designing soft-body quadrupedal robots using PN model that were resilient to harsh condition[9], capable of rapid and stable actuation[10], and even environmental camouflage[11].

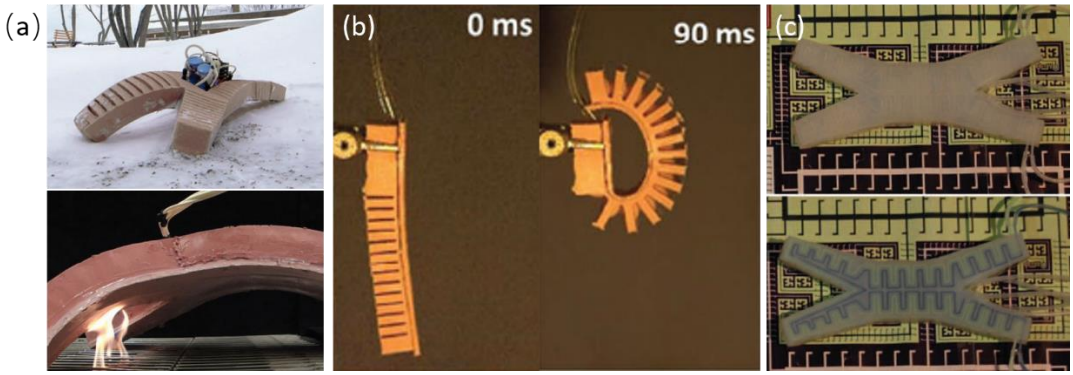

Figure 3. (a) Resilience of the untethered soft robot in various harsh environments: snowstorm and fire[9], Copyright © 2014, Mary Ann Liebert, Inc.; (b) Images from high-speed cameras of the actuation of a fast pneu-net (fPN) actuator[10], Copyright © 2014 WILEY‐VCH Verlag GmbH & Co. KGaA, Weinheim; (c) An uncamouflaged (top) soft robot in an artificial condition and the same robot camouflaged (bottom)[11], Copyright © 2012, American Association for the Advancement of Science.

Besides locomotive robots, the FEAs have also been used in manipulators. OctArm, a continuum manipulator inspired from octopus, used pneumatical actuators and was able to function amphibiously[12]. A Human hand-like robot that allowed for rapid grasping was designed by modified PN system named PenuFlex[13]. Similarly, a gripper was fabricated using PN architecture coupled with lithography was also reported[14]. Other than finger grasping, another study has designed the robot by helically arranged tubes to examine the rotational motion of wrist[15].

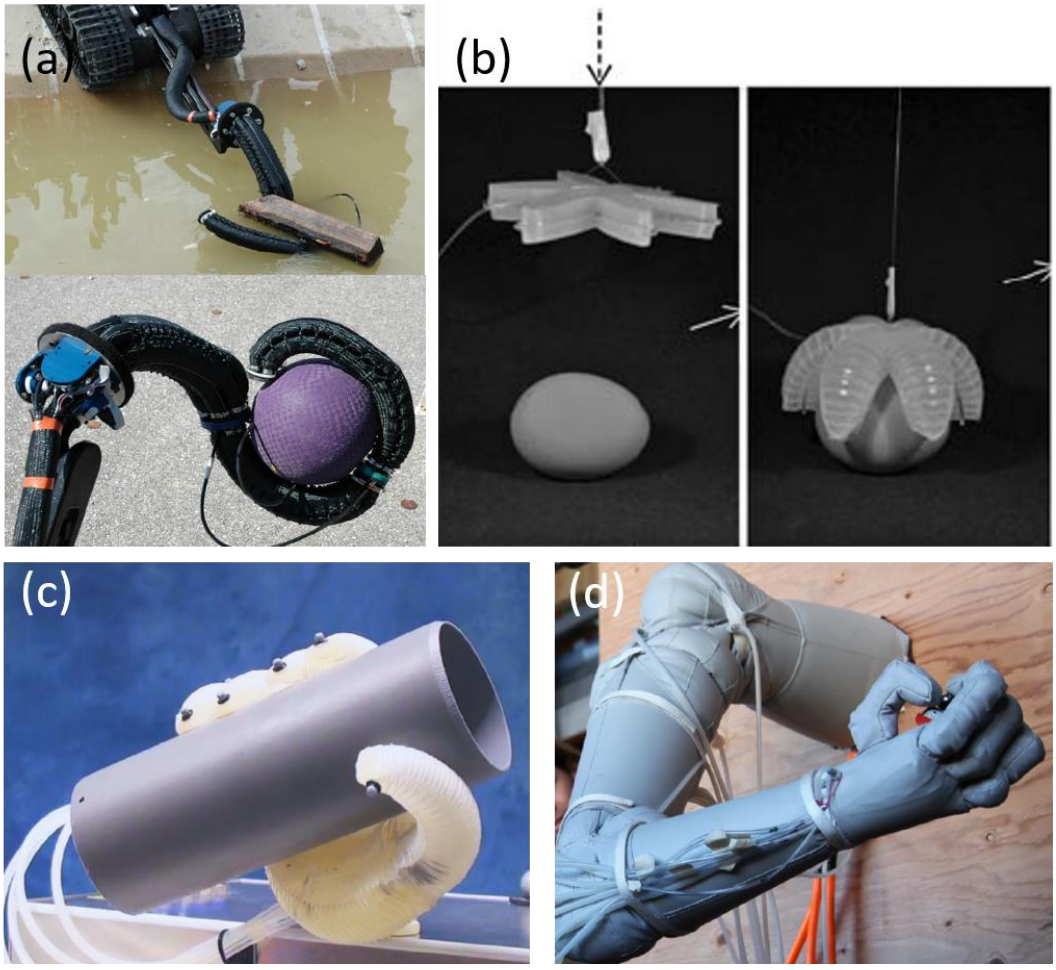

Figure 4. (a) The OctArm operating in water and on ground[12], Copyright © 2006, IEEE. (b) A tip-to-tip PneuNet holding an egg[14], Copyright © 2011 WILEY‐VCH Verlag GmbH & Co. KGaA, Weinheim. (c) A pneumatically driven soft robotic hand gripping a cylinder[13], Copyright © 2016, © SAGE Publications. (d) The PneuArm inflatable manipulator prototype[15], Copyright © 2014 by ASME.

Electro-active polymers (EAPs) was first reported by Wihelm Rontgen in 1880s, are biocompatible polymers that deform accordingly upon electrical stimulation. In general, EAPs are classified into two types: electronic and ionic EAP[16]. The electronic EAPs usually function under very high electrical fields (>150V) and the induced displacement is maintained under a DC voltage. Although high energy density is required, the electronic EAPs can response in milliseconds[16]. In contrast, the ionic EAPs demand low activating voltages (<5V) and they have a natural bi-directional actuation property that enables directional deformation based on the applied polarity of voltage[17]. As compared to electronic EAPs, ionic EAPs such as ionic polymer-

metal composite (IPMC) have the advantages of larger deformation at relatively small electric field and thus have higher efficiency and safety, which make miniaturization of soft robots probable[18]. However, IPMCs require encapsulation in order to operate in open air condition and they also generate less bending force than electronic EAPs[17]. Some research works have used IPMCs to build soft robots, such as serpent-like swimming robot[19]. Previously, only simple strip-shaped IPMC was studied, resulting in robots with simple bending motion[20, 21]. In the later stage, patterned IPMCs that could perform multi-DOF motions due to the ability of controlling invidual IPMC segment[22], were proposed.

In short, there are three types of actuation systems in soft robots: variable length tendon, fluidic actuation, and EAPs. Each possesses unique strengths and has shown potentials in different applications. In particular, pneumatic pressure based soft robot is the most popular one among the rest due to its versatility in many applications.

2.1.2 Materials

Unlike conventional robots that are manufactured from rigid materials such as metals and crosslinked thermoset, soft robots are mostly made from silicone and rubber because the soft robotics system requires large flexibility[23-26]. Silicone rubber is an elastomer that is widely used in industry due to its excellent resistance to extreme temperatures (-100 to 300 ℃). Silicone rubber is chemically inert and non-toxic, which makes it suitable for products that contact humans directly. Some robotics system such as a multigait soft robot used elastomeric polymers in order to maximize its flexibility[27].

Since traditional electrical motors used in rigid robots cannot be installed in most of the soft robotic systems, SMAs are commonly utilized to make the actuators to reduce the size and weight of soft robots[5, 7, 28]. Furthermore, SMAs also exhibit long life cycles, large force-weight ratio and negligible noise during operation, which

make this technology in soft robotics competitive[29]. However, high current requirements, inefficient transduction and non-linear behaviors have led to difficulty in precision control.

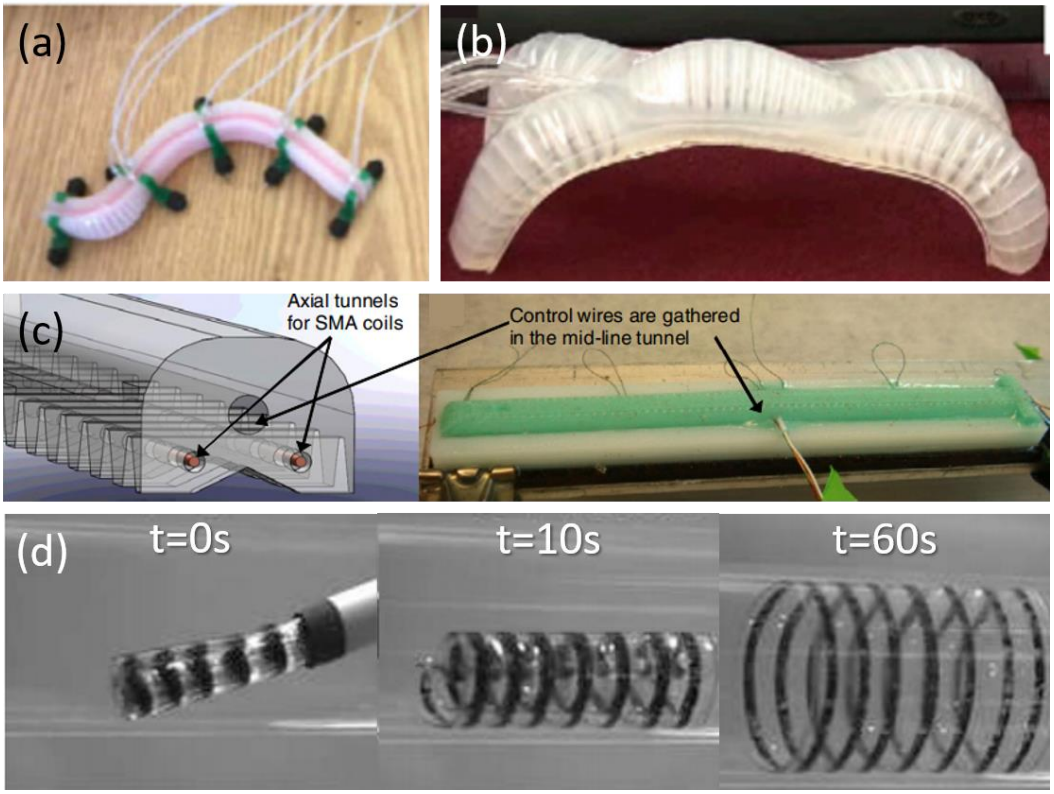

Figure 5. Various material applications in soft robots. (a) A soft-bodied snake robot made by silicone rubber[23], Copyright © 2013 IOP Publishing. (b) A tethered soft robot based on elastomeric material (Ecoflex)[14], Copyright © 2011 John Wiley & Sons. (c) An artificial caterpillar bot with a silicone rubber body and SMA backbones[28], Copyright © 2011 IOP Publishing Ltd. (d) Time series of a SMP stent recovering in water at 52 °C[30], © 2007 Springer Nature Switzerland AG.

Shape Memory Polymers (SMPs) which function similarly as SMAs but not limited to electrical activation, are deemed as a good substitute to SMAs. Other stimuli such as chemical, thermal, light and magnetic fields are more commonly utilized, resulting in greater transduction efficiency but longer response durations[31]. In addition, SMPs are cheaper, lighter and easier to process than SMAs, which make then more suitable in micro-electromechanical systems and actuators in biomedical devices[30]. As compared to metallic materials, SMPs are better in terms of flexibility, biocompatibility and modifications[32].

2.1.3 Bioinspiration in Soft Robots Designs

Studying the nature has been sparking miraculous ideas for progression of science and technology. In biology, many impressive structures and processes have been discovered and studied by researchers, and in fact, the key idea behind them is function: how the squid's tentacles work? The scientists and engineers are focusing in mimicking the functional processes and structures. Therefore, 'bioinspiration' provides insights in biological phenomena to explore new research fields for non-biological science and technology[33]. For example, the camouflage ability of cuttlefish or chameleon[34] originate researches in optical metamaterials[35, 36] and smart composites[11].

Soft robots as defined previously, are robots made with materials with moduli similar to soft biological matters and capable of autonomous movements[3]. The characteristics of these robots are softness and body compliance, which are primary features possessed by living organisms that enable fast interaction and adaptation to the surrounding environments[37]. There are two contributing factors in advancements of soft robotics: (1) There were many developed researches on replication and enhancement of motions and features of large mammals and these ideas were applied to fabricate robots that could exert large forces or operate at high speeds. However, they were metal based, electrically or hydraulically actuated, heavy and unsafe to work around humans. (2) Besides large mammals, other life forms include mollusks, reptiles, plants, etc. are fact soft, and they make up for the major organisms on Earth.

One major source of inspirations of soft robot designs come from marine lives, or more specifically, mollusks. Mollusks are animals without segmented parts, soft in nature and bilaterally symmetrical[38]. Mollusks are the second largest phylum in the world and the largest marine phylum, which accounts for nearly 23% of all named marine organisms[39]. Among all mollusk phylum, cephalopod mollusks, namely squid and octopuses, are the most neurologically advanced among invertebrates. Cephalopods have a set of sophisticated sensory system that enables them to detect

food, avoid predators and communicate among one another, which make them excellent adaptors and survivors in all marine environments[40].

Octopuses have no rigid body structure and they can squeeze into very small apertures to escape from their predators. Octopuses have eight arms that can grasp objects, bend in all directions and enable locomotion on various surfaces underwater. Their arms have an unique peculiar muscular structure, known as muscular hydrostat, that allow for contractions of different muscles to vary the stiffness of arms and exert forces[41]. Hence, the octopus serves as a good model for soft robotics. For example, a robot arm prototype using artificial muscular hydrostat has been developed, with the ability to contract longitudinally and transversely[6]. Similar arm robot arms were also designed based on this mechanism[5, 12]. The octopuses hyper-inflate their mantle cavity with water and rapidly eject it to escape from predators. An ultra-fast jet-propelled robot was fabricated emulating this function was proposed, with 53% of kinetic energy conversion efficiency, which matches the best of fasting-starting fish[42]. Furthermore, some cephalopods can alter their body color to blend into the surroundings to hunt food[43]. An interesting work done by Whitesides' group deploying a microfluidic network that was capable of color changing, contrasting, patterning, shape-shifting, luminescence and surface temperature changing to build a soft machine[11].

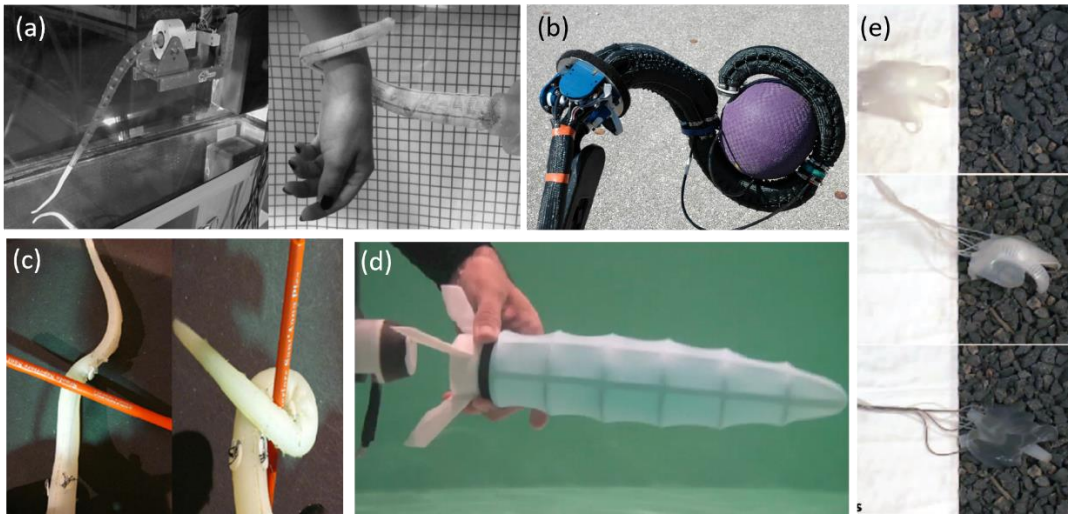

Figure 6. Various octopus-inspired soft robots. (a) Octopus arm-like robot prototype in waster at rest and wrapping human wrist[6], Copyright © Taylor & Francis. (b) OctArm grasping a ball[12], Copyright © 2006, IEEE. (c) A continuum soft arm grasping a pencil[5], Copyright © 2011 IOP Publishing Ltd. (d) Prototype of a flexible hull inflatable robot inspired by octopuses[42], Copyright © 2015 IOP Publishing Ltd. (e) Camouflaging of a soft robot crawling across a rock bed[11], Copyright © 2012, American Association for the Advancement of Science.

Some other examples include a gripper inspired by starfish with pneumatically inflated networks of microchannels embedded in PDMS, to provide anisotropic movements[27]. By studying the crawling locomotion of snakes and the anisotropic frictional properties of snake skin, an autonomous self-contained snake-like soft robot integrating actuation, energy source, computation and control functions was developed, allowing for serpentine locomotion[23]. Also, a free swimming cownose ray robot propelled by IPMC-based artificial fins was proposed[44].

Besides mollusks, arthropods, which accounts for over 80 percent of all known living species on Earth[45], are extensively studied in many research areas. An arthropod is an invertebrate animal with an exoskeleton, a segmented body and paired appendages, which include insects, arachnids, myriapods, and crustaceans. Insects have been receiving attention due to their complex structure. and functions. By studying specialized joints, springs and latches, a wide range of novel actuators, such as electro-elastomers[46] and ionic polymeric-conductor composite materials[47] have been developed and applied in robotics. Also, engineers are intrigued by the fabulous dynamic stability of insects when moving in high speed and strong maneuverability.

Caterpillars usually deter the predators by releasing noxious chemicals, cryptic coloration, or even rapid striking[48]. Sometimes they also will curl up quickly and escape from danger. A soft-bodied ballistic rolling robot, named GoQbot, was designed based on this curling movement of caterpillars, providing insights for fast locomotion for linear shaped robotic devices[28]. Besides rolling, most of soft-bodied animals use peristalsis for locomotion. This combination has several advantages such as ability to pass through small apertures, reshaping from falling and large impact[49]. Although peristaltic locomotion is slow, minimum noise is generated as compared to other

forms of locomotion such as legging or wheeling[50]. Owing to these advantages, a soft worm-like crawling robot that was fabricated based on NiTi SMA, which significantly reduces the size of the robot and enables large deformation[7]. A similar study using SMA wires, polydimethylsiloxane (PDMS), and a thin polyvinyl chloride (PVC) plate to form a smart soft composite. This soft inchworm-mimicking machine is able to move linearly in a two-way manner, and turn in all directions[51].

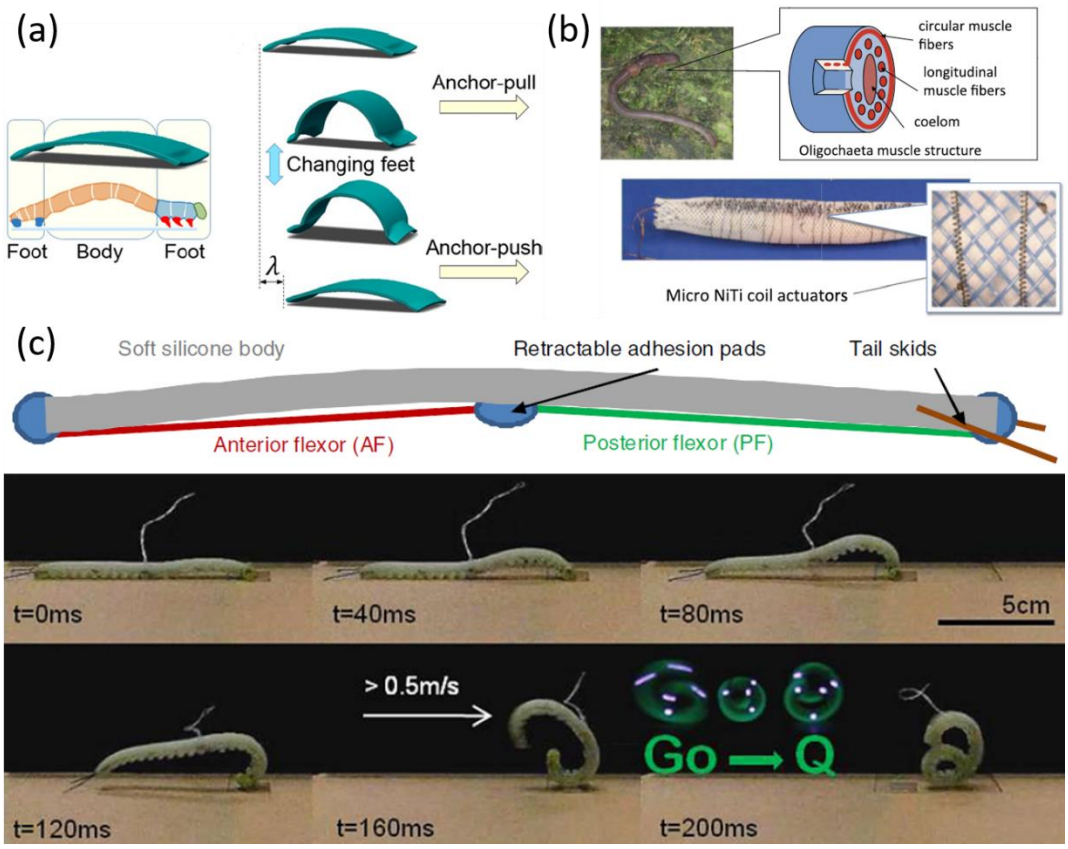

Figure 7. Demonstration of several worm-inspired soft robots. (a) A structural comparison between the robot and an inchworm, and schematic display of the robot during locomotion[51], Copyright © 2014 IOP Publishing Ltd. (b) Dissection of an Oligochaeta and prototype designed using micro NiTi coil actuators based on its structural arrangement[7], Copyright © 2013, IEEE. (c) GoBbot, a soft robot with two actuation components: anterior and posterior flexors, which together helped to generate ballistic rolling[28], Copyright © 2011 IOP Publishing Ltd.

In this section, a summary of different sources of inspiration help to design various soft robots was presented. Despite animals, plants are also the basis of most of Earth's ecosystems. Green plants generate oxygen, which is crucial to our survival. Humans

and animals also get the food from them. In nature, there are many amazing mechanisms that plant exhibit in adaptation, photosynthesis, reproduction or even hunting, which will be discussed in the next section.

2.2 Plant Intelligence

Legg and Hunter have summarized the concept of intelligence as the followings: Intelligence (1) is a property that individual possesses when it interacts with its environments, (2) reflects the ability to succeed or profit with respect to some goal, (c) indicates how well the agent adapts to different environments[52].

From McNamara and Houston's work, these three definitions can be used to describe 'plant intelligence': (1) wild plants use competitive and other biotic and abiotic signals to interact and respond to the surrounding environment; (2) the strongest and fitted ones produce more offspring, which is the primary goal of survival; (3) fitness to plants refer to the skills that individual best adapt to their environments throughout their lifetimes[53].

As compared to animals, plants have been treated as passive creatures, due to the lack of obvious movement. Therefore, people tend to think that plants do not possess intelligence. However, plants make up of 99% of the Earth biomass, which intrigues scientists to investigate the mystery behind. Unlike human beings and animals, whose intelligent behaviors are easily recognizable, organisms without a defined nervous system, such as plants, are regarded as unintelligent lives by the opponents.

Competition of resources among plants or other microorganisms can be viewed as different forms of game theory. The core value of game theory is to defeat competitors by changing its strategy. To achieve that, self-recognition must be present[54]. For example, competition via rot systems can be treated as a form of tit-for-tat situation, where competitors proliferate their roots as far as possible to occupy soil to

others. However, they leave gaps to avoid direct contact with one another[55]. These features have been observed in various species, suggesting plants have territory awareness. Interestingly, when a plant is facing water-stressful situations (resulting in growth reductions), it can transmit this message to other surrounding conspecifics via root systems. As a result, others will take actions in anticipation of future water stress even they do not experience it in the first place[56]. This serves as a good strategy to ensure its survival while other competitors do not take advantage during its growth reduction period.

Volatile organic chemicals (VOCs) are high vapor pressure organic compounds at ambient temperature, that are vital in plants communication, and even messages from plants to animals. When herbivorous or disease organisms attack the plant, specific VOCs are released to attract parasitoids of the herbivorous pests, which serve as a burglar alarm and to active defense mechanisms[57]. Emitted VOCs can also induce defense mechanisms in nearby conspecifics, if they are in the range of 50 centimeters. Holopainen and Blande proposed a creative view that the complexity and species individuality of VOCs can be seen as a plant language: individual volatiles represent words and the VOC signature represent sentences[58]. Absence of one or two words (VOCs) will result in communication failure[59]. Therefore, emission of VOCs can be regarded as a form of self-recognition or even altruism[60].

Furthermore, those plants that have experienced herbivory or disease turn primed to prepare themselves more readily for similar events in the future. This priming effect could last for years or even throughout meiosis. Many researches use priming mechanisms to cultivate plants with certain desire resistance including salt, heat, disease resistivity[61-63]. Through artificial exposure to certain environmental stimuli, the experience is learned and remembered.

In short, plant behaves cognitively in an analogous way to that of a human. It accumulates and updates various information from its surroundings, combines with its present information and makes decisions to react in the future. Although the response

time is much longer than humans and animals, plants still possess certain level of intelligence to survive.

2.2.1 Plant Electrophysiology

Plant electrophysiology is defined as the study of electrochemical phenomena related to biological cells and tissues in plants, which involves measurements of electrical potential and currents at different scales ranging from single ionic channels to entire plant. Although the so-called neuro systems in plants do not match the same complexity level as animals, a simple neural network within the phloem still enables long-distance communications in plants. These electrical signal transmission pathways are believed to be developed to respond in time to various environmental stimuli. Unlike hormones, which is a chemical signal, electrical signals propagate at a faster speed and longer distance, usually about 0.01-0.2 m s^{-1} for most plants. In some cases, such as soybean, its action potentials transmission rate can be as high as 30 s^{-1}, which is comparable to that in animal nerves[64].

Environmental changes such as variations in temperature, humidity, touching or wounding, will trigger electrical signals at the location of the symplastic continuum. Other stimuli such as acid rain[65], or even irradiation [66] will induce action potentials in plants. After perception, electrical signals are transmitted through plasmodesmata to other symplastic cells[67]. Firstly, depolarization of plasmatic membrane is observed in *Chara* via mechanical stimulation[68], which leads to formation of receptor potential. The receptor potential replicates of the stimulus when it is present. When the stimulus exceeds the depolarization threshold, an action potential (AP) is generated. Next, a large transient depolarization induced by this AP enables the information to be rapidly conducted by plasmodesmata. The schematic demonstration of origination and propagation of electrical signals is displayed in Fig.8.

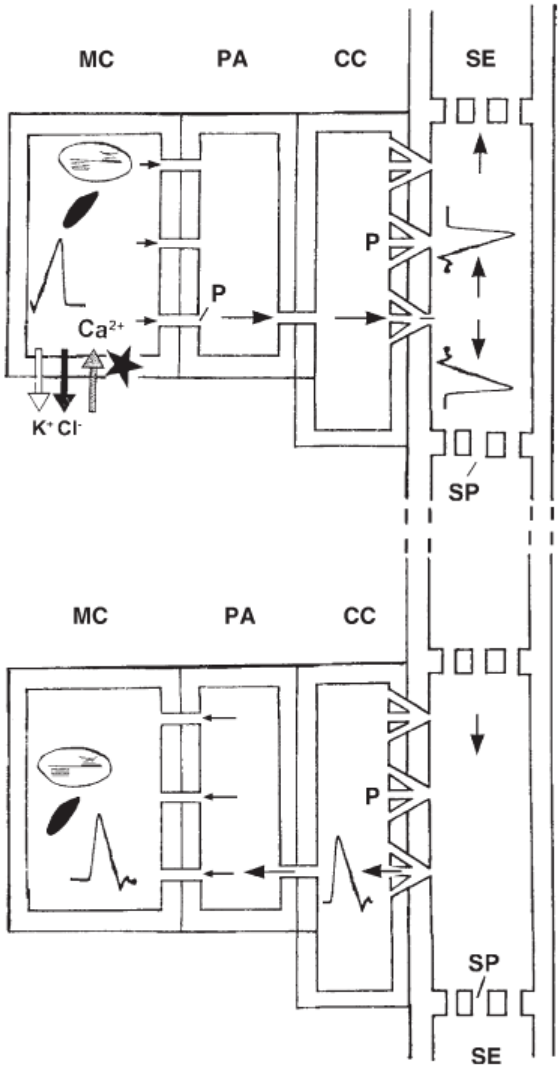

Figure 8. Electrical signaling in higher plants. Stimulations such as touch or cold shock (star) triggers calcium ions influx into a living cell, e.g. a mesophyll cell (MC). The membrane potential drops after the depolarization, and an AP is evoked by chloride and potassium efflux. This AP is then transmitted over short distances via plasmodesmal (P) networks and enters the SE/CC-complex in order to be propagated over longer distances. Sieve pores (SP) that have large diameters provide pathways with small resistance for fast electrical signal transmission along the SE plasma membrane and exit the phloem through plasmodesmata to elicit physiological reactions in the surrounding tissue[69], Copyright © Springer-Verlag Berlin Heidelberg 2006.

The first plant AP was recorded from the Venus flytrap (*Dionea muscipula* Ellis) in 1863 by John Burdon-Sanderson. Darwin then declared that *Dionea* was the "most animal-like plant" due to its fast reflex when trapping preys with its lobe[70]. The trap-closing phenomenon of *Dionea* was regarded as a good example to demonstrate the comparable function of APs in plants to nerve–muscle preparations in animals[71].

An AP usually takes place in an all-or-none manner, and it can be self-amplified and propagate at constant speed and magnitude[72]. Electrical coupling via plasmodesmata was found in many species such as *Nitella*[73], *Elodea* and *Avena*[74] and *Lupinus*[75], showing that plasmodesmata act as relay stations in the signaling network.

For long-distance transmission between organs, low resistance pathways that connect continuously throughout the whole plant are required. From Figure 8, the sieve pores or the sieve tube system serves as the bridges for electrical signal conduction over long distance due to the relatively big, unblocked sieve pores and the continuous plasma membrane[76].

2.2.2 Electrical Signals in Plants

Electrical signals were first discovered in plants by Berthelon in 1793, which was long before Darwin hypothesized the presence of chemical signals in plants in 1881. When a plant is electrically stimulated, or a voltage is applied to it, an electrical signal is evoked and propagated through the plant. There is a range of electrical signals discovered by scientists: action potentials (APs); variation potentials (VPs); voltage transients (VT) or voltage spikes (VS); system potentials (SPs) and rhythmical electrical activity (REA).

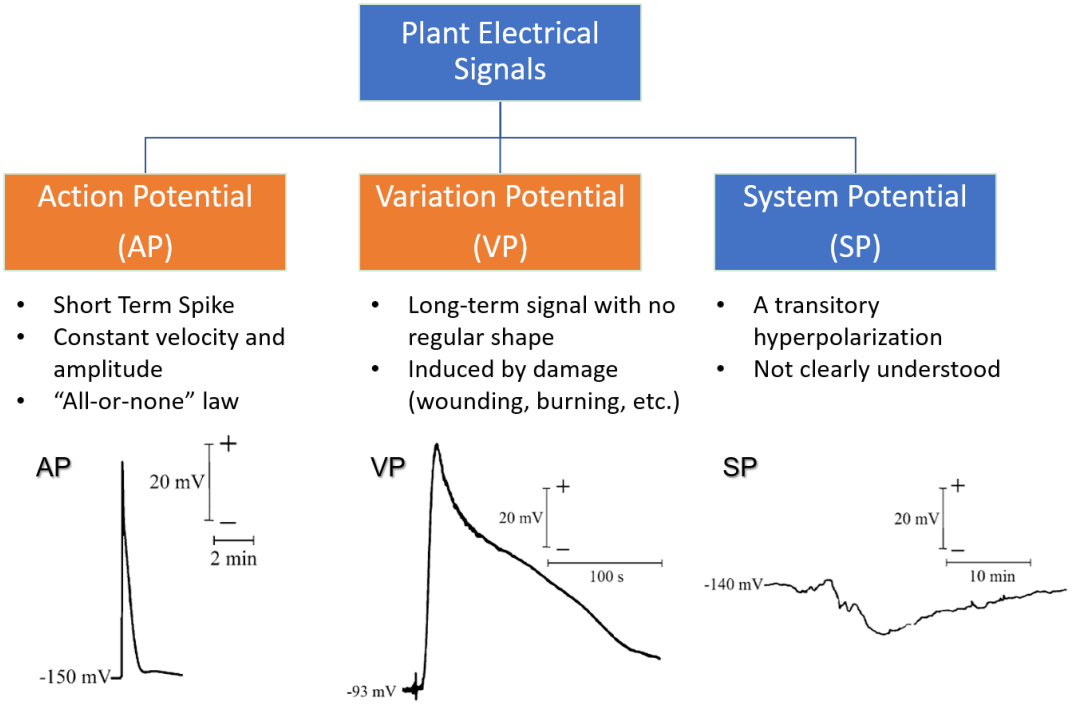

Figure 9. Three types of electrical signals in plants: action potential (AP), variation potential (VP) and system potential (SP)[77]. AP and VP are two most thoroughly studied electrical signals in plants. For SP, there is still a lack of systematic understanding of this signal, hence it will not be discussed further in this work.

In general, only those signals involve membrane potential (V_m) changes and capable of long-distance transmission attract the research attentions, namely two major signals, APs and VPs.

2.2.2.1 Action Potentials (APs)

In animals, APs are fast electrical signals that propagate along the axons in the nervous system and some muscle surfaces and glandular cells. AP are transient (within milliseconds) and travel at constant speed and amplitude in axons[72]. AP usually take place in an all-or-none manner, and their amplitude and shape will not change after the membrane has been depolarized. AP are self-propagating and hence, they rely heavily on ionic channels that respond to variations in membrane potential. Generally, plant cells are excited by Ca^{2+}, Cl^- and K^+ ions. The APs in the giant internodal cells

of the green algae *Chara* and *Nitella* is the most well studied, as those cells possess vigorous protoplasmic streaming that aided AP propagation at a speed of 10-20 mm s^{-1}[73].

One example of AP propagation in higher plants is *Mimosa pudica*, whose leaflets close in sequence upon transmission of APs. The AP also results in bending of tertiary pulvini. Specifically, after passing through the pulvinus, the AP is propagated from plasmodesmata to the motor cortex cells, which then cause loss of hydraulic pressure by ion efflux[78]. Another good example will be Venus flytrap, where touching of trigger hairs on the upper leaf epidermis activates mechanosensitive ion channels and induce APs to shut the trap[79].

In summary, the APs in plants work very similarly to those in animal cells except the propagation speed is significantly slower[80]. Calcium influx leads to depolarization, which is amplified by chloride efflux, and later repolarized by potassium efflux. In addition, when an AP is generated, a refractory period is present where subsequent AP cannot be generated immediately, which could be attributed to temporary channel inactivation[81].

2.2.2.2 Variation Potentials (VPs)

Variation potentials (VPs), are electrical signals which cause local changes in membrane potentials, inducing from the passage of other signals. The major difference between VP and AP is that VP cause a longer and more delayed repolarization and a greater variation range in magnitude[82]. The VP can be excited by damaging to plants such as wounding[83], excision[84] or even flaming[85]. Furthermore, the AP are transmitted mainly in the living phloem whereas the VP can propagate in the dead xylem[86, 87]. However, their magnitudes and speeds damp when they are further away from the damaged location. The xylem tension plays a vital part in generation of the

VP: when humidity is very high, VPs cannot be evoked due to negligible xylem tension.

Using *mimosa pudica* as an example: A VP is generated in the rhachis when a leaf pinna tip was cut, which has an irregular shape and lasts longer than an AP. While the AP stops at the base of a pinna, the VP is able to pass through it and continues to propagate into the neighboring pinna to induce closing of all leaflets. In addition, a VP can transmit basipetally through the petioles, leading to the bending of the petioles. In short, an AP is confined to the base of a pinna, but a VP can propagate all the way through the secondary and primary pulvini, resulting in both leaflets folding and petiole bending.

2.2.2.3 Physiological Effects of Electrical Signals

Both APs and VPs are capable of delivering local stimuli to distant cells and tissues so that they can take respective actions. For example, insectivorous plants such as *Drosera* and *Dionaea* that grow in nitrogen-deficient regions, utilizes APs to catch insects effectively as nitrogen source[88, 89]. In *Dionaea*, once the mechanical pressure of any trigger hairs increase, Ca^{2+} is first injected into the cytosol of the sensor cells, which generates an AP without trap closing[90]. Next, if any of the trigger hairs are touched within 40 seconds, the second AP will be evoked to close the trap. The successive APs are to prevent activation of trap by accidents. Short-distance electrical signals also have impacts on the respiration rate of *Vicia faba* seedlings[91] and after the pollination of flowers[92].

Besides short-distance transmission, long-distance signaling is also very important in many plants. In *Mimosa*, both APs and VPs help to close the pinnules and bend the petioles to make itself less appealing to the predators. Furthermore, VPs caused by flaming could transiently reduce the photosynthesis activity of *mimosa*[93]. In maize, APs evoked by watering the plants in dry land increase the carbon dioxide

and water vapor exchange of the leaves[94]. On the other hand, freezing of leaf tips also trigger APs to reduce the phloem transportation of distant leaf parts[95].

In addition, some long-lasting effects can also be inflicted by plant excitation. For instance, Ca^{2+} signal initiated by touching the Arabidopsis could result in modification of cell wall and increase in disease resistance, and also the change in gene expression were observed after several minutes upon touching[96]. In *Luffa cylindrica*, evocation of a single AP would reduce the stem growth rate [97].

2.3 Traditional Signal Measurement Techniques

Conventionally, external electrodes were the only feasible tool to measure potentials for the plant surface and animal organs. This potential is also known as the extracellular potential. Extracellular potential measurements have been widely used in the old days because it could detect the electrical potential differences continuously over several days. In contrast, intracellular potentials measured via invasive glass microelectrodes last for a short period of 1 to 2 hours only as the electrolyte within the electrode diffuses into the measuring cells and alters the original bioelectric state. However, intracellular measurements are more accurate and precise because electrical signals and membrane potentials (V_m) could be reckon from specific cells.

2.3.1 Extracellular Potential Measurement

Extracellular measurements are extensively studied from animal electrophysiology and are summation of the total bioelectrical activity in large cell groups. Electrocardiograms (ECG) and electroencephalograms (EEG) are two readily commercialized examples of extracellular measurement techniques in medical area. In higher plant,

these two measurements can also be done using inserted metal electrodes. However, the insertion often results in wounding reactions and therefore, metal wires with small diameters (e.g. Ag/AgCl-wires with a diameter 0.4–1.0 mm) are used to minimize the damage, shown in Fig.10. The principle behind is to make contact with the tissue that consists of large cell groups upon insertion. For example, such setup was used in measuring the electrical signals of *mimosa* upon physical and electrical stimulation of its pinnules and petioles[98].

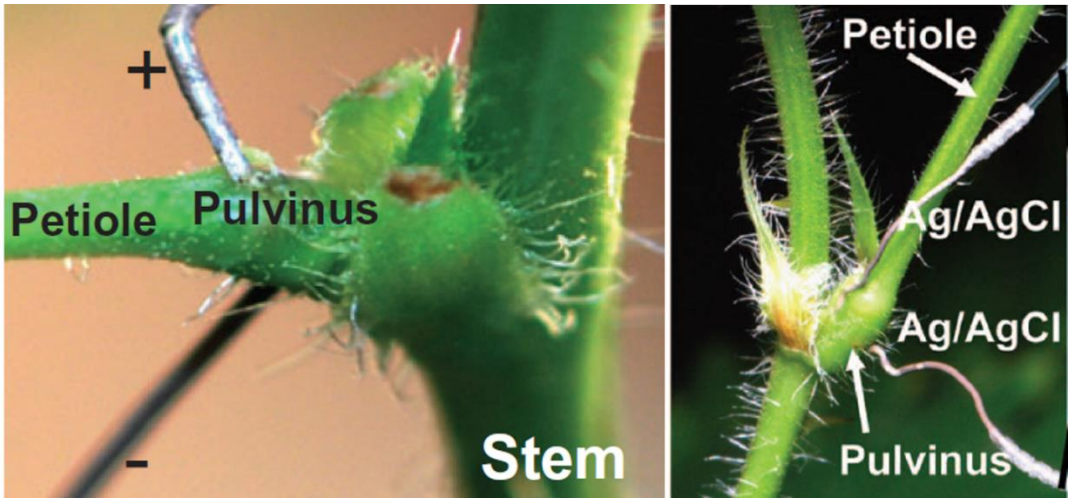

Figure 10. Examples of invasive metal electrodes in *Mimosa pudica*[98], Copyright © 2009 Blackwell Publishing Ltd.

However, although this invasive method is useful for plants that exhibit large physical movement, it causes damage to the plant tissues, nonetheless. Surface measurement appears to be a better solution due to the non-invasiveness and physical stability. It can be coupled with other measuring technique such as gas exchange recordings simultaneously [94] (Fig.11). In general, it uses electrodes that include Ag/AgCl wires, soaked with 0.1 w/v % KCl in agar and covered using cotton to enlarge measuring surface area[99], or pelleted Ag/AgCl and a conducting aqueous gel commonly used in ECG[86].

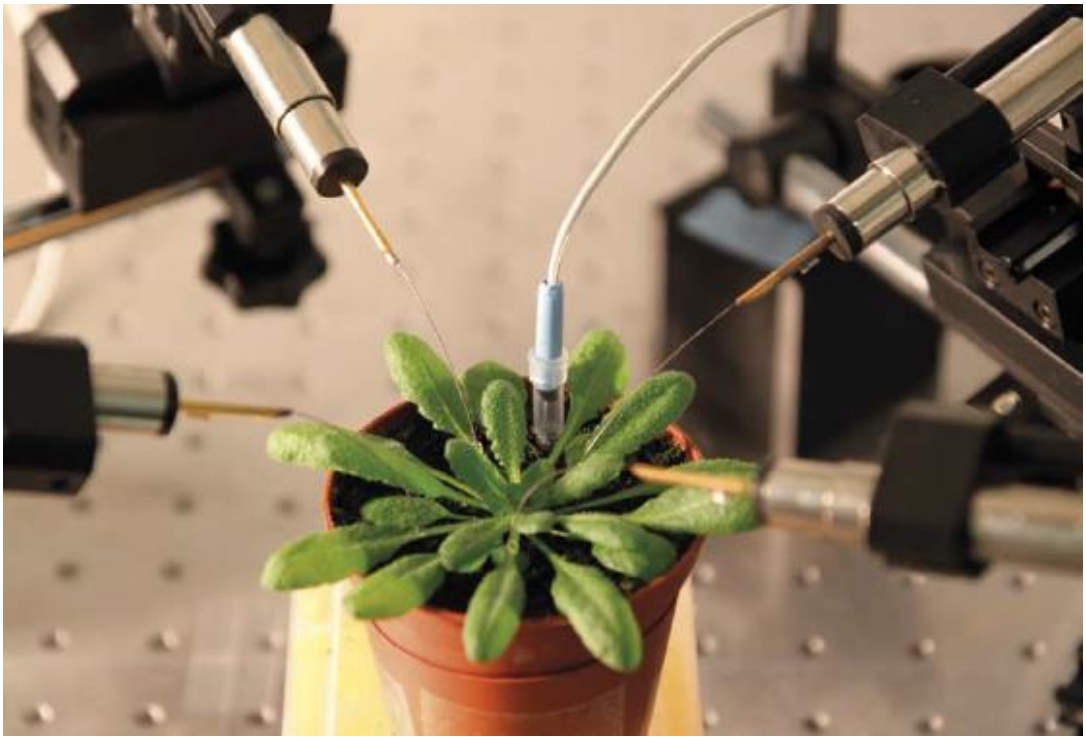

Figure 11. Illustration of a recording setup for surface potential changes measurement of *Arabidopsis* using Ag/AgCl electrode with KCl/agar solution[100], Copyright © 2014, Springer Nature.

Although these two extracellular measurements are relatively easy to prepare, intracellular information cannot be accurately obtained by these methods.

2.3.2 Intracellular Potential Measurement

In the early years, internal potential of cells, as known as the intracellular potential, can only be deduced by measuring the "wound potentials" via the abovementioned techniques[101]. The membrane theory established by Bernstein provided a way to directly measure the cell membrane potentials[102]. Later, intracellular potential, also known as membrane potential (V_m) measurement was greatly facilitated by using microelectrodes, which were KCI-filled glass micropipettes with very tiny tip diameter to insert into living cells, proposed by Pletcher[103]. This method was first deployed onto giant axon cells of cephalopods and charophytic algae. However, insertion of microelectrodes usually led to long-lasting damage and very small membrane

potential[104]. In 1940s, introduction of electronic amplifiers and voltage clamp circuits made measurement of ion currents rather than voltages and even monitoring of ion channel activities possible. This advancement promoted the understanding of the ionic species and mechanisms related to changes in V_m, especially action potentials (APs)[105].

As mentioned in the previous section, phloem cells are crucial in long-distance signal conduction because of low resistance pathways (sieve pores), accurate intracellular measurement of sieve elements is the key for high speed signals detections. However, insertion of microelectrodes seems impossible as the phloem is positioned inside the plant, and precise insertions can hardly be achieved. A very interesting approach known as the 'aphid electrode' was proposed by Fromm and Bauer in 1994, which successfully detected V_m of sieve tubes and the variation upon stimulation[95]. Aphids are placed on a mature leaf overnight and separated from its stylet using laser pulse on the next day, as shown in Fig.12. The remaining stylet serves as a great connection between the cytoplasm and the microelectrode, and the solidified saliva has electrically insulated the stylet.

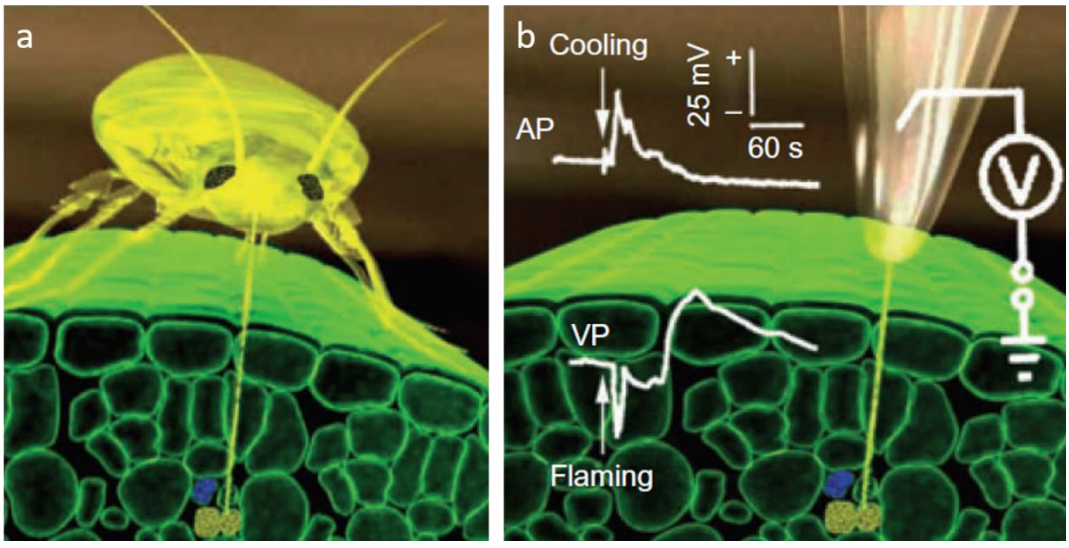

Figure 12. Aphid electrode. (a) An aphid inserting stylet into a sieve element on the leaf surface. (b) After separation of aphid from the stylet using laser pulse, the stylet served as a connection between the sieve tube and the microelectrode. An AP was produced by cooling the shoot while a VP was generated from flaming of a leaf[106], Copyright © 2006 John Wiley & Sons Ltd.

2.4 Mimosa Pudica

As compared to animals, plants generally give the impression of motionless creatures. In general, plant movements are categorized into two: (1) the spontaneous movements as the results of endogenous metabolism, such as the 'nycthemeral' movements of leaves caused by the change of day and night periods. (2) the induced movements as the results of external stimuli (temperature alteration, feeding actions by predators, etc.), for example, leaves of *mimosa pudica* will fold upon physical touch[107]. However, most plants do not exhibit observable induced movements and hence, fast moving plants such as venus trap and *mimosa pudica* have raised immense attention as good research models for the study of plants excitability and motility.

Mimosa pudica is a seismonastic plant which fold its pinnules and bend its petiole when it is mechanical stimulated by touch, vibration or wind, and this protective mechanism makes it less attractive to some herbivores[108]. In the same book, it also mentioned that *mimosa pudica* can also be electrically stimulated. Both electrical and physical stimulation can lead to the folding of leaflets and the bending of the petiole, shown in Fig.13.

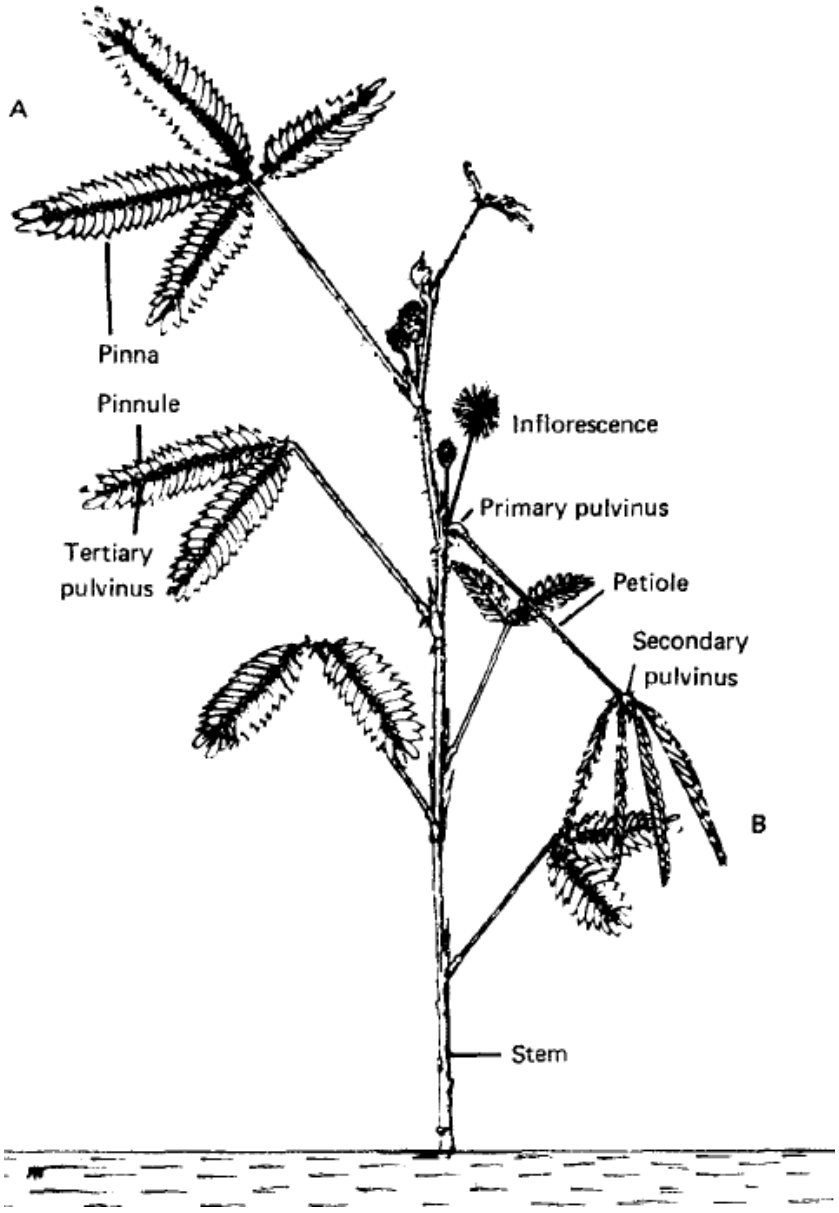

Figure 13. General appearance of *Mimosa pudica*. The leaf A is in normal state whereas the leaf B displays the position after excitation[107], Copyright © Cambridge Philosophical Society.

From Figure 13, these two movements are resulted from different elements in the primary and secondary pulvini, that attribute to voltage-gated potassium, chloride and calcium ionic channels[109, 110],H^+-ATPases[111], aquaporins[112], actin[113], Ricca's factor[114] or gallic acid 4-*O*-(*β*-D-glucopyranosyl-6'-sulfate)[115], neurotransmitters[116] and osmotic pressure[117]. All these different mechanisms have experimental

evidence and should be combined together to give a comprehensive description of the seismonastic properties in *Mimosa Pudica*[118].

The main types of electrical signals in *Mimosa Pudica* are APs and VPs, which were discussed in the previous sections. The major difference in these two signals are shown in Figure 13. An AP generally takes a shape of sharp spike after stimulation, whereas a VP has no regular shape. An AP travels at a higher speed (20-30 mm s^{-1}) than that of a VP (5-6 mm s^{-1}) but stopped at the base of a pinna, whereas the VP is able to propagate all the way through the secondary and primary pulvini, leading to folding of neighboring pinnules and bending of the petiole.

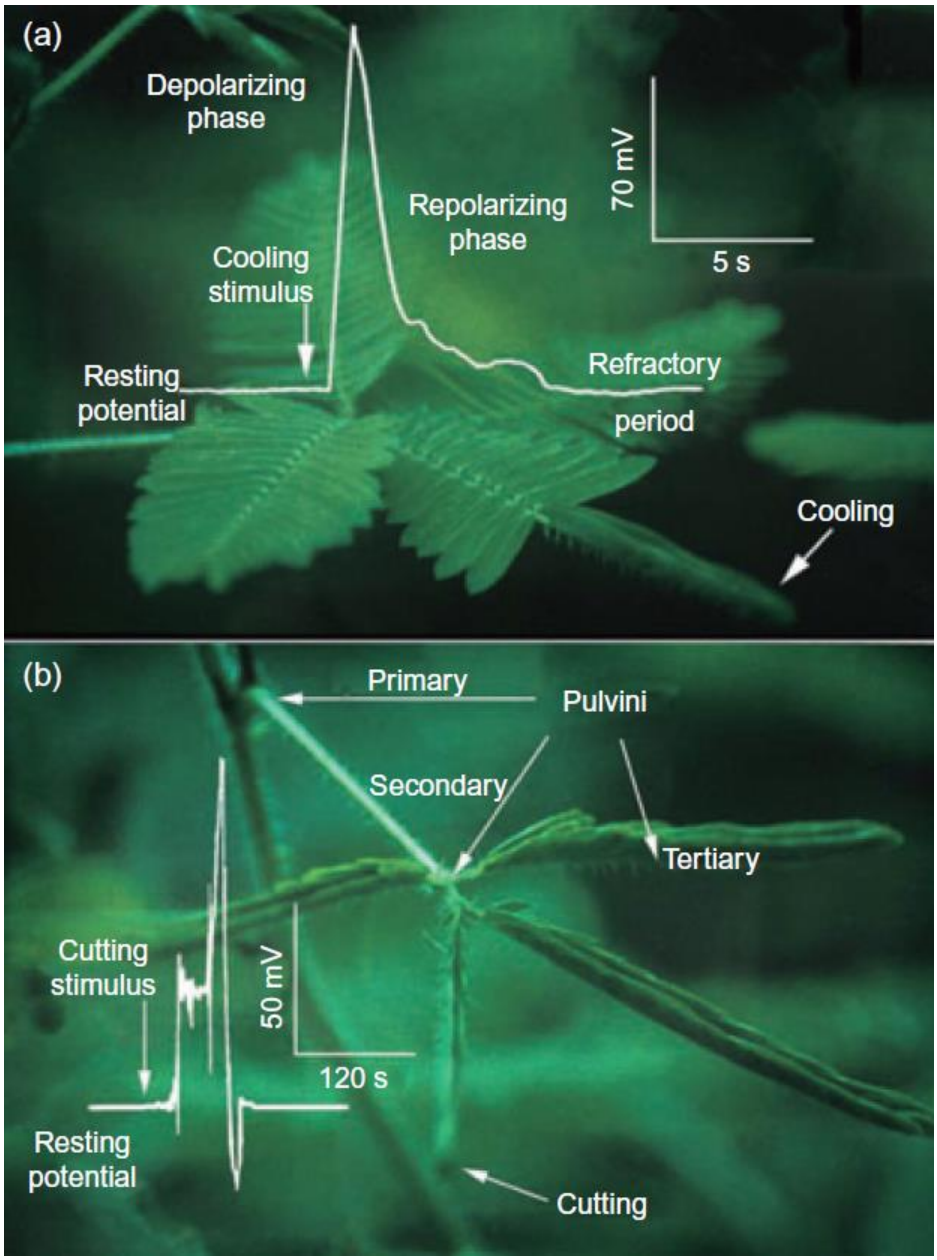

Figure 14. Electrical signals in *Mimosa pudica*. (a) An AP is generated when a pinna tip is touched or cooled by ice and transmitted basipetally within the rhachis at 20-30 mm s^{-1}. The AP is limited to the base of pinna and cannot propagate further. (b) A VP is evoked when the pinna is cut, which has an irregular shape and last for a longer time than AP. In addition, it travels at a lower speed (5-6mm s^{-1}) but is capable of transmitting over the secondary pulvini at the base of pinna, causing the neighboring pinnules to fold and also the falling of the petiole at the primary pulvinus[106], Copyright © John Wiley & Sons Ltd.

In general, an extracellular measurement using Ag/AgCl electrodes piercing through the pulvini is used to measure the electrical signals and provide electrical stimulation to study the relationship between the two major movements and amount of electricity

used[98, 118, 119]. Due to the large motion of the petiole bending, this invasive electrode has the advantage of good contact as compared to other non-invasive methods such as Ag/AgCl and agar electrodes. However, the insertion of the electrodes inevitably causes tissue damage to the plants and hence, resting period (3-25 hours) is required for *Mimosa* to recover[98]. Volkov's team used the Charged Capacitor Method to estimate the accurate amount of electrical energy required to initiate the movements in *Mimosa[98] and Dionaea muscipula* Ellis[79, 120].

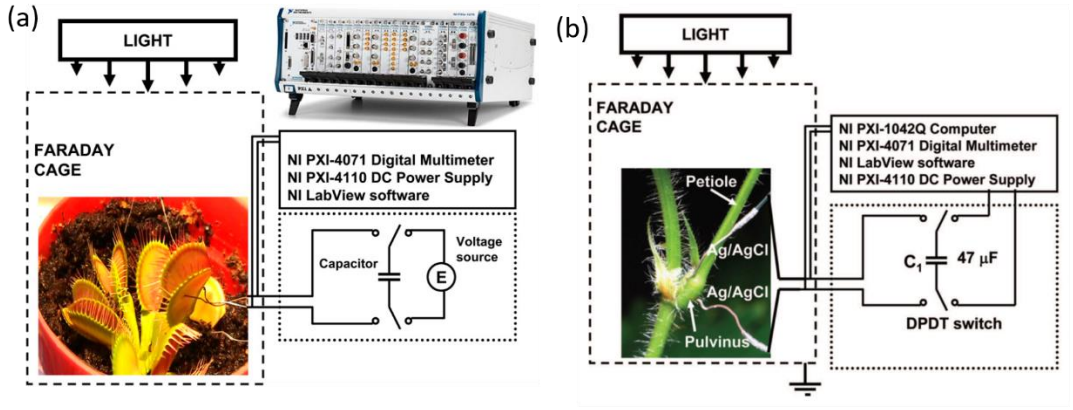

Figure 15. Experimental setup for the Charged Capacitor Method in (a) *Dionaea muscipula* Ellis[79] and (b) *Mimosa pudica*[118], Copyright © 2010 Landes Bioscience and © 2008 Elsevier B.V, respectively. A double pole-double throw (DPDT) switch connects a capacitor to one 1.5V battery for charging and to the plant for stimulation.

Since capacitance is known by choosing the capacitor, the amount of charge delivered can be calculated and the voltages applied can also be controlled, using this equation Q = CU.

The pinnules closing and the petiole bending movements are characteristic to *Mimosa pudica* and the mechanisms behind offer a different insight for designing a soft robotic system that mimic the grasping motion of human hands.

2.5 Plant Applications in Materials and Devices

The nature provides fabulous insights for engineers and researchers to design artificial materials or devices that have novel performance. This bioinspired rich heritage filled with fascinating ideas to ameliorate basic needs and comforts is waiting to be unlocked by scientists. The zest and breakthroughs in nanotechnology serve as bridge between the disparity between the artificial and natural art pieces. In addition, devices such as smart sensors, power electronics manifested from nature's mimicry mark the new era of technological advancement[121].

2.5.1 Plant Applications in Smart Fabrics

Smart textiles have emerged to be a fast-developing area of research due to the unique feature to sense and/or respond to environmental changes[122]. Natural existing biomaterials possess structural and functional advantages which perform beyond the limits of artificial materials[123]. Plants are generally regarded as static and passive organisms, however they also exhibit a wide range of autonomous movements upon external stimuli. Some examples include the trap closing in insectivorous Venus flytrap (*Dionaea muscipula*)[79], the pinnules folding in *mimosa*[98], and the opening and closing of pinecones[124]. The actuation mechanisms and physiological characteristics related to these movements can be incorporated into smart textiles design.

The glassy lotus leaf (*Nelumbo nucifera*) has excellent water repellent and anti-dust properties due to its unique surface micro-morphology[125]. Owing to this superb hydrophobicity of lotus leaf, scientists have fabricated superhydrophobic poly-lactic acid (PLA) fabrics using UV-photografting of hydrophobic silica particles functionalized with vinyl functional group over silica microstructure as shown in Fig.16**Figure 16**[126]. Such technique shows a promising fabric design that repels water and dust.

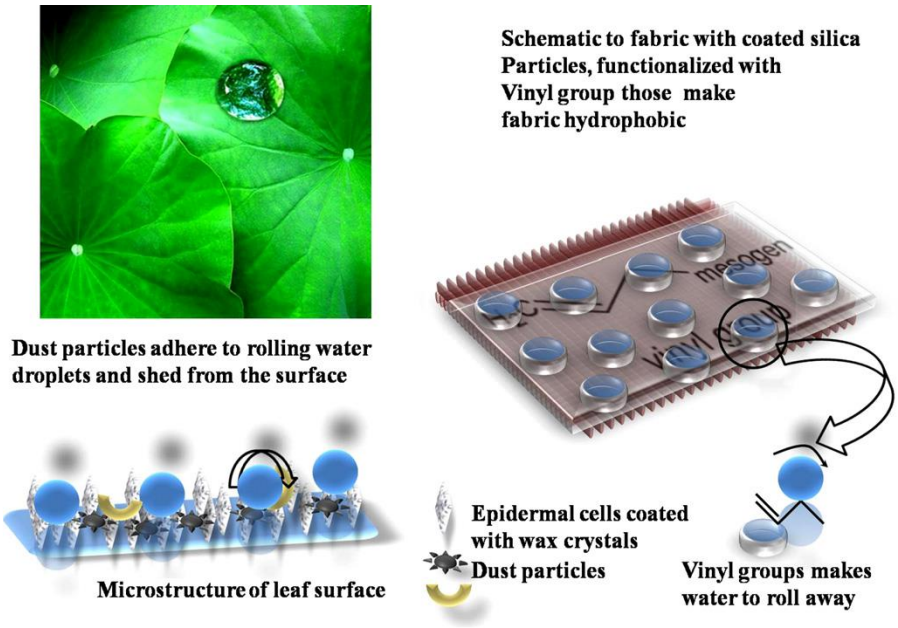

Figure 16. Lotus-like fabrics with water and dust repelling characteristic[127], Copyright © 2011 Elsevier Ltd.

The sensitive plant *mimosa pudica* demonstrates quick sensing and hydraulic actuation – the folding of leaflets and the bending of petioles, which are caused by the rapid loss of water in pulvini[117]. This underlying mechanism put forth an idea in designing fabrics that are capable of shrinking and inflation upon touching. A therapeutic fabric embedded with actuators sensors was invented to provide massaging and aromatizing during walks, inspiring from the functional replicate of the *Mimosa* pulvinus, shown in Fig.17.

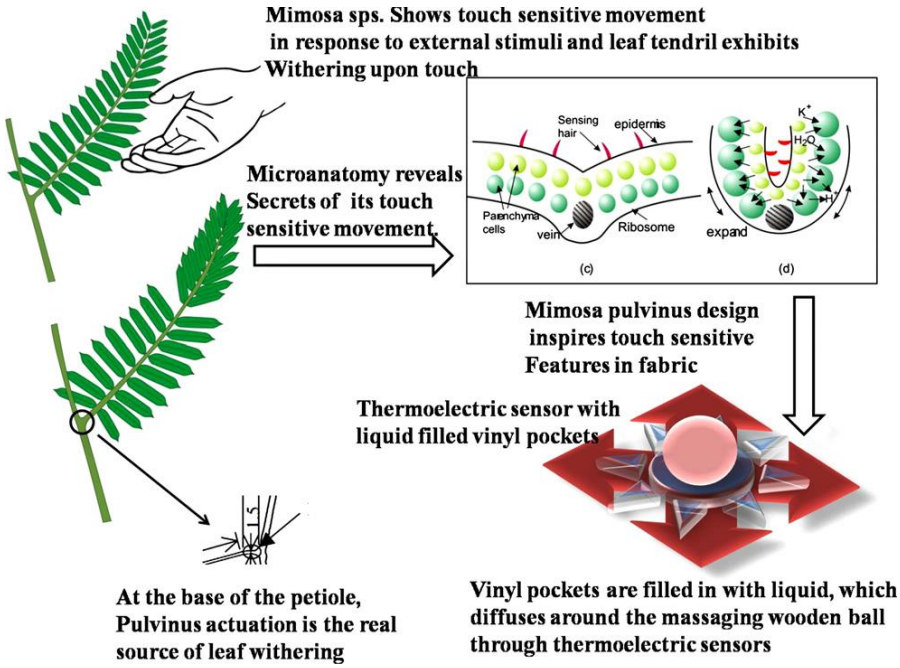

Figure 17. A sensitive cloth design mimicking the *Mimosa pudica* pulvinus. Reduction of turgor pressure causes a rapid shrinking movement fueled by rearrangement of water and ion influx. A touch sensitive fabric model is designed to mimic pulvinus features[127], Copyright © 2011 Elsevier Ltd.

The scales of *Pinus radiate* cones move upon changes in surrounding humidity, which automatically opens up to disperse seeds when it is dry and closes up in the moist environment[128]. This hygroscopic movement of pine scales was then studied and utilized to fabricate a humid-sensitive adaptive textile, which can keep the body cool by moisture in microclimate (Fig.18).

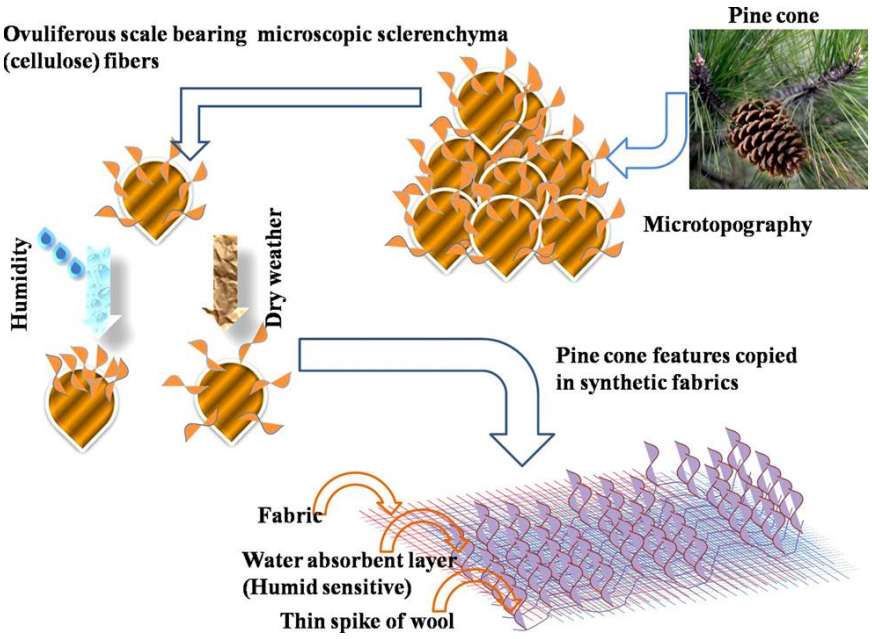

Figure 18. Schematic illustration of humid sensitive fabric which experience cumulative movements when hygroscopic components below changes, inspired by pinecone's unique actuation responds to surrounding humidity variations[127], Copyright © 2011 Elsevier Ltd.

2.5.2 Plant Applications in Morphing and Actuation System

As compared to animals, whose movements mainly come from muscular activity, plant movements are based on integrative fluidic motions. Plant cells and tissues provide both structural stability and movement capability without clear differentiation between the actuation and structure parts, which are commonly distinct in animals and other man-made systems. In short, plant movements is a combination of the hydraulic actuating strengths (e.g high power to density ratio[129]) and also the compliant nature and hence, many new engineered system benefit from plants.

In small scaled soft-robots and some biomedical applications, it is very difficult to install pumping devices. To address this, soft resin based osmotic actuation system with fluid filled capsules are developed based on the osmotic principle of plants[130]. The capsules are covered with artificial semi-permeable membranes which deliver

fluid and produce pressure, and hence achieving shape shifting and actuation in absence of external pressure applied. Two mechanisms have been studied so far: (1) the active pressure formation via selective transport of ions and molecules across the membrane to generate pressure[131-133]; (2) the passive pressure formation by direct water diffusion based on concentration gradients[134, 135]. Technical barriers such as slow pressurization (ranging from minutes to hours), low filtration coefficient semi-permeable membranes and scalable fabrication of such systems remain to be solved.

Hygroscopic materials such as hydrogels gain energy from the surrounding humidity alterations to achieve shape morphing, which is more efficient than morphing and actuation system relying on pressurization. Furthermore, hygroscopic tissues are ubiquitous in plants, and able to swell up to 10 times when the surrounding humidity increases and vice versa[136]. Such feature is ideal for applications that cannot carry power sources. Besides variations in humidity, scientists have fabricated inorganic hydrogels that swell/shrink upon different stimulations such as temperature[137], enzymes[138], electric signals[139] and light[140]. Hygroscopic materials are fabricated together with other materials to form different functional structures: (1) Biomorph: a hygroscopic layer that changes its volume upon humidity variations and a passive layer that constrains physically[141]; (2) Multi-material modulation: a twisting hygroscopic material with an in-plane microscale modulation coupled with two constituent materials stripes[142]; (3) Fiber reinforcement: a passive matrix incorporating hygroscopic fibers[143] or vice versa[144].

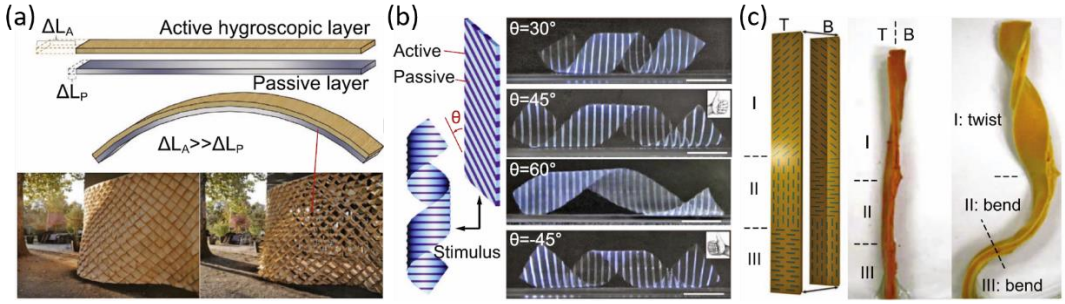

Figure 19. Different utilization of material anisotropy to obtain desired hygroscopic deformation. (a) Biomorph inspired by pinecones as responsive building skins[145, 146], Copyright © 2012 John Wiley & Sons, Ltd and Copyright © 2015 Elsevier Ltd, respectively. (b) Multi-material modulation capable of helical twisting[142], Copyright © 2013, Springer Nature. (c) Programmable short fiber-reinforced ribbon for complex deformation[144], Copyright © The Royal Society of Chemistry 2014.

Although many advancements in design and synthesis were made towards practical applications, challenges such as hard to achieve complicated and greater dimensional shape changes and actuation, and performance degradation of hygroscopic materials still remain to be solved.

2.5.3 Plant Applications in Flexible Devices

The maturation of the modern electronics industry established on semiconductors and nanotechnology has improved the quality of our lives. However, most of the devices are fabricated from complementary metal oxide semiconductors (CMOS), which materials with large moduli such as metals and semiconducting materials are used[147]. Recently, the development of flexible electronics has caught immense attentions as they could possibly overturn the idea of rigid electronics and revolutionize the way of living[148, 149]. Unfortunately, most materials with outstanding electrical properties has poor mechanical performance in complex stress conditions, which render them unsuitable to manufacture flexible and stretchable devices. Living creatures have evolved wide range of well-developed structures and materials via natural selection and hence, nature is a perfect source to harvest solutions for the future of flexible electronics[150].

Mechanical sensors used to detect physical strain which transform the geometry deformation into electrical signals for detection. Among all mechanical sensors, biosensors with efficient transduction of external mechanical information into bio-signals exhibit fascinating strengths in ensuring the survival of living organisms in complicated conditions[151]. The micro- or even nanostructures found on plant surfaces serve as good models for ultrahigh sensitive pressure sensors. For example, *Mimosa pudica*'s leaves demonstrate remarkable responsiveness upon external stimuli, which was used as a template for fabricating a micro-structured PDMS electrode via a two-step negative/positive molding[152]. Other plant organ surfaces such as rose petal also inspired a resistive PDMS-based sensor coated with Cu-Ag nanowires[153]. On the

other hand, a sponge-like structural PDMS dielectric layer inspired *by spongia officinalis* which has a hierarchically porous structure, that is capable of accommodating larger deformation and hence a higher sensitivity[154].

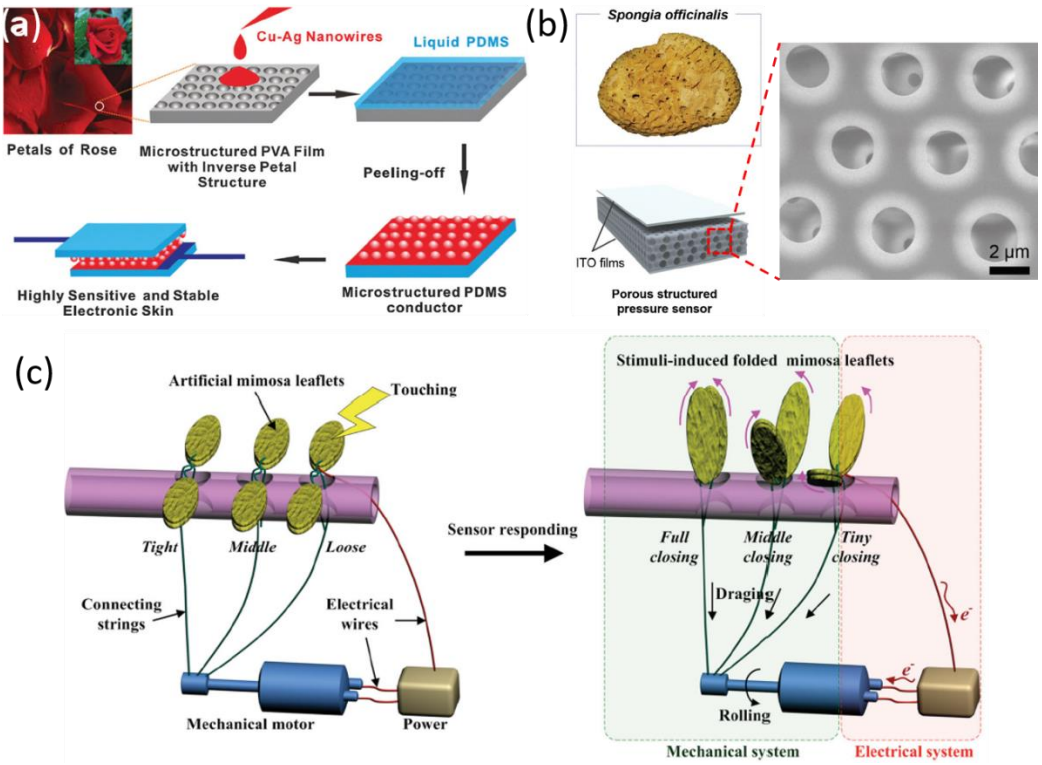

Figure 20. Nature-inspired structural materials for pressure sensing. (a) Schematic fabrication process of flexible micro-structured e-skin inspired by rose petals[153], Copyright © The Royal Society of Chemistry 2015. (b) Photograph of a *Spongia officinalis* and schematic demonstration of a porous structured pressure sensor that has a spongy structure of PDMS thin film dielectric layer, and a top view SEM image that reveals the uniform formation of pores in the multilayer configuration[154], © 2016 WILEY‐VCH Verlag GmbH & Co. KGaA, Weinheim. (c) A flexible pressure sensor mimicking the leaves movement of *Mimosa pudica*[152], Copyright © 2014 WILEY‐VCH Verlag GmbH & Co. KGaA, Weinheim.

Mechanical interactions such as adhesion effect is also an essential element in flexible electronic design. In particular, due to the large mechanical deformation, the interfacial adhesion between materials of different elastic moduli becomes a challenge. Engineers have come up with ideas such as introducing adhesive Cr and Ti metal layers to improve the adhesion between different layers on elastic substrates[155-157]. In order to survive in complex and hostile environments, plants have evolved various types of root systems. Inspired by this, the structure of root systems was introduced

to enhance interfacial adhesion and stretchability between electrodes and soft substrates, namely an interlocking layer with biomimetic roots protruding into the PDMS substrate underneath the gold layer[158]. The presence of gold nanopiles increases the contact area with the substrates and hence a higher adhesive strength is achieved. However, this structure suffers from a lower stretchability as compared to other electrodes.

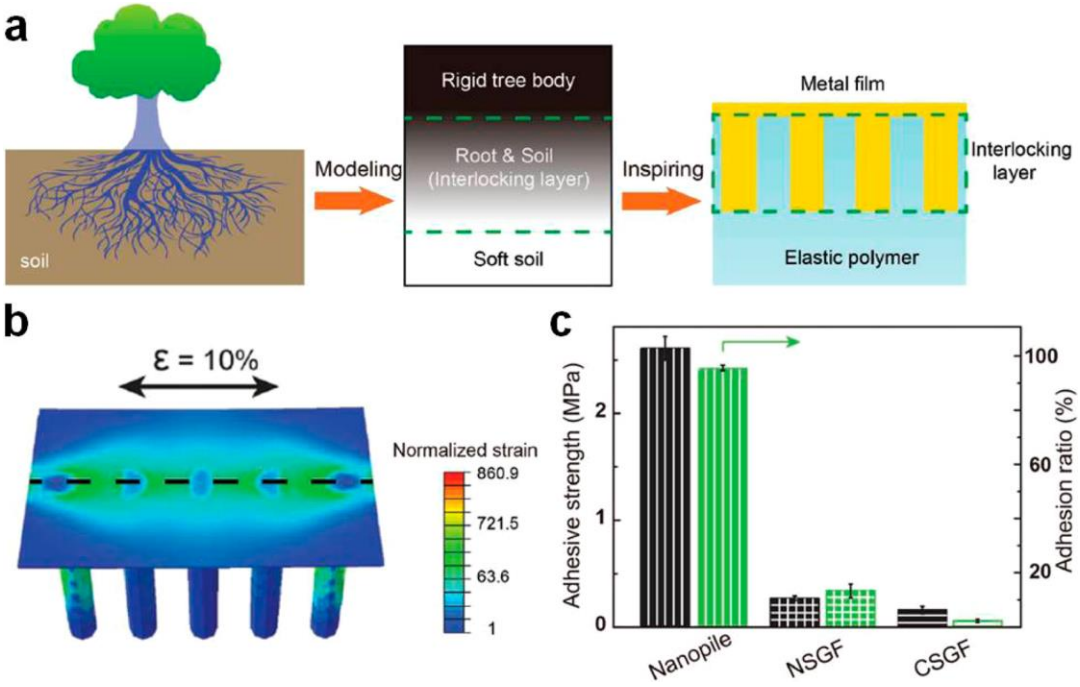

Figure 21. A flexible electrode made with a gold/PDMS composite film with strong interlayer adhesion mimicking the plants root system. (a) Illustration of the interlocking nanopile structure combining the "hard" and "soft" materials together. (b) The strain distribution in the film under FEM simulations. (c) Comparison of the adhesive strength of nanopile film to a crack-based stretchable film and a flat non-stretchable film[158],

2.6 Stretchable Electrodes Design

Flexible and conductive electrodes remain the research frontier in order to ensure the rapid advancements of functional and flexible devices. Recent researches have shifted attentions to electronics fabricated using elastic substrates, which are capable of high-degree deformation, and maintaining high electrical and mechanical performance and stability[159-161].

The conventional method to fabricate stretchable electronics is using stretchable substrates with "rigid islands" – rigid active components connected to the surrounding substrate through stretchable interconnects[162, 163]. These rigid islands protect the active components from mechanical failure while the stretchable substrate and conductors bear the strain created and ensure the electricity connections of the whole device. The major advantage of this design is the capability to integrate rigid electronic devices[164]. However, the mechanical durability is hindered as the stress concentrated at the interface of rigid-to-stretchable materials. To solve this problem, a "fully stretchable" structure where all the components are made flexible and stretchable, can accommodate deformations to a much higher extend as compared to "rigid islands" structure[165, 166]. However, materials with various functionalities, such as stretchable electrodes, dielectrics, semiconductors and sensors, are needed to make this structure workable. Apart from stretchability, electrodes also need to be transparent, and process compatible with other materials, and possess modifiable conductivity.

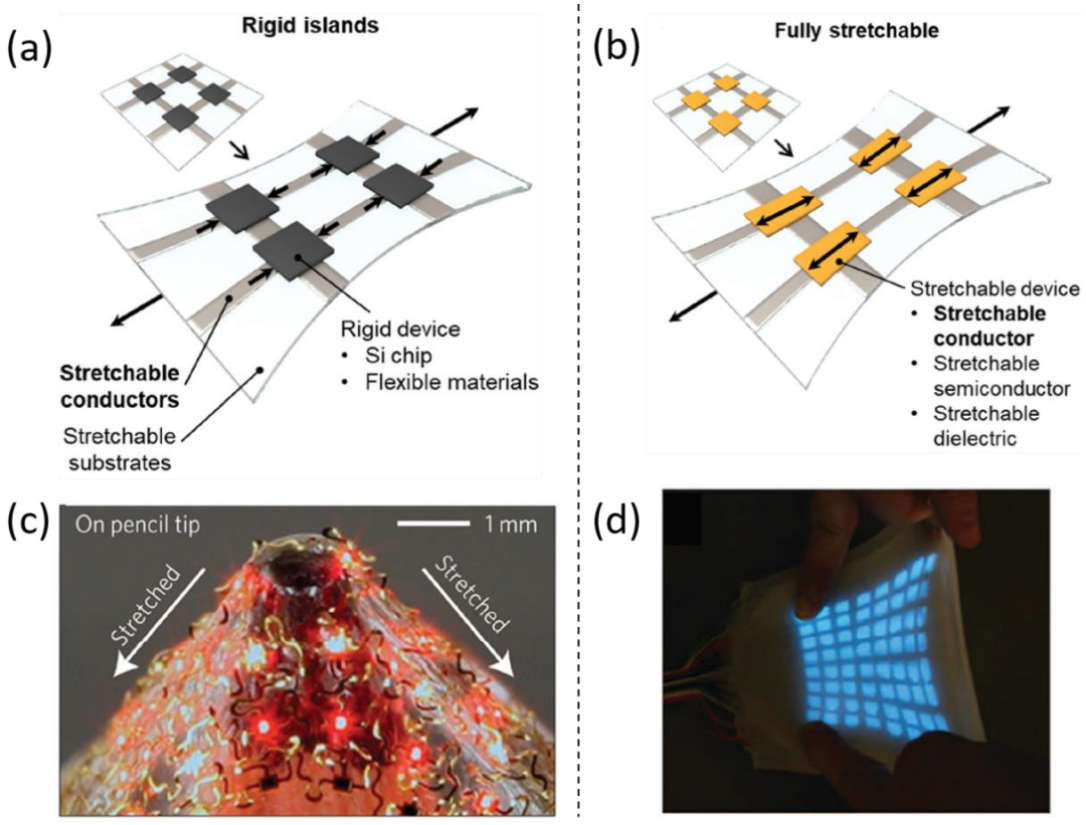

Figure 22. Stretchable electronic device designs. A schematic illustration of (a) "rigid islands" and (b) "fully stretchable" structure[167], Copyright ©The Royal Society of Chemistry 2019. Stretchable light emitting devices adapting (c) the "rigid islands"[168] and (d) "fully stretchable"[166] approaches, Copyright © 2010, Springer Nature and © 2016, American Association for the Advancement of Science, respectively.

In the following sections, the different advancements in stretchable electrode designs will be discussed.

2.6.1 Structure-based Stretchable Electrodes

To achieve stretchable interconnects, the stretchable electrode based on its structural designs is the one of the most commonly adapted methods. The different structures designed to minimize bending can obtain good conductivity and yet excellent stretchability.

2.6.1.1 Wavy structures

The wavy structure is one of the most commonly adapted templates for stretchable thin-film electrodes. This structure is obtained by deposition or coating of conductive materials onto the pre-strained elastic polymer substrates and subsequently the pre-strain is released[169], which can acquire a stretchability up to 400% without significant resistance variation[170]. After the release, a highly periodic wavy structure with distinct wavelengths and amplitudes is formed. Another strategy to generate the wavy structures is by thermal expansion. The temperature difference creates incongruity between thin metal films and elastomer substrate, yielding a stretchability ranging from 22% to 40%[171, 172]. In addition, a substrate that swells with ambient moisture and causes thin metal films such as Au and Pt to wrinkle is another method[173]. A stretchability of 50% was achieved for Ag and Pt films used. Despite the relatively easy fabrication methods, to achieve desirable stretchability on the device, considerably large wavy deformation is required, which limits the usability.

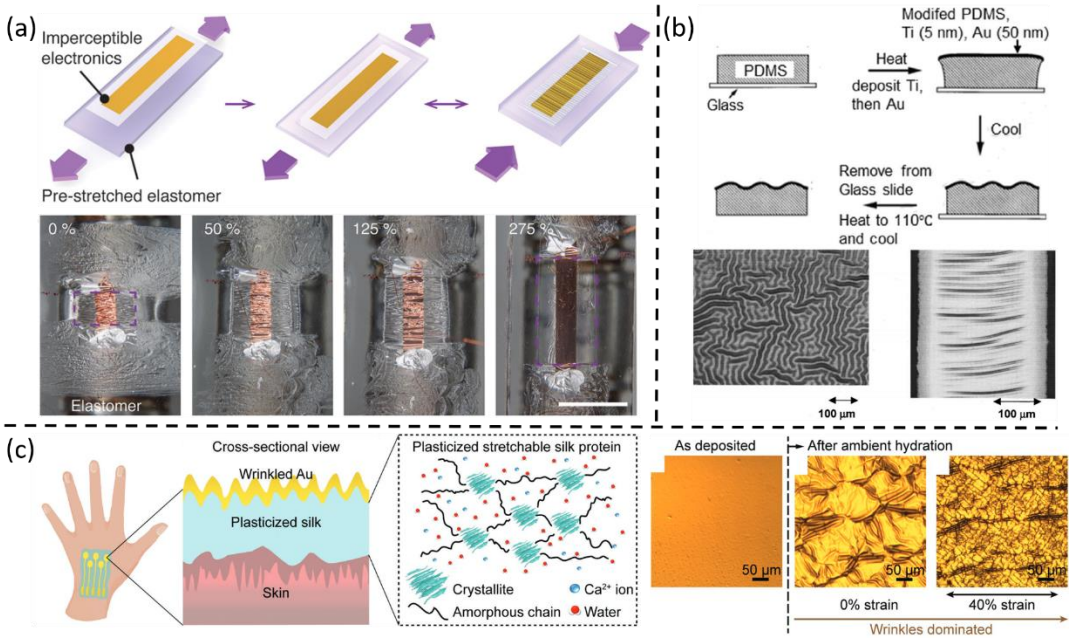

Figure 23. The wavy structure stretchable electrodes. (a) Illustration of the preparation of the electrodes by pre-strained elastomer and the image sequence showing the stretchable electrodes in different strain rate[170], Copyright © 2014 The Authors. Published by WILEY‐VCH Verlag GmbH & Co. KGaA, Weinheim. (b) Schematic preparation of metal films on PDMS via thermal expansion[172] and the optical images of the wave pattern formed[171], Copyright © 1998, Springer Nature and © 2003 American Institute of Physics, respectively. (c) A schematic of on-skin electrodes fabricated from plasticized silk protein, synthesized by substrates hydration, and optical images of Au on plasticized silk at various strain conditions[173], Copyright © 2018 WILEY‐VCH Verlag GmbH & Co. KGaA, Weinheim.

2.6.1.2 Serpentine Structures

A serpentine structure is a network of meandering metal nanowires, where its stretchability is decided by both the in-plane electrode structure and the out-of-plane structural flexibility. Upon tensile stress, the wavelengths of the structure increases while the magnitudes of the tortuous part decreases. Conversely, when the stress is removed, the wavelengths decrease and the magnitudes increase, as shown in Fig. 2.6-3(a). The excellent stretchability is a result of the macroscopic deformation of the entire structure rather than the microscopic dimensional changes in the electrode materials, and hence a very high stretchability (>1600%) can be acquired without the substrate[174]. However, most of time this superb stretchability cannot be achieved: (1) the flexibil-

ity of the whole structure is limited by the serpentine wire thickness[175]; (2) the adhesion between the wire and the substrate constrains the large deformation[176]; (3) the stiffness of substrate also hinders the stretchability of the entire structure[177].

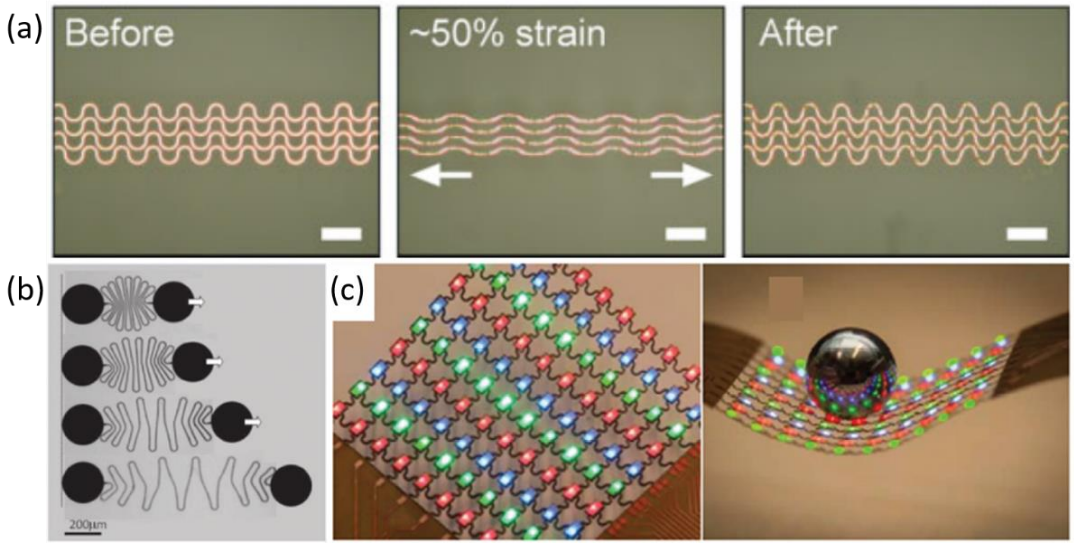

Figure 24. Serpentine structured stretchable conductors. (a) Pictures of the original and deformed serpentine structure gold nanowires[178], Copyright © 2004 WILEY‐VCH Verlag GmbH & Co. KGaA, Weinheim. (b) Photo of extendible microwire under an optical microscope[174], Copyright © 2010 WILEY‐VCH Verlag GmbH & Co. KGaA, Weinheim. (c) The 10x10 RGB LED matrix fabricated using a serpentine structure[179], Copyright © 2015 John Wiley and Sons.

2.6.1.3 Nanomesh

A mesh is a structure that is similar to a web or a net in that it has many attached or woven strands. Similar to serpentine structure, out-of-plane deformability is critical in preserving stretchability. Due to its relatively simple structure, various fabrication approaches can be used to make stretchable mesh electrodes. For instance, stretchable metal nanomesh can be formed by vacuum deposition of metals (Au, Cu, Ag, Al) onto a nanofiber mat (PVA), and transferred to various substrates by dissolving PVA with water[180-182]. The Au Nanomesh transferred on PDMS demonstrated a 50% stretchability with a high transparency (>90%) at 550 nm[181]. The advantages of high intrinsic conductivity, the low reflectance and immense apertures of Au nanomesh facilitate excellent optoelectronic properties. In addition, Au is chemically inert and hence it is ideal to be used to manufacture electrodes on skin for electromyogram

measurement. For lower strain, the reconfiguration of the mesh in the in-plane direction helps to accommodate the strain. However, when strain becomes greater, the mesh structure becomes instable and deflects out-of-plane, causing breakage of the connections of the entire structure, as shown in Fig.

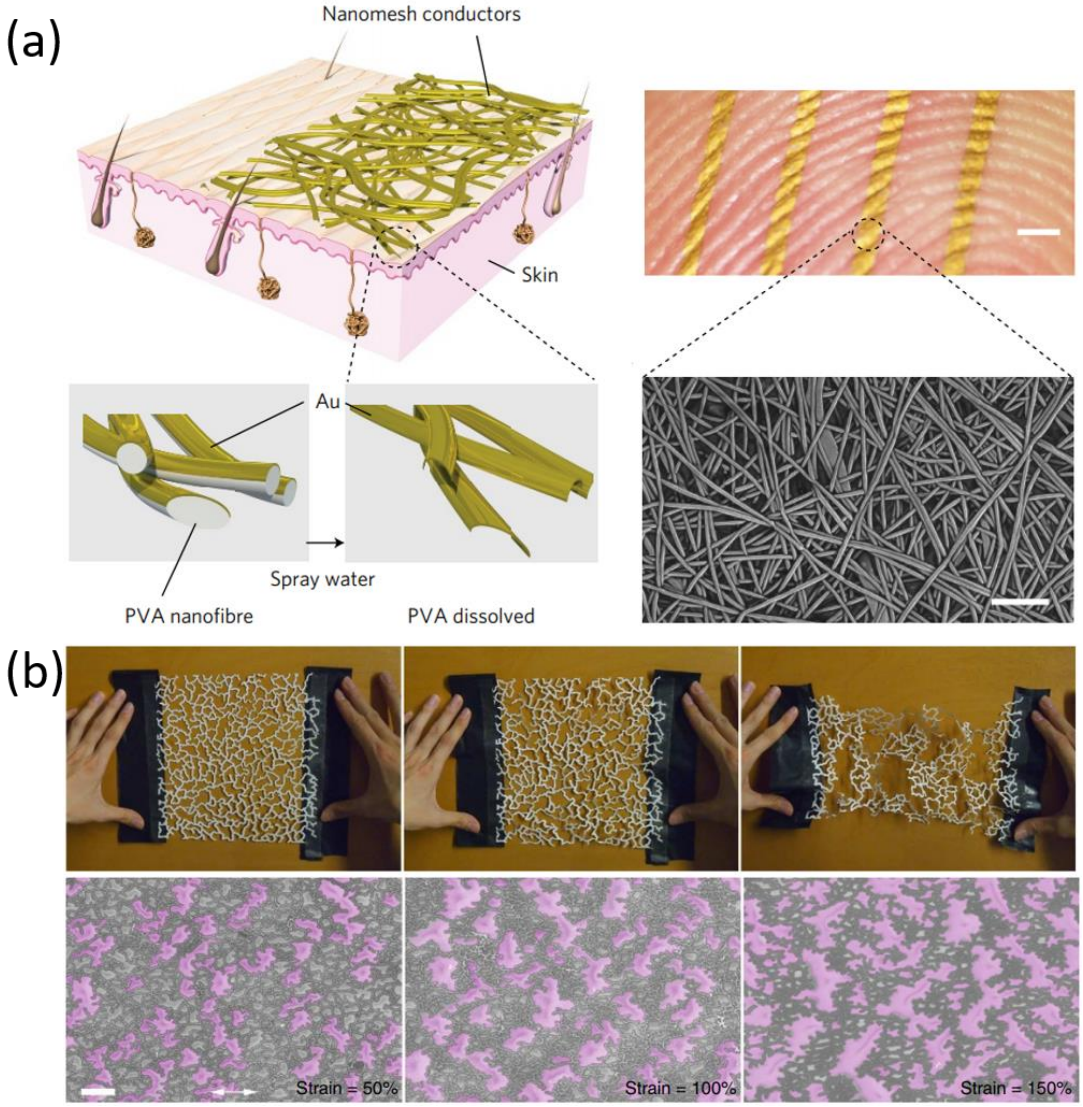

Figure 25. Nanomesh structure electrodes. (a) Schematic showing how the Au nanomesh is obtained: Au is first deposited onto electrospun PVA nanofibers, which are dissolved by water and the Au nanomesh is adhered onto the skin. The Au nanomesh on the human fingertips showed good conformability. An SEM image shows the microscopic structure of the Au nanomesh[180], Copyright © 2017, Springer Nature. (b) A paper replicate of the nanomesh experiencing strain and the SEM images of Au nanomesh/PDMS electrode under different strain conditions[183], Copyright © 2014, Springer Nature.

2.6.1.4 Microcracks

Microcracks are another structure providing stretchability to the electrodes. For instance, the flat Au thin films cannot be stretched. However, growth of Au thin film could be interrupted through vacuum depositing on elastomer substate at specific parameters, leads to numerous microcrack formations[184]. Due to the presence of these microcracks, the Au thin films showed a small initial sheet resistance (10 Ohm sq^{-1}), extremely high stretchability (4100%) and excellent cyclic strain durability (20%, 250000 cycles)[185-187]. For this structure, strain-induced crack propagation is the key in determining the performance of stretchable electrodes. Several researches focused on inhibiting crack propagation by introducing specialized micro-pattern into the substrate[158, 188, 189]. Furthermore, the surface morphology of the substrate materials and the deposition parameters of Au are two important factors in formation of microcracks[184].

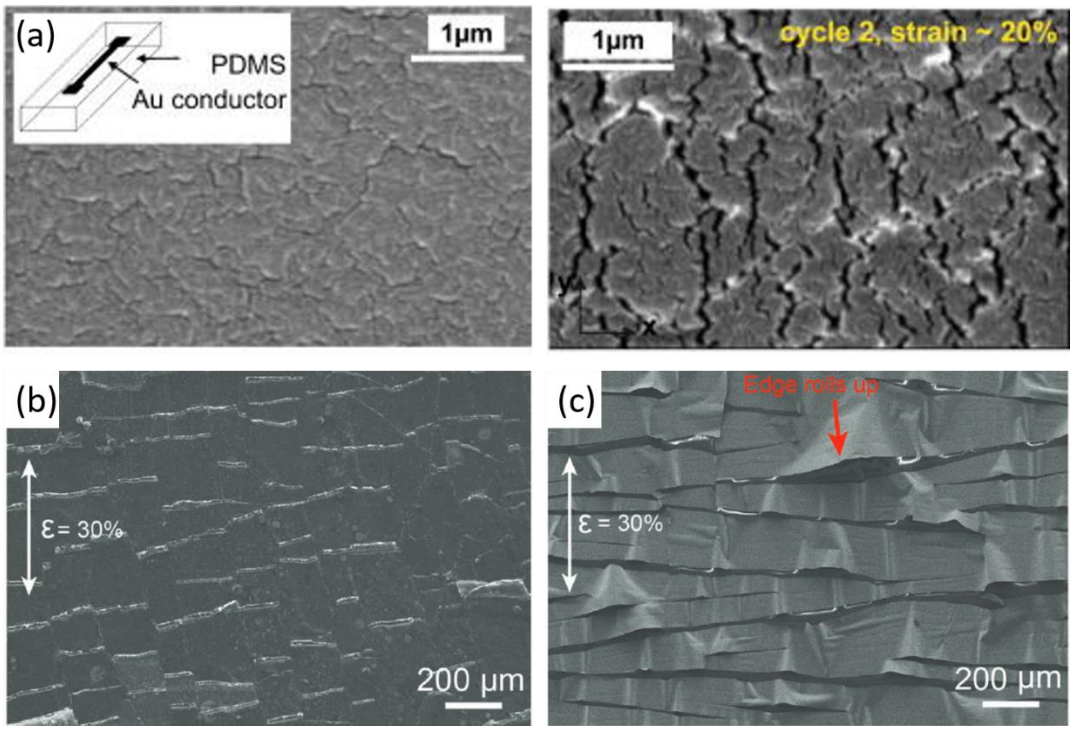

Figure 26. Microcrack based stretchable electrodes. (a) SEM images of microcrack morphology of Au thin film on PDMS with 0% and 20% strains, respectively[187], Copyright © AIP Publishing. SEM images of microstructures of the gold films (b) with and (c) without nanopiles under 30% tensile strain, respectively[158], Copyright © 2016 WILEY‐VCH Verlag GmbH & Co. KGaA, Weinheim. Due to the weak adhesion in the nostretchable film, the crack edge rolled up, but in the nanopile-enhanced film, microcracks propagation are suppressed.

2.6.2 Novel Stretchable Electrode Materials

Although structural innovations in thin film electrodes help to achieve good stretchability, these approaches also increase the process complexity (vacuum deposition, chemical etching, etc.) and wire resistance. Thus, development of conductive materials-based stretchable electrodes, which are mechanically durable and able to be industrially manufactured, is still very crucial.

2.6.2.1 Liquid Metal

A liquid metal is an alloy with very low melting points which form a eutectic that is in liquid form at ambient temperature. Liquid metals demonstrate almost infinite stretchability and high conductivity (>10^4 S cm^{-1})[190]. Initially, toxic Hg was used[191], and it was replaced with low toxicity liquid metals made of Ga-In alloy (EGaIn)[192], and Ga-In-Sn alloy (Galinstan)[193]. However, the superb stretchability also indicates the high likelihood of flowing, which post a challenge in precise patterning of liquid metals[194]. Soft fluidics filling[195], photolithography[196] and laser writing[197] are common methods to pattern liquid metals. In addition, liquid metals are commonly mixed with elastomers to achieve high mechanical toughness[198] and high thermal conductivity[199]. The liquid metal can also act as adhesive agents to connect the conducting networks of a metal-based stretchable electrodes[200].

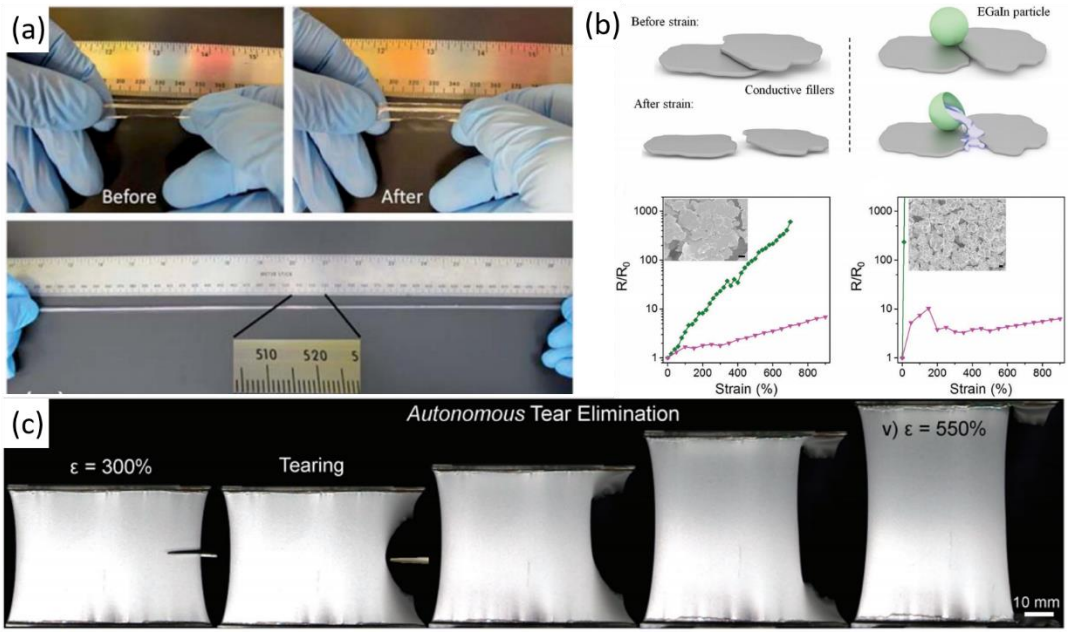

Figure 27. Liquid metals based stretchable electrodes. (a) EGain liquid metals filled into a fluidic channel made of thermoplastic elastomer gel (TPEG) subjected to a 1000% strain to demonstrate ultra-stretchability and elasticity[195], Copyright © The Royal Society of Chemistry 2013. (b) Liquid metals serve as bridges between other metal-based conductors[200], Copyright © 2018 WILEY - VCH Verlag GmbH & Co. KGaA, Weinheim. (c) The excellent tear resistance of liquid metal embedded elastomer (LFEE) is shown by creating a notch stretched to 300% strain and is totally blunted via an autonomous tear elimination mechanism[198], Copyright © 2018 WILEY - VCH Verlag GmbH & Co. KGaA, Weinheim.

2.6.2.2 Ionic Conductor

Ionic stretchable electrodes fabricated from hydrogels containing ions show remarkable high stretchability (>600%), high transparency and negligible influence on ionic conduction upon mechanical deformation[201, 202]. When interfaced with conventional electronic conductors, the ionic conductors become electrical double layer capacitors, which is difficult to be used in continuous direct current (DC) current. On the other hand, in microscale devices, these ionic conductors perform better than conventional electrical double layer capacitors and can function under alternate current (AC) conditions[201]. One major hinderance of wide applications of these ionic conductors is

the dehydration due to the addition of ionic salts[202]. Many approaches such as elastomer encapsulation[203], hygroscopic salts addition[173], nonvolatile ionic liquids incorporation[204] are investigated to solve this problem.

2.6.2.3 Conducting Polymer

Conducting polymeric electrodes are fabricated from solid molecular-level stretchable materials. As compared to ionic conductors based on hydrogels, conducting polymers have both ionic and electronic conductions[205], which decrease the interfacial resistance between electron-conducting and ion-conducting materials. Poly(2,3-dihydrothieno-1,4-dioxin)–poly(styrenesulfonate) or PEDOT:PSS in short, is a promising candidate for stretchable electrodes fabrication, due to very high conductivity[206]. However, PEDOT and PSS are intrinsically semi-crystalline, a plasticizer is required to improve the intrinsically low stretchability[207, 208]. Ionic salts are used to enhance conductivity and stretchability: by neutralizing electrostatic interactions to soften the PSS molecules, which increase the stretchability, and to increase the conductive crystalline domain of PEDOT, higher conductivity is achieved[209]. Blending with other soft polymers is another method to increase stretchability in PEDOT:PSS. Strain-induced electrical properties are introduced by microphase separation of the elastomer and PEDOT:PSS. For instance, high conductivity of 48 S cm^{-1} and stretchability of 100% was achieved by blending with polyurethane nanoparticles (PUD) dispersed in water[210]. Blending with hydrophilic and stretchable polymers (high molecular weight poly(ethylene oxide) (PEO), poly(vinyl alcohol) (PVA), etc.) generates uniform films[211, 212]. A PEO (M_n:5 000 000) blended PEDOT:PSS demonstrated a stretchability of 55% and conductivity of 356 S cm^{-1}[212]. Furthermore, polymerization of PEDOT:PSS in the form of hydrogel can significantly soften the entire network (~10-100 kPa)[213]. However, the conductivity is generally low (0.022 S cm^{-1}) due to limited PEDOT interpenetration. By intertwining the PEDOT:PSS network with a secondary polymer network, conductivity can be increased[213]. This approach

also makes tailoring the Young's modulus probable by adjusting the extent of inter-penetration and keeping conductivities greater than 0.1 S cm^{-1}.

2.6.3 Composite Stretchable Electrode

Although some novel conducting stretchable materials have been fabricated, most of the readily commercialized conductive materials are not stretchable. Hence, by layering and patterning of non-stretchable conductors and stretchable insulators, a stretchable composite electrode can be realized.

2.6.3.1 Bilayer Composites

In the bilayer composite, the conductivity comes from the percolated conducting pathway of fillers, which bridges the gap in the stretchable electrodes. One typical example of conductive fillers is single walled carbon nanotube (SWCNT), which is dispersed into polymeric solvent to form stretchable composite electrodes[214-216]. The conductivity of SWCNT networks is low, though, it still qualifies to be incorporated into capacitive sensors, resistive sensors and organic semiconductors[214, 217].

On the other hand, conductive network fabricated from silver nanowires (AgNWs), demonstrates higher conductivity. By embedding AgNWs into elastomer such as PMDS, high stretchability (~200%) and small resistance variation can be obtained[218-220]. In addition, high transparency of the electrodes can be achieved by tailoring the amount of AgNWs used, and this feature is deployed in making a stretchable light emission device[218]. A self-healable electrode fabricated from PDMS-MPU-IU polymer, which can dynamically reconstruct the embedded AgNWs network upon mechanical damage, displays good electrical conductivity[221]. Stretchable electrodes based on Cu nanowires were also reported as a cheap alternative to AgNWs[222, 223]. In addition, pre-strain methods are used to enhance stretchability (up to 460%) of the bilayer composites by creating wavy structure[224], which has been discussed in the previous section.

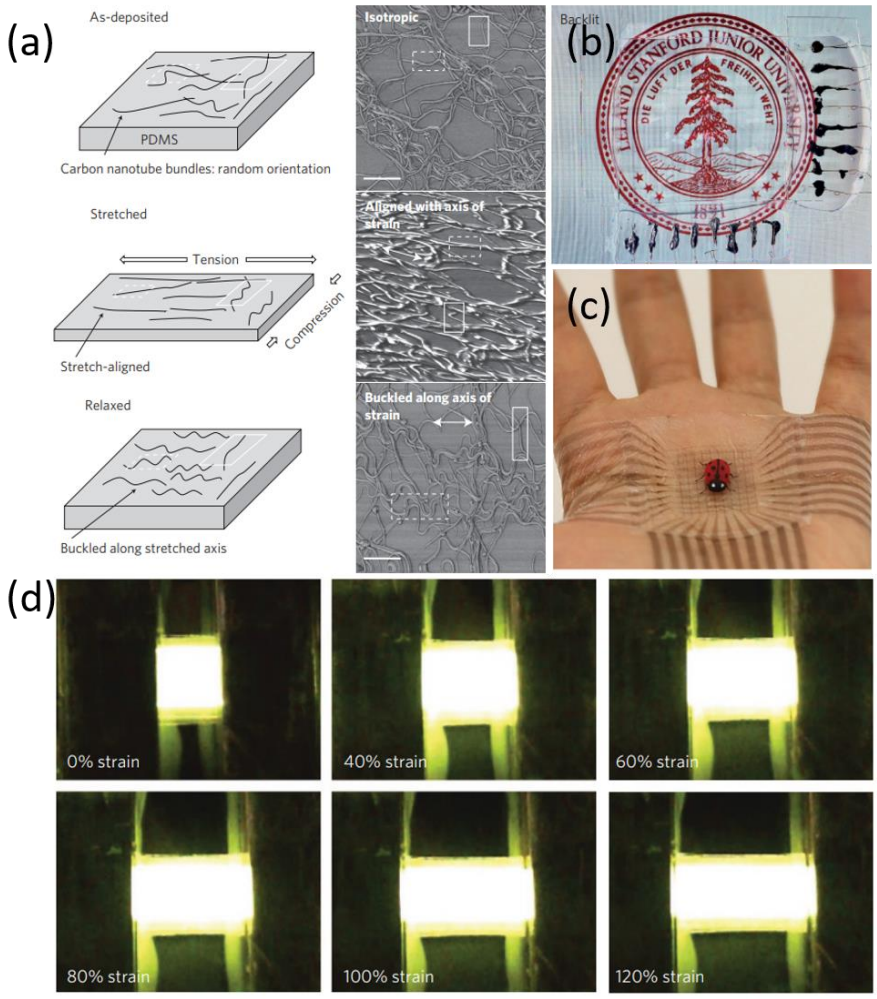

Figure 28. Nanowire based bilayer stretchable electrodes. (a) Schematics and AEM images of SWCNTs on PDMS substrates, and (b) picture of the actual device demonstrating good transparency[214], Copyright © 2011, Springer Nature. (c) The flexible SEBS -based sensing array with CNT pattern on a human palm that is conformable and able to detect location of a artificial ladybug with six conductive legs[217], Copyright © 2018, Springer Nature. (d) Images of a polymer light-emitting electrochemical cell (PLEC) based on a patterned AgNW-Polyurethane acrylate composites illuminates under different strain levels[218], Copyright © 2013, Springer Nature.

2.6.3.2 Printable Elastic Electrodes

For large area stretchable devices to be feasibly applicable, they must have low sheet resistance (<0.1 Ohm sq.$^{-}$1), high stretchability (>400%), and high processability. In addition, thicker film (>10 μm) is also important, which can be achieved by large area printing method using proper formulating of conducting fillers and stretchable

elastomers. The key in obtaining stretchability is to homogenously disperse the conductive fillers and shape them into a net structure. For instance, a printable elastic conductor consists of well distributed SWCNTs in a highly elastic fluorinated copolymer rubber is prepared using an imidazolium ion-based ionic liquid, followed by a jet-milling process[225]. The jet milling helps to distribute the SWCNTs into the elastomer matrix while maintaining the length, thus increase the percolation of conductive SWCNTs network and viscosity of composite ink. Extra process such as coating are not needed for this printable elastic conductor, and a stretchability of 118% and remarkably high conductivity of 102 S cm^{-1} were reported.

Silver-based conductive fillers such as AgNWs have shown higher conductivities than SWCNTs. For larger area flexible devices, Ag flaks are more suitable due to a better aspect ratio that enables percolation, dispersibility in different solvent matrixes and lower cost. An ink comprising of Ag flasks, fluorine rubber (P(VDF-HFP)), fluorine surfactant water solution and methylisobutylketone can achieve a conductivity of 182 S cm^{-1} at 215% strain[226]. This excellent performance was a result of the fluorine surfactant solution used, which improves the Ag flasks affinity to the polymer matrix. After printing, when the solvent evaporated, the phase separation and self-organization of Ag flakes occurred, forming a homogenous conductive pathways of Ag flakes on the rubber matrix surface. This phase separation method was also reported to fabricate a conductive pathway using Au-coated AgNWs and poly(styrene-block-butadiene-block-styrene) (SBS)[227]. Yet, low density of conductive fillers restricts the conductivity and cyclic durability due to the limited conducting pathways available.

Another filler is the metal nanoparticles (NPs), which can react upon different stimuli, such as mechanical strain[228], or electrical fields[229]. Compared with flasks and wire forms, nanoparticles have a lower percolation threshold when the size is similar to the tunneling conduction length[230, 231]. A homogenous distribution of Ag NPs was achieved via the *in situ* formation from micron-sized Ag flakes[230]. The as-synthesized Ag NPs enhanced the connective pathways that link the Ag flakes and were

able to align under strain. The resultant conductor showed a conductivity of 935 S cm^{-1} at 400% strain.

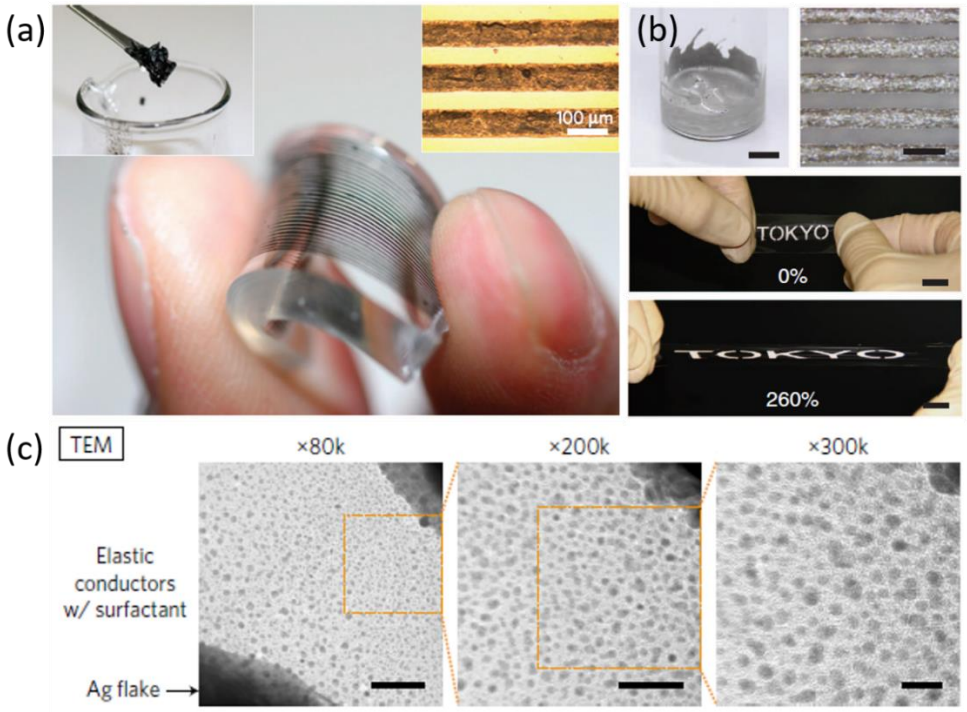

Figure 29. Printable elastic conductors based on various conductive fillers. (a) SWCNTs[225], Copyright © 2009, Springer Nature. (b) Self-organized Ag flakes[226], Copyright © 2015, Springer Nature. (c) *In situ* Ag NPs formed with Ag flakes[230], Copyright © 2017, Springer Nature.

The easy processability of printable elastic conductors have enabled many large area stretchable devices to be fabricated, such as stretchable transistor matrices based on the "rigid islands" approaches[226, 232], stretchable display[225], electronic textiles[233].

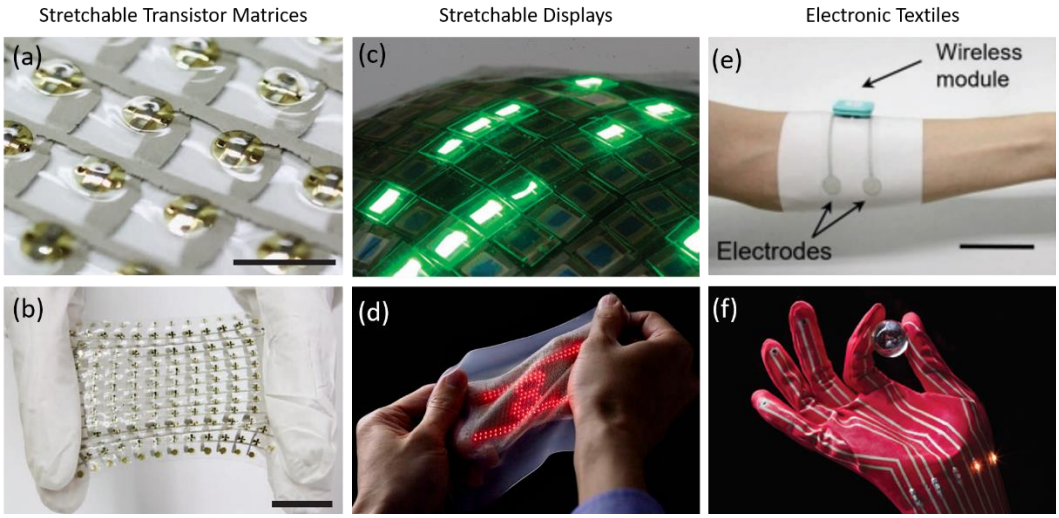

Figure 30. Large area stretchable electronics fabricated from printable elastic conductors. (a,b) Stretchable transistor matrices[226], Copyright © 2015, Springer Nature. (c,d) Stretchable displays utilizing organic LEDs[225], and micro-LEDs[234], Copyright © 2009, Springer Nature and © 2018 Takao Someya Research Group, respectively. (e) E-textiles with multipoint EMG measurement electrodes and (f) Pressure sensing e-textiles groves[230], Copyright © 2017, Springer Nature.

References

[1] C. Lee, M. Kim, Y. J. Kim, N. Hong, S. Ryu, H. J. Kim, S. Kim, International Journal of Control, Automation and Systems 2017, 15, 3.
[2] C. Majidi, Soft Robotics 2014, 1, 5.
[3] D. Rus, M. T. Tolley, Nature 2015, 521, 467.
[4] G. Robinson, J. B. C. Davies, "Continuum robots - a state of the art", presented at *Proceedings 1999 IEEE International Conference on Robotics and Automation (Cat. No.99CH36288C)*, 10-15 May 1999, 1999.
[5] M. Calisti, M. Giorelli, G. Levy, B. Mazzolai, B. Hochner, C. Laschi, P. Dario, Bioinspiration & Biomimetics 2011, 6, 036002.
[6] C. Laschi, M. Cianchetti, B. Mazzolai, L. Margheri, M. Follador, P. Dario, Advanced Robotics 2012, 26, 709.
[7] S. Seok, C. D. Onal, K. Cho, R. J. Wood, D. Rus, S. Kim, IEEE/ASME Transactions on Mechatronics 2013, 18, 1485.
[8] C. Ching-Ping, B. Hannaford, IEEE Transactions on Robotics and Automation 1996, 12, 90.
[9] M. T. Tolley, R. F. Shepherd, B. Mosadegh, K. C. Galloway, M. Wehner, M. Karpelson, R. J. Wood, G. M. Whitesides, Soft Robotics 2014, 1, 213.
[10] B. Mosadegh, P. Polygerinos, C. Keplinger, S. Wennstedt, R. F. Shepherd, U. Gupta, J. Shim, K. Bertoldi, C. J. Walsh, G. M. Whitesides, Advanced Functional Materials 2014, 24, 2163.
[11] S. A. Morin, R. F. Shepherd, S. W. Kwok, A. A. Stokes, A. Nemiroski, G. M. Whitesides, Science 2012, 337, 828.

[12] W. McMahan, V. Chitrakaran, M. Csencsits, D. Dawson, I. D. Walker, B. A. Jones, M. Pritts, D. Dienno, M. Grissom, C. D. Rahn, "Field trials and testing of the OctArm continuum manipulator", presented at *Proceedings 2006 IEEE International Conference on Robotics and Automation, 2006. ICRA 2006.*, 15-19 May 2006, 2006.
[13] R. Deimel, O. Brock, The International Journal of Robotics Research 2015, 35, 161.
[14] F. Ilievski, A. D. Mazzeo, R. F. Shepherd, X. Chen, G. M. Whitesides, Angewandte Chemie International Edition 2011, 50, 1890.
[15] S. Sanan, P. S. Lynn, S. T. Griffith, Journal of Mechanisms and Robotics 2014, 6.
[16] S. T. Kwang j. Kim, *Electroactive Polymers for Robotic Applications: Artificial Muscles and Sensors*, Springer-Verlag London, 2007.
[17] E. N. Gama Melo, O. F. Aviles Sanchez, D. Amaya Hurtado, Ingenier á y Desarrollo 2014, 32, 279.
[18] Y. Bar-Cohen, Proceedings of SPIE - The International Society for Optical Engineering 2004.
[19] K. Ogawa, Y. Nakabo, T. Mukai, K. Asaka, N. Ohnishi, Transactions of the Society of Instrument and Control Engineers 2006, 42, 80.
[20] G. Shuxiang, T. Fukuda, K. Asaka, IEEE/ASME Transactions on Mechatronics 2003, 8, 136.
[21] M. Mojarrad, M. Shahinpoor, "Biomimetic robotic propulsion using polymeric artificial muscles", presented at *Proceedings of International Conference on Robotics and Automation*, 25-25 April 1997, 1997.
[22] Y. Nakabo, T. Mukai, K. Asaka, "Kinematic Modeling and Visual Sensing of Multi-DOF Robot Manipulator with Patterned Artificial Muscle", presented at *Proceedings of the 2005 IEEE International Conference on Robotics and Automation*, 18-22 April 2005, 2005.
[23] C. D. Onal, D. Rus, Bioinspiration & Biomimetics 2013, 8, 026003.
[24] E. Steltz, A. Mozeika, N. Rodenberg, E. Brown, H. M. Jaeger, "JSEL: Jamming Skin Enabled Locomotion", presented at *2009 IEEE/RSJ International Conference on Intelligent Robots and Systems*, 10-15 Oct. 2009, 2009.
[25] K. Suzumori, S. Endo, T. Kanda, N. Kato, H. Suzuki, "A Bending Pneumatic Rubber Actuator Realizing Soft-bodied Manta Swimming Robot", presented at *Proceedings 2007 IEEE International Conference on Robotics and Automation*, 10-14 April 2007, 2007.
[26] Y. Zheng, X. Ding, C. C. Y. Poon, B. P. L. Lo, H. Zhang, X. Zhou, G. Yang, N. Zhao, Y. Zhang, IEEE Transactions on Biomedical Engineering 2014, 61, 1538.
[27] R. F. Shepherd, F. Ilievski, W. Choi, S. A. Morin, A. A. Stokes, A. D. Mazzeo, X. Chen, M. Wang, G. M. Whitesides, Proceedings of the National Academy of Sciences 2011, 108, 20400.
[28] H.-T. Lin, G. G. Leisk, B. Trimmer, Bioinspiration & Biomimetics 2011, 6, 026007.
[29] M. Cianchetti, A. Arienti, M. Follador, B. Mazzolai, P. Dario, C. Laschi, Materials Science and Engineering: C 2011, 31, 1230.
[30] D. Ratna, J. Karger-Kocsis, Journal of Materials Science 2008, 43, 254.
[31] C. Liu, H. Qin, P. T. Mather, Journal of Materials Chemistry 2007, 17, 1543.
[32] A. Lendlein, S. Kelch, Angewandte Chemie International Edition 2002, 41, 2034.
[33] G. M. Whitesides, Interface Focus 2015, 5, 20150031.
[34] M. Stevens, S. Merilaita, Philosophical Transactions of the Royal Society B: Biological Sciences 2009, 364, 423.
[35] V. M. Shalaev, W. Cai, U. K. Chettiar, H.-K. Yuan, A. K. Sarychev, V. P. Drachev, A. V. Kildishev, Opt. Lett. 2005, 30, 3356.
[36] U. Leonhardt, Nature Materials 2009, 8, 537.
[37] M. H. Dickinson, C. T. Farley, R. J. Full, M. A. R. Koehl, R. Kram, S. Lehman, Science 2000, 288, 100.

[38] *Handbook of the Marine Fauna of North-West Europe*, Oxford University Press, Oxford 2017.
[39] A. Joseph, in *Investigating Seafloors and Oceans*, (Ed: A. Joseph), Elsevier, 2017, 493.
[40] R. Villanueva, V. Perricone, G. Fiorito, Front Physiol 2017, 8, 598.
[41] W. M. KIER, K. K. SMITH, Zoological Journal of the Linnean Society 1985, 83, 307.
[42] G. D. Weymouth, V. Subramaniam, M. S. Triantafyllou, Bioinspiration & Biomimetics 2015, 10, 016016.
[43] L. M. Mäthger, R. T. Hanlon, Cell and Tissue Research 2007, 329, 179.
[44] Z. Chen, T. Um, J. Zhu, H. Bart-Smith, ASME 2011 International Mechanical Engineering Congress and Exposition, IMECE 2011 2011, 2.
[45] F. ØDegaard, Biological Journal of the Linnean Society 2000, 71, 583.
[46] Q. Pei, R. Pelrine, S. Stanford, R. Kornbluh, M. Rosenthal, Synthetic Metals 2003, 135-136, 129.
[47] D. Silvera-Tawil, D. Rye, M. Velonaki, Robotics and Autonomous Systems 2015, 63, 230.
[48] E. Walters, P. Illich, J. Weeks, M. Lewin, Journal of Experimental Biology 2001, 204, 457.
[49] N. Taro, I. Tomohide, "Locomotion strategy for a peristaltic crawling robot in a 2-dimensional space", presented at *2008 IEEE International Conference on Robotics and Automation*, 19-23 May 2008, 2008.
[50] N. Saga, T. Nakamura, Smart Materials and Structures 2004, 13, 566.
[51] W. Wang, J.-Y. Lee, H. Rodrigue, S.-H. Song, W.-S. Chu, S.-H. Ahn, Bioinspiration & Biomimetics 2014, 9, 046006.
[52] S. Legg, M. Hutter, Advances in Artificial General Intelligence: Concepts, Architectures and Algorithms 2007, 157.
[53] J. M. McNamara, A. I. Houston, Nature 1996, 380, 215.
[54] T. Trewavas, BioScience 2016, 66, 542.
[55] M. Gersani, J. Brown, E. O'Brien, G. Maina, Z. Abramsky, Journal of Ecology 2001, 89, 660.
[56] O. Falik, Y. Mordoch, L. Quansah, A. Fait, A. Novoplansky, PLOS ONE 2011, 6, e23625.
[57] N. Dudareva, F. Negre, D. Nagegowda, I. Orlova, Critical Reviews in Plant Sciences 2006, 25, 417
[58] J. Holopainen, J. Blande, Advances in experimental medicine and biology 2012, 739, 17.
[59] Y. Kikuta, H. Ueda, K. Nakayama, Y. Katsuda, R. Ozawa, J. Takabayashi, A. Hatanaka, K. Matsuda, Plant & cell physiology 2011, 52, 588.
[60] R. Karban, K. Shiojiri, S. Ishizaki, W. Wetzel, R. Evans, Proceedings. Biological sciences / The Royal Society 2013, 280, 20123062.
[61] E. Sani, P. Herzyk, G. Perrella, V. Colot, A. Amtmann, Genome biology 2013, 14, R59.
[62] Y. Ding, M. Fromm, Z. Avramova, Nature communications 2012, 3, 740.
[63] R. C. Ackerson, Plant Physiology 1980, 65, 455.
[64] A. Volkov, D. Collins, J. Mwesigwa, Plant Science 2000, 153, 185.
[65] T. Shvetsova, J. Mwesigwa, A. Labady, S. Kelly, D. J. Thomas, K. Lewis, A. Volkov, Plant Science - PLANT SCI 2002, 162, 723.
[66] A. Volkov, T. Dunkley, S. Morgan, D. Ruff, Y. Boyce, A. Labady, Bioelectrochemistry (Amsterdam, Netherlands) 2004, 63, 91.
[67] A. van Bel, K. Ehlers, 2007, 263.
[68] K. U, Ann Rep Biol Works, Fac Sci, Osaka Univ 1968, 16, 61.

[69] J. Fromm, in *Plant Electrophysiology: Theory and Methods*, (Ed: A. G. Volkov), Springer Berlin Heidelberg, Berlin, Heidelberg 2006, 269.
[70] C. Darwin, London: John Murray. 1875.
[71] P. Simons, *The Action Plant: Movement and Nervous Behaviour in Plants*, Blackwell, 1992.
[72] T. Zawadzki, E. Davies, H. Dziubinska, K. Trębacz, Physiologia Plantarum 2006, 83, 601.
[73] R. M. Spanswick, J. W. F. Costerton, Journal of Cell Science 1967, 2, 451.
[74] R. M. Spanswick, Planta 1972, 102, 215.
[75] A. J. E. van Bel, H. V. M. van Rijen, Planta 1994, 192, 165.
[76] R. F. Evert, W. Eschrich, S. E. Eichhorn, Planta 1972, 109, 193.
[77] E. Sukhova, E. Akinchits, V. Sukhov, The Journal of Membrane Biology 2017, 250, 407.
[78] J. Fromm, W. Eschrich, Trees 1988, 2, 7.
[79] A. G. Volkov, T. Adesina, E. Jovanov, Bioelectrochemistry 2008, 74, 16.
[80] M. R. Sussman, Science 1992, 256, 619.
[81] E. Davies, in *Plant Electrophysiology: Theory and Methods*, (Ed: A. G. Volkov), Springer Berlin Heidelberg, Berlin, Heidelberg 2006, 407.
[82] R. Stahlberg, R. E. Cleland, E. Van Volkenburgh, in *Communication in Plants: Neuronal Aspects of Plant Life*, (Eds: F. Baluška, S. Mancuso, D. Volkmann), Springer Berlin Heidelberg, Berlin, Heidelberg 2006, 291.
[83] R. Stahlberg, D. J. Cosgrove, Plant, Cell & Environment 1994, 17, 1143.
[84] R. Stahlberg, D. J. Cosgrove, Planta 1992, 187, 523.
[85] A. G. Volkov, L. O'Neal, M. I. Volkova, V. S. Markin, Journal of Plant Physiology 2013, 170, 1317.
[86] S. Mancuso, Australian journal of plant physiology 1999, 26.
[87] M. Malone, J. J. Alarcon, L. Palumbo, Planta 1994, 193, 181.
[88] T. Sibaoka, Annual Review of Plant Physiology 1969, 20, 165.
[89] S. E. Williams, B. G. Pickard, Planta 1972, 103, 193.
[90] D. Hodick, A. Sievers, Planta 1988, 174, 8.
[91] M. Filek, J. Kościelniak, Plant Science 1997, 123, 39.
[92] A. M. Sinyukhin, E. A. Britikov, Nature 1967, 215, 1278.
[93] C. Koziolek, T. E. E. Grams, U. Schreiber, R. Matyssek, J. Fromm, New Phytologist 2004, 161, 715.
[94] J. Fromm, H. Fei, Plant Science 1998, 132, 203.
[95] J. Fromm, T. Bauer, Journal of Experimental Botany 1994, 45, 463.
[96] E. McCormack, L. Velasquez, N. A. Delk, J. Braam, in *Communication in Plants: Neuronal Aspects of Plant Life*, (Eds: F. Baluška, S. Mancuso, D. Volkmann), Springer Berlin Heidelberg, Berlin, Heidelberg 2006, 249.
[97] T. Shiina, M. Tazawa, Plant and Cell Physiology 1986, 27, 1081.
[98] A. G. VOLKOV, J. C. FOSTER, T. A. ASHBY, R. K. WALKER, J. A. JOHNSON, V. S. MARKIN, Plant, Cell & Environment 2010, 33, 163.
[99] J. Fromm, R. Spanswick, Journal of Experimental Botany 1993, 44, 1119.
[100] S. A. R. Mousavi, C. T. Nguyen, E. E. Farmer, S. Kellenberger, Nature Protocols 2014, 9, 1997.
[101] R. Beutner, Klinische Wochenschrift 1922, 1, 2535.
[102] B. J, 1912.
[103] D. Pletcher, in *Microelectrodes: Theory and Applications*, (Eds: M. I. Montenegro, M. A. Queirós, J. L. Daschbach), Springer Netherlands, Dordrecht 1991, 3.
[104] S. C. Brooks, S. Gelfan, Protoplasma 1928, 5, 86.
[105] A. L. Hodgkin, B. Katz, J Physiol 1949, 108, 37.

[106] J. FROMM, S. LAUTNER, Plant, Cell & Environment 2007, 30, 249.
[107] G. Roblin, Biological Reviews 1979, 54, 135.
[108] J. C. Bose, *Life Movements in Plants*, Anmol, 1993.
[109] T. Abe, The botanical magazine = Shokubutsu-gaku-zasshi 1981, 94, 379.
[110] G. Roblin, P. Fleurat-Lessard, Planta 1987, 170, 242.
[111] P. Fleurat-Lessard, S. Bouche-Pillon, C. Leloup, J. Bonnemain, Plant physiology 1997, 113, 747.
[112] Y. Temmei, S. Uchida, D. Hoshino, N. Kanzawa, M. Kuwahara, S. Sasaki, T. Tsuchiya, FEBS letters 2005, 579, 4417.
[113] H. Yao, Q. Xu, M. Yuan, Plant Signal Behav 2008, 3, 954.
[114] R. U, Nuovo Giornale Botanico
Italiano Nuovo Serie 1916, 51.
[115] R. L. Satter, H. L. Gorton, T. C. Vogelmann, 1990, v. 3.
[116] P. Wojtaszek, Ann Bot 2003, 92, 166.
[117] T. Tamiya, T. Miyazaki, H. Ishikawa, N. Iriguchi, T. Maki, J. J. Matsumoto, T. Tsuchiya, The Journal of Biochemistry 1988, 104, 5.
[118] A. G. Volkov, J. C. Foster, K. D. Baker, V. S. Markin, Plant Signal Behav 2010, 5, 1211.
[119] A. G. Volkov, *Plant Electrophysiology: Signaling and Responses*, Springer Berlin Heidelberg, 2012.
[120] A. Volkov, H. Carrell, V. Markin, Plant physiology 2009, 149, 1661.
[121] P. Ball, Nature 2001, 409, 413.
[122] D. Ahmed, "HYBRIDIZATION OF SMART TEXTILES IN MEDICAL AND HEALTHCARE MANAGEMENT", presented at *AUTEX 2009 World Textile Conference* İzmir, Turkey, 2009.
[123] M. Sarikaya, Proceedings of the National Academy of Sciences of the United States of America 1999, 96, 14183.
[124] E. Reyssat, L. Mahadevan, J R Soc Interface 2009, 6, 951.
[125] Z. Guo, W. Liu, Plant Science 2007, 172, 1103.
[126] G. Y. Bae, J. Jang, Y. G. Jeong, W. S. Lyoo, B. G. Min, Journal of Colloid and Interface Science 2010, 344, 584.
[127] A. V. Singh, A. Rahman, N. V. G. Sudhir Kumar, A. S. Aditi, M. Galluzzi, S. Bovio, S. Barozzi, E. Montani, D. Parazzoli, Materials & Design (1980-2015) 2012, 36, 829.
[128] C. Dawson, J. F. V. Vincent, A.-M. Rocca, Nature 1997, 390, 668.
[129] J. Huber, N. Fleck, M. Ashby, Proceedings of The Royal Society A: Mathematical, Physical and Engineering Sciences 1997, 453, 2185.
[130] A. Volkov, S. Harris, C. Vilfranc, V. Murphy, J. Wooten, H. Paulicin, M. Volkova, V. Markin, Journal of plant physiology 2012, 170.
[131] V. B. Sundaresan, H. Tan, D. Leo, *Investigation on High Energy Density Materials Utilizing Biological Transport Mechanisms*, Vol. 69, 2004.
[132] L. Matthews, V. B. Sundaresan, V. Giurgiutiu, D. Leo, Journal of Materials Research - J MATER RES 2006, 21, 2058.
[133] V. B. Sundaresan, D. Leo, Smart Materials and Structures 2007, 16, S207.
[134] E. Sinibaldi, G. Puleo, F. Mattioli, V. Mattoli, F. Michele, L. Beccai, F. Tramacere, S. Mancuso, B. Mazzolai, Bioinspiration & biomimetics 2013, 8, 025002.
[135] B. R. Bruhn, T. B. H. Schroeder, S. Li, Y. N. Billeh, K. W. Wang, M. Mayer, PLOS ONE 2014, 9, e91350.
[136] A. Cadino, S. Fréour, F. Jacquemin, P. Casari, Front Chem 2014, 1, 43.
[137] J. Wang, Z. Chen, M. Mauk, K.-S. Hong, M. Li, S. Yang, H. H. Bau, Biomedical Microdevices 2005, 7, 313.

[138] N. Bassik, A. Brafman, A. M. Zarafshar, M. Jamal, D. Luvsanjav, F. M. Selaru, D. H. Gracias, Journal of the American Chemical Society 2010, 132, 16314.
[139] E. Smela, O. Inganäs, I. Lundström, Science 1995, 268, 1735.
[140] X. Zhang, C. L. Pint, M. H. Lee, B. E. Schubert, A. Jamshidi, K. Takei, H. Ko, A. Gillies, R. Bardhan, J. J. Urban, M. Wu, R. Fearing, A. Javey, Nano Letters 2011, 11, 3239.
[141] E. Reyssat, L. Mahadevan, Journal of the Royal Society, Interface / the Royal Society 2009, 6, 951.
[142] Z. L. Wu, M. Moshe, J. Greener, H. Therien-Aubin, Z. Nie, E. Sharon, E. Kumacheva, Nature Communications 2013, 4, 1586.
[143] A. Le Duigou, M. Castro, Industrial Crops and Products 2015, 71, 1.
[144] S. Armon, H. Aharoni, M. Moshe, E. Sharon, Soft Matter 2014, 10, 2733.
[145] A. Menges, S. Reichert, Architectural Design 2012, 82.
[146] A. Holstov, B. Bridgens, G. Farmer, Construction and Building Materials 2015, 98, 570.
[147] Y. Liu, K. He, G. Chen, W. R. Leow, X. Chen, Chemical Reviews 2017, 117, 12893.
[148] A. M. Hussain, M. M. Hussain, Advanced Materials 2016, 28, 4219.
[149] D. Lipomi, Advanced materials (Deerfield Beach, Fla.) 2015, 28.
[150] D.-H. Kim, N. Lu, Y. Huang, J. A. Rogers, MRS Bulletin 2012, 37, 226.
[151] P. Fratzl, F. G. Barth, Nature 2009, 462, 442.
[152] B. Su, S. Gong, Z. Ma, L. W. Yap, W. Cheng, Small 2015, 11, 1886.
[153] Y. Wei, S. Chen, Y. Lin, Z. Yang, L. Liu, Journal of Materials Chemistry C 2015, 3, 9594.
[154] S. Kang, J. Lee, S. Lee, S. Kim, J.-K. Kim, H. Algadi, S. Al-Sayari, D.-E. Kim, D. Kim, T. Lee, Advanced Electronic Materials 2016, 2, 1600356.
[155] H. Guo, J. Tang, M. Zhao, W. Zhang, J. Yang, B. Zhang, X. Chou, J. Liu, C. Xue, W. Zhang, Nanoscale Research Letters 2016, 11, 112.
[156] C. F. Guo, Y. Chen, L. Tang, F. Wang, Z. Ren, Nano Letters 2016, 16, 594.
[157] T. Li, Z. Suo, International Journal of Solids and Structures 2007, 44, 1696.
[158] Z. Liu, X. Wang, D. Qi, C. Xu, J. Yu, Y. Liu, Y. Jiang, B. Liedberg, X. Chen, Advanced Materials 2017, 29, 1603382.
[159] M. Kaltenbrunner, T. Sekitani, J. Reeder, T. Yokota, K. Kuribara, T. Tokuhara, M. Drack, R. Schwödiauer, I. Graz, S. Bauer-Gogonea, S. Bauer, T. Someya, Nature 2013, 499, 458.
[160] J. van den Brand, M. de Kok, M. Koetse, M. Cauwe, R. Verplancke, F. Bossuyt, M. Jablonski, J. Vanfleteren, Solid-State Electronics 2015, 113, 116.
[161] D. J. Lipomi, B. C. K. Tee, M. Vosgueritchian, Z. Bao, Advanced Materials 2011, 23, 1771.
[162] J. Xu, S. Wang, G.-J. N. Wang, C. Zhu, S. Luo, L. Jin, X. Gu, S. Chen, V. R. Feig, J. W. F. To, S. Rondeau-Gagné, J. Park, B. C. Schroeder, C. Lu, J. Y. Oh, Y. Wang, Y.-H. Kim, H. Yan, R. Sinclair, D. Zhou, G. Xue, B. Murmann, C. Linder, W. Cai, J. B.-H. Tok, J. W. Chung, Z. Bao, Science 2017, 355, 59.
[163] S. Wagner, H. Gleskova, I. C. Cheng, J. Sturm, Z. Suo, 2005, 263.
[164] S. Xu, Y. Zhang, L. Jia, K. E. Mathewson, K.-I. Jang, J. Kim, H. Fu, X. Huang, P. Chava, R. Wang, S. Bhole, L. Wang, Y. J. Na, Y. Guan, M. Flavin, Z. Han, Y. Huang, J. A. Rogers, Science 2014, 344, 70.
[165] A. Chortos, G. I. Koleilat, R. Pfattner, D. Kong, P. Lin, R. Nur, T. Lei, H. Wang, N. Liu, Y.-C. Lai, M.-G. Kim, J. W. Chung, S. Lee, Z. Bao, Advanced Materials 2016, 28, 4441.
[166] C. Larson, B. Peele, S. Li, S. Robinson, M. Totaro, L. Beccai, B. Mazzolai, R. Shepherd, Science 2016, 351, 1071.
[167] N. Matsuhisa, X. Chen, Z. Bao, T. Someya, Chemical Society Reviews 2019, 48.

[168] R.-H. Kim, D.-H. Kim, J. Xiao, B. H. Kim, S.-I. Park, B. Panilaitis, R. Ghaffari, J. Yao, M. Li, Z. Liu, V. Malyarchuk, D. G. Kim, A.-P. Le, R. G. Nuzzo, D. L. Kaplan, F. G. Omenetto, Y. Huang, Z. Kang, J. A. Rogers, Nature Materials 2010, 9, 929.
[169] W. M. Choi, J. Song, D.-Y. Khang, H. Jiang, Y. Y. Huang, J. A. Rogers, Nano Letters 2007, 7, 1655.
[170] M. Drack, I. Graz, T. Sekitani, T. Someya, M. Kaltenbrunner, S. Bauer, Advanced Materials 2015, 27, 34.
[171] S. P. Lacour, S. Wagner, Z. Huang, Z. Suo, Applied Physics Letters 2003, 82, 2404.
[172] N. Bowden, S. Brittain, A. G. Evans, J. W. Hutchinson, G. M. Whitesides, Nature 1998, 393, 146.
[173] G. Chen, N. Matsuhisa, Z. Liu, D. Qi, P. Cai, Y. Jiang, C. Wan, Y. Cui, W. R. Leow, Z. Liu, S. Gong, K.-Q. Zhang, Y. Cheng, X. Chen, Advanced Materials 2018, 30, 1800129.
[174] G. Lanzara, N. Salowitz, Z. Guo, F.-K. Chang, Advanced Materials 2010, 22, 4643.
[175] Y. Zhang, S. Wang, X. Li, J. A. Fan, S. Xu, Y. M. Song, K.-J. Choi, W.-H. Yeo, W. Lee, S. N. Nazaar, B. Lu, L. Yin, K.-C. Hwang, J. A. Rogers, Y. Huang, Advanced Functional Materials 2014, 24, 2028.
[176] D.-H. Kim, Z. Liu, Y.-S. Kim, J. Wu, J. Song, H.-S. Kim, Y. Huang, K.-c. Hwang, Y. Zhang, J. A. Rogers, Small 2009, 5, 2841.
[177] S. Yang, B. Su, G. Bitar, N. Lu, International Journal of Fracture 2014, 190, 99.
[178] D. S. Gray, J. Tien, C. S. Chen, Advanced Materials 2004, 16, 393.
[179] H. Ohmae, Y. Tomita, M. Kasahara, J. Schram, E. Smits, J. van den Brand, F. Bossuyt, J. Vanfleteren, J. De Baets, SID Symposium Digest of Technical Papers 2015, 46, 102.
[180] A. Miyamoto, S. Lee, N. F. Cooray, S. Lee, M. Mori, N. Matsuhisa, H. Jin, L. Yoda, T. Yokota, A. Itoh, M. Sekino, H. Kawasaki, T. Ebihara, M. Amagai, T. Someya, Nature Nanotechnology 2017, 12, 907.
[181] H. Wu, D. Kong, Z. Ruan, P.-C. Hsu, S. Wang, Z. Yu, T. J. Carney, L. Hu, S. Fan, Y. Cui, Nature Nanotechnology 2013, 8, 421.
[182] K. J. Seo, X. Han, Y. Qiang, X. Zhao, Y. Zhong, Z. Shi, H. Fang, Applied Physics Letters 2018, 112, 263101.
[183] C. F. Guo, T. Sun, Q. Liu, Z. Suo, Z. Ren, Nature Communications 2014, 5, 3121.
[184] O. Graudejus, P. Görrn, S. Wagner, ACS Applied Materials & Interfaces 2010, 2, 1927.
[185] I. M. Graz, D. P. J. Cotton, S. P. Lacour, Applied Physics Letters 2009, 94, 071902.
[186] S. P. Lacour, J. Jones, S. Wagner, L. Teng, S. Zhigang, Proceedings of the IEEE 2005, 93, 1459.
[187] S. P. Lacour, D. Chan, S. Wagner, T. Li, Z. Suo, E. Division of, H. U. C. M. Applied Sciences, Applied Physics Letters 2006, 88.
[188] H. Vandeparre, Q. Liu, I. R. Minev, Z. Suo, S. P. Lacour, Advanced materials (Deerfield Beach, Fla.) 2013, 25, 3117.
[189] V. Venugopalan, R. Lamboll, D. Joshi, K. S. Narayan, ACS Applied Materials & Interfaces 2017, 9, 28010.
[190] M. D. Dickey, Advanced Materials 2017, 29, 1606425.
[191] H. E. Holling, H. C. Boland, E. Russ, American Heart Journal 1961, 62, 194.
[192] S. J. French, D. J. Saunders, G. W. Ingle, The Journal of Physical Chemistry 1938, 42, 265.
[193] P. Surmann, H. Zeyat, Analytical and Bioanalytical Chemistry 2005, 383, 1009.
[194] I. D. Joshipura, H. R. Ayers, C. Majidi, M. D. Dickey, Journal of Materials Chemistry C 2015, 3, 3834.
[195] K. P. Mineart, Y. Lin, S. C. Desai, A. S. Krishnan, R. J. Spontak, M. D. Dickey, Soft Matter 2013, 9, 7695.

[196] C. W. Park, Y. G. Moon, H. Seong, S. W. Jung, J.-Y. Oh, B. S. Na, N.-M. Park, S. S. Lee, S. G. Im, J. B. Koo, ACS Applied Materials & Interfaces 2016, 8, 15459.
[197] C. Pan, K. Kumar, J. Li, E. J. Markvicka, P. R. Herman, C. Majidi, Advanced Materials 2018, 30, 1706937.
[198] N. Kazem, M. D. Bartlett, C. Majidi, Advanced Materials 2018, 30, 1706594.
[199] M. D. Bartlett, N. Kazem, M. J. Powell-Palm, X. Huang, W. Sun, J. A. Malen, C. Majidi, Proceedings of the National Academy of Sciences 2017, 114, 2143.
[200] J. Wang, G. Cai, S. Li, D. Gao, J. Xiong, P. S. Lee, Advanced Materials 2018, 30, 1706157.
[201] C. Keplinger, J.-Y. Sun, C. C. Foo, P. Rothemund, G. M. Whitesides, Z. Suo, Science 2013, 341, 984.
[202] C. Yang, Z. Suo, Nature Reviews Materials 2018, 3, 125.
[203] J.-Y. Sun, C. Keplinger, G. M. Whitesides, Z. Suo, Advanced Materials 2014, 26, 7608.
[204] B. Chen, J. J. Lu, C. H. Yang, J. H. Yang, J. Zhou, Y. M. Chen, Z. Suo, ACS Applied Materials & Interfaces 2014, 6, 7840.
[205] J. Rivnay, S. Inal, B. A. Collins, M. Sessolo, E. Stavrinidou, X. Strakosas, C. Tassone, D. M. Delongchamp, G. G. Malliaras, Nature Communications 2016, 7, 11287.
[206] L. Groenendaal, F. Jonas, D. Freitag, H. Pielartzik, J. R. Reynolds, Advanced Materials 2000, 12, 481.
[207] S. Savagatrup, E. Chan, S. M. Renteria-Garcia, A. D. Printz, A. V. Zaretski, T. F. O'Connor, D. Rodriquez, E. Valle, D. J. Lipomi, Advanced Functional Materials 2015, 25, 427.
[208] J. Y. Oh, S. Kim, H.-K. Baik, U. Jeong, Advanced Materials 2016, 28, 4455.
[209] Y. Wang, C. Zhu, R. Pfattner, H. Yan, L. Jin, S. Chen, F. Molina-Lopez, F. Lissel, J. Liu, N. I. Rabiah, Z. Chen, J. W. Chung, C. Linder, M. F. Toney, B. Murmann, Z. Bao, Science advances 2017, 3, e1602076.
[210] C.-L. Choong, M.-B. Shim, B.-S. Lee, S. Jeon, D.-S. Ko, T.-H. Kang, J. Bae, S. H. Lee, K.-E. Byun, J. Im, Y. J. Jeong, C. E. Park, J.-J. Park, U. I. Chung, Advanced Materials 2014, 26, 3451.
[211] P. Li, K. Sun, J. Ouyang, ACS Applied Materials & Interfaces 2015, 7, 18415.
[212] S. G. R. Bade, X. Shan, P. T. Hoang, J. Li, T. Geske, L. Cai, Q. Pei, C. Wang, Z. Yu, Advanced Materials 2017, 29, 1607053.
[213] V. R. Feig, H. Tran, M. Lee, Z. Bao, Nature Communications 2018, 9, 2740.
[214] D. J. Lipomi, M. Vosgueritchian, B. C. K. Tee, S. L. Hellstrom, J. A. Lee, C. H. Fox, Z. Bao, Nature Nanotechnology 2011, 6, 788.
[215] L. Hu, D. S. Hecht, G. Grüner, Chemical Reviews 2010, 110, 5790.
[216] Z. Yu, X. Niu, Z. Liu, Q. Pei, Advanced Materials 2011, 23, 3989.
[217] S. Wang, J. Xu, W. Wang, G.-J. N. Wang, R. Rastak, F. Molina-Lopez, J. W. Chung, S. Niu, V. R. Feig, J. Lopez, T. Lei, S.-K. Kwon, Y. Kim, A. M. Foudeh, A. Ehrlich, A. Gasperini, Y. Yun, B. Murmann, J. B. H. Tok, Z. Bao, Nature 2018, 555, 83.
[218] J. Liang, L. Li, X. Niu, Z. Yu, Q. Pei, Nature Photonics 2013, 7, 817.
[219] K. Tybrandt, F. Stauffer, J. Vörös, Scientific Reports 2016, 6, 25641.
[220] K. Tybrandt, J. Vörös, Small 2016, 12, 180.
[221] D. Son, J. Kang, O. Vardoulis, Y. Kim, N. Matsuhisa, J. Y. Oh, J. W. F. To, J. Mun, T. Katsumata, Y. Liu, A. F. McGuire, M. Krason, F. Molina-Lopez, J. Ham, U. Kraft, Y. Lee, Y. Yun, J. B. H. Tok, Z. Bao, Nature Nanotechnology 2018, 13, 1057.
[222] Y. Cheng, S. Wang, R. Wang, J. Sun, L. Gao, Journal of Materials Chemistry C 2014, 2, 5309.
[223] S. Ding, J. Jiu, Y. Gao, Y. Tian, T. Araki, T. Sugahara, S. Nagao, M. Nogi, H. Koga, K. Suganuma, H. Uchida, ACS Applied Materials & Interfaces 2016, 8, 6190.

[224] P. Lee, J. Lee, H. Lee, J. Yeo, S. Hong, K. H. Nam, D. Lee, S. S. Lee, S. H. Ko, Advanced Materials 2012, 24, 3326.
[225] T. Sekitani, H. Nakajima, H. Maeda, T. Fukushima, T. Aida, K. Hata, T. Someya, Nature Materials 2009, 8, 494.
[226] N. Matsuhisa, M. Kaltenbrunner, T. Yokota, H. Jinno, K. Kuribara, T. Sekitani, T. Someya, Nature Communications 2015, 6, 7461.
[227] S. Choi, S. I. Han, D. Jung, H. J. Hwang, C. Lim, S. Bae, O. K. Park, C. M. Tschabrunn, M. Lee, S. Y. Bae, J. W. Yu, J. H. Ryu, S.-W. Lee, K. Park, P. M. Kang, W. B. Lee, R. Nezafat, T. Hyeon, D.-H. Kim, Nature Nanotechnology 2018, 13, 1048.
[228] Y. Kim, J. Zhu, B. Yeom, M. Di Prima, X. Su, J.-G. Kim, S. J. Yoo, C. Uher, N. A. Kotov, Nature 2013, 500, 59.
[229] T. Koshi, E. Iwase, Japanese Journal of Applied Physics 2015, 54, 06FP03.
[230] N. Matsuhisa, D. Inoue, P. Zalar, H. Jin, Y. Matsuba, A. Itoh, T. Yokota, D. Hashizume, T. Someya, Nature Materials 2017, 16, 834.
[231] J. Li, J.-K. Kim, Composites Science and Technology 2007, 67, 2114.
[232] T. Sekitani, Y. Noguchi, K. Hata, T. Fukushima, T. Aida, T. Someya, Science 2008, 321, 1468.
[233] H. Jin, N. Matsuhisa, S. Lee, M. Abbas, T. Yokota, T. Someya, Advanced Materials 2017, 29, 1605848.
[234] T. S. R. Group, 2018.

Chapter 3 Experimental Methodology

This chapter elaborates the synthesis methods of the plant conformable electrodes and various characterization techniques including optical microscopy, tensile testing et al. Mechanical and electrical stimulation experiment set-ups are also discussed.

3.1 Rationale of Selection

The objective of this thesis is to fabricate an electrode that is able to adhere onto the petioles of *Mimosa pudica* plant and measure the electrical signals. The basic requirements for this electrode are: (1) good electrical conductivity; (2) good stretchability and (3) good adhesion on plant surface.

The electricals signals, mainly the action potentials (APs) and variation potentials (VPs), are vital for simulating mechanical movements of *Mimosa pudica* (leaflets folding, petioles bending). Since our goal is to develop an electrode that is non-invasive in nature, hence the electrical signal induction and measurement can only be extracellular. The problem associated with this measurement is that the signals are very weak, therefore electrode materials with high electrical conductivity are selected. Since physical movements of *Mimosa* plant would be involved, it is therefore important for the electrodes to be able to adhere tightly to the plant during the test.

Polydimethylsiloxane (PDMS), is the most commonly used silicon-based organic polymer with its application ranging from contact lenses to industrial elastomers. PDMS is chemically inert, non-toxic and transparent in nature, and has low elastic modulus, which allows it to be easily deformed into various shapes[1]. Its rubbery behavior makes it suitable as the substrate for our conformable electrode. By adjusting the proportion of the crosslinking agent and the polymer base, we could easily obtain PDMS substrates with different elasticity.

Subsequently, gold (Au), which is a very good electrical conductor, could be deposited onto the cured PDMS substrate to form an electrically connective layer via vacuum deposition technique. With only 80nm of Au layer, the whole substrate could be highly conductive, which has negligible effect on the thickness of the electrode.

However, the exposed Au layer does not have any adhesive ability. Hence, hydrogel, a three-dimensional hydrophilic polymer network that is rich in water content, is introduced to be the adhesive agent between the conductive electrode and the plant. The adhesion of hydrogel comes from the covalent forces of polymer networks. Addition of ionic compounds such as lithium chloride, the hydrogel becomes ionically conductive and hygroscopic (ability to absorb moisture from air).

By combining these three layers of materials, the conformable plant electrode now satisfies all three requirements, which are stretchable, electrically conductive and adhesive to plant surface.

3.2 Synthesis of Electrodes

The chemicals used in this section were from Sigma-Aldrich, unless otherwise stated.

3.2.1 Fluorination of the Silicon Wafers

The silicon wafers used were polished single-crystal silicon wafers doped with boron (Si100, thickness 525 ± 25 μm). Clean the silicon wafers with ethanol thoroughly and dried in a nitrogen gas stream. Place the cleaned silicon wafers with a glass substrate loading a drop of 1H, 1H, 2H, 2H perfluoro-octyl-trichlorosilane into a vacuum chamber. After vacuum the chamber with a rotary pump, wait for 1 hour to complete the fluorination before taking out. This is to improve the hydrophobicity of the wafer surface to facilitate the removal of the coated polydimethylsiloxane (PDMS) and ease of cleaning for later usages[2].

3.2.2 Preparation of PDMS Substrates

PDMS precursor solution was formed by blending the prepolymer and cross-linking agent thoroughly (weight ratio of 10:1). 100 µm thick PDMS substrates were obtained from spin-coating the precursor solutions onto the fluorinated silicon wafers at 800 rpm for 60 s. After spin-coating, substrates were crosslinked at 60 ℃ for 24 hours.

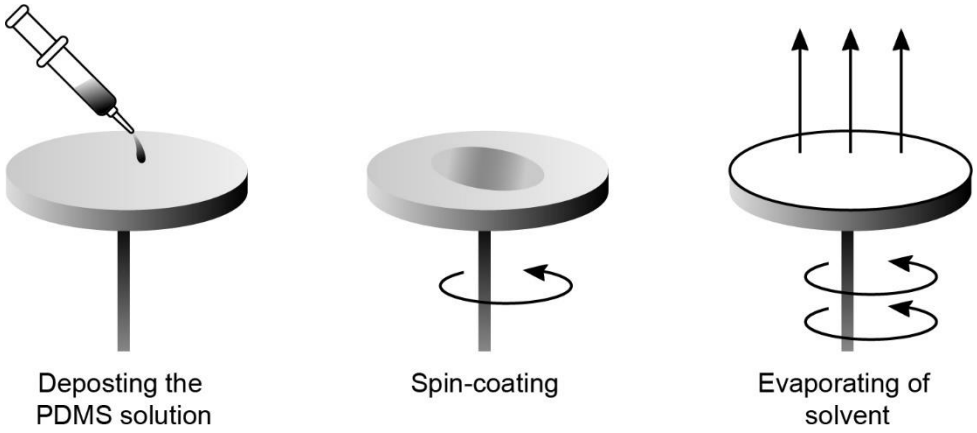

Figure 31 . Schematic of the PDMS spin coating process.

3.2.3 Vacuum Deposition of Conducting Layers

The cured PDMS samples are placed into a thermal vacuum evaporator (Nano 36, Kurt. J. Lesker). Vacate the chamber until the pressure is below 10^{-4} Pa. The evaporation source and samples were kept 30 cm apart. Rotation of sample holder was done to obtain uniform metal thin films during evaporation. A layer of 80nm Au using Au bullet (purity: >99.9%, Kurt. J. Lesker) was deposited at a rate of 0.5 Å s^{-1}.

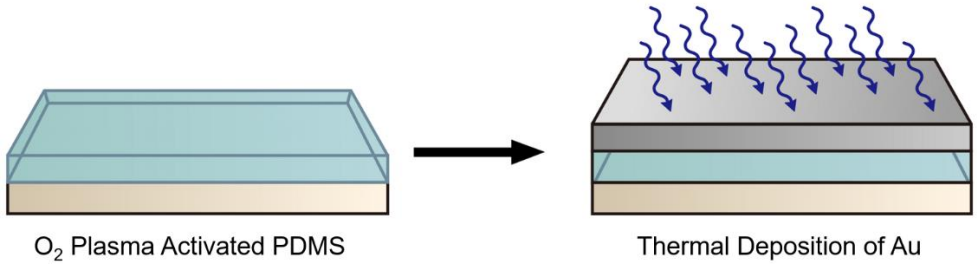

Figure 32. Schematic illustration of thermal vacuum deposition of the composite electrode.

3.2.4 Hydrogel Precursor Preparation

For hydrogel precursor selection, a double-network of polyacrylamide and alginate was designed. For the polyacrylamide (PAAm) network, acrylamide (AAm) was used as monomer. A alginate network that acts as mechanical energy dissipator, was introduced to the hydrogels to form an interpenetrated structure that enhanced the toughness of the hydrogel[3].

The precursor solution was formed by 6g of AAm (12%wt) and 1g of sodium alginate (2%wt) adding into 44mL of deionized water, together with 4.25g of lithium chloride (2M), 1.1g of glucose, 3.6 μg of N,N′-Methylenebisacrylamide (MBAA).

The hydrogel precursor solution was then refrigerated at -5 ℃.

3.2.5 Oxygen Plasma Etching

Half of the as-deposited PDMS substrates were covered by a rectangular PDMS molds to prevent exposure to the plasma, and placed into the plasma etching machine (Cute, Femto Science). The chamber was vacuumed and filled with pure oxygen gas. Plasma etching was performed under a power rate of 100W for 30s. The etched samples were quickly sealed to prevent exposure in the ambient environment. PDMS material consists of repeated —O−Si$(CH_3)_2$− units that produce hydroxyl groups (−OH) once being exposed to oxygen plasma[4]. Increase in hydroxyl groups due to the surface layer oxidation can form strong intermolecular bonds, and thus enhancing the interfacial adhesion between the deposited Au layer and the toughened hydrogel[5, 6].

3.2.6 Hydrogel Grafting on the Plasma-etched Substrates

The prepared hydrogel precursor was taken out from the freezer and put onto a magnetic stirrer to defrost to room temperature. After defrosting, 1ml of the precursor solution was extracted into a 15ml centrifugal tube. The plasma-etched substrates and the centrifugal tube were both placed into a vacuum chamber for 5 minutes to remove the oxygen gas in the precursor solution. Nitrogen gas was pumped into the chamber during venting. Since dissolved oxygen in the solution can consume radicals, inhibiting polymerization and crosslinking of the hydrogel[7, 8]. Hence it is important to savage the oxygen in order to fully polymerize the hydrogel. 10 ul of glucose oxidase (GOx) solution (1ml of deionized water, 1mg of GOx) was added into the precursor solution. The enzyme GOx speeds up the conversion of glucose to gluconic acid and hydrogen peroxide, and oxygen is consumed during this process[9]. After addition of GOx solution, the precursor solution was vacuumed again and vented with nitrogen gas.

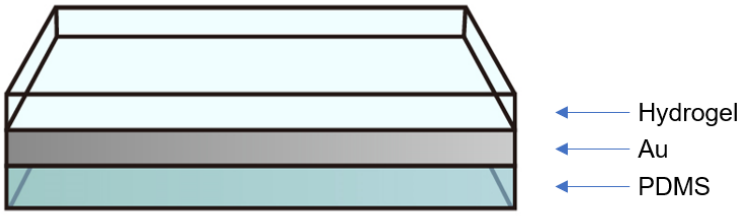

Figure 33. Schematic illustration of plant conformable electrode.

The toughened hydrogel was prepared by mixing 1ml of degassed precursor solution with 10 µl of Irgacure 2959 (photo-initiator) and 10 µl of diluted TEMED solution (2ml of deionized water, 2 µl of TEMED) and 45 µl of calcium carbonate slurry. Calcium ions in calcium carbonate were to crosslink the sodium alginate. The mixture was mixed thoroughly and casted at the amount of 40 µl per cm^2 onto the exposed part of plasma-etched substrate and crosslinked under ultraviolet light irradiation for 30 minutes.

3.3 Characterization Techniques

The morphology of as-synthesized conformal electrodes was obtained from an optical microscopy. The physical properties such as adhesion strength of the electrode on leaf, adhesion strength between the PDMS substrates and hydrogel would be characterized by a mechanical tester (C42, MTS Systems Corporation). The effect of electrodes on leaf would be evaluated by a chlorophyll meter (SPAD 502 Chlorophylll Meter). The stretchability of the electrode would be evaluated by a mechanical tester and a parameter analyzer (Keithley 4200, Tektronix). The interfacial impedance between Au-PDMS substrates and hydrogel was measured by an electrochemical workstation (Zennium E, Zahner Ennium).

3.3.1 Optical Microscope

The optical microscope is a microscope that utilizes visible light and a series of lenses to produce magnified images of small objects. The maximum magnification power of optical microscopes is typically capped to around 1000x due to the limited resolving power of visible light.

Under the optical microscope, the cross sections of the plant conformable electrodes and the plant conformable electrodes warping onto the Mimosa stem were taken.

3.3.2 Adhesion Strength on Plant Surface

Tensile testing is a basic material testing where a tension is applied on a sample until failure. Mechanical properties such as ultimate tensile strength, breaking strength and maximum elongation can be directly measured by a tensile test. Other characteristics such as Young's modulus, yield strength and Poisson's ratio can also be obtained[10].

To measure steady signals from plants, the electrodes are expected to stay closely adhered to plants. The adhesion strength was evaluated by the 90 °peeling-off experiment. The conformable plant electrodes were cut into strips with a dimension of 3.0 x 1.0 cm^2 and pressed onto the leave surface mounted on the mechanical tester with one end fixing on the upper grip. The strain rate was set at 0.1 mm/s and the hydrogel was slowly peeled off from the leaf. The plateau of force during peeling was averaged and divided by the hydrogel width as adhesive strength.

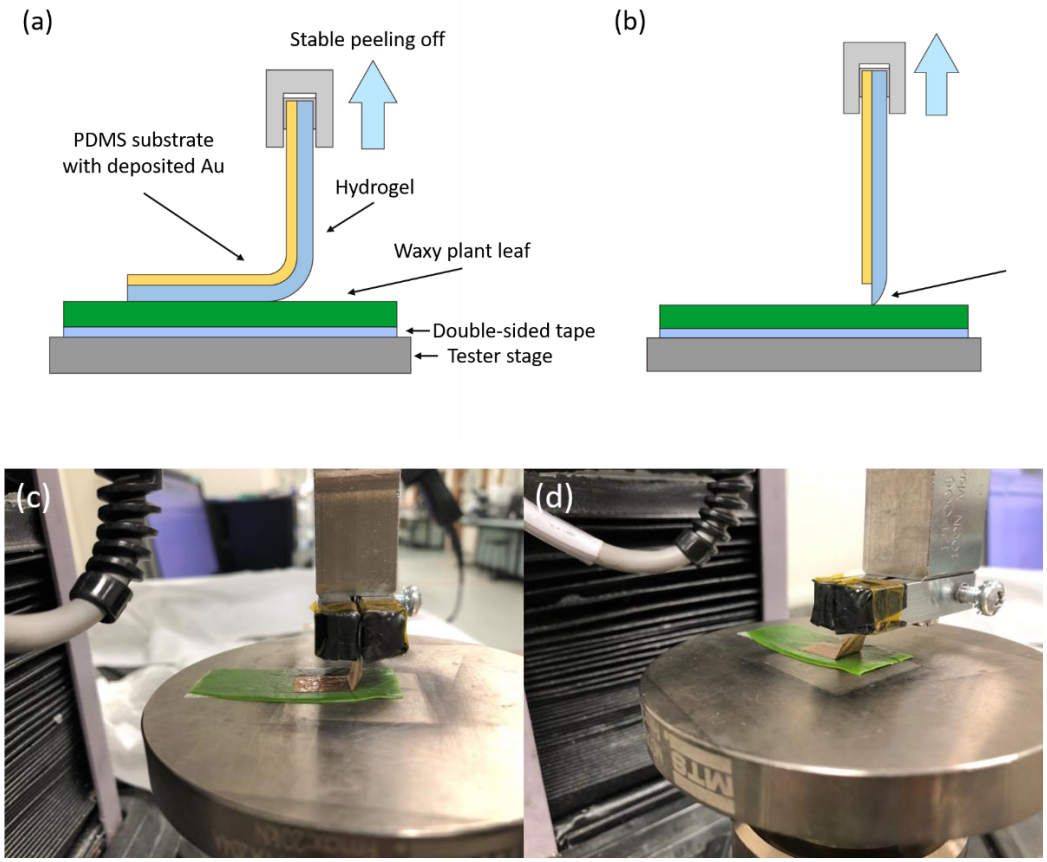

Figure 34. Illustration of peel test of electrodes on leaves: (a) & (b) schematic of the peeling test; (c)&(d) actual peeling test set-up.

3.3.3 Interfacial Adhesion Strength of Plant Conformable Electrodes

The generation of electrical signals in *mimosa* involves physical movements, while strong adhesion between hydrogel and petiole is important, close attachment of hydrogel on the PDMS substrates is also very crucial to maintain a closed electrical circuit. The adhesion strength could be measured by attaching two electrodes (the hydrogel side) together, and slowly pulled one of them apart at a speed of 0.1 mm per second. The electrodes were mounted onto PET film for ease of grasping.

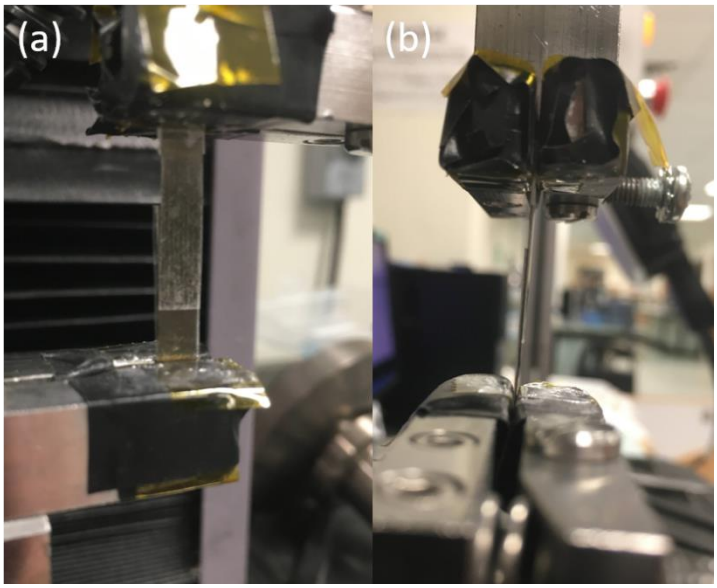

Figure 35. Illustration of the sliding resistance test of the electrodes: (a) front view, (b) side view.

3.3.4 Effect of Plant Conformable Electrodes on Plant Leaves

Ideally, the synthesized electrodes should have minimum negative impact on plants. Hence, the effect of electrodes on leaves can be quantified by two indicators: (1) chlorophylls and (2) leaf nitrogen content. Chlorophyll is a green photosynthetic pigment in plants and algae that absorbs light and converts into energy during photosynthesis process[11]. Insufficient chlorophyll in leaves will render inability to generate carbohydrates via photosynthesis and may result in withering of plants, which is also known as chlorosis[12]. Lack of nitrogen is a common cause of chlorosis, as nitrogen constitutes an essential structural and functional component of chlorophylls[13].

Hence, we chose *Epipremnum aureum* (also known as devil's ivy) as the test subject. The chlorophyll and nitrogen content of 6 leaves were measured by a chlorophyll meter, and the measured regions were covered by the electrodes. The electrodes were then removed after 48 hours and these two readings were measured again to see the difference.

Figure 36. The electrodes attached onto the devil's ivy leaves with numerical markings.

3.3.5 Stretchability of Plant Conformable Electrodes

Resistance–strain characteristic is vital for plant signal measurements. Since the generation of electrical signals in the *mimosa* usually accompanied with physical movements of the *mimosa* plants, hence, the electrodes should remain conductive while being stretched by the plants. The testing samples were cut into 3.0 cm (length) ×0.5 cm (width) rectangular strips. The liquid metal (eutectic GaIn) and thin copper wires were used to make electrical contact on the samples. The electrodes were stretched

at a tensile strain rate of 0.1mm/s using a mechanical tester until rupture and the resistance was measured by a parameter analyzer during stretching.

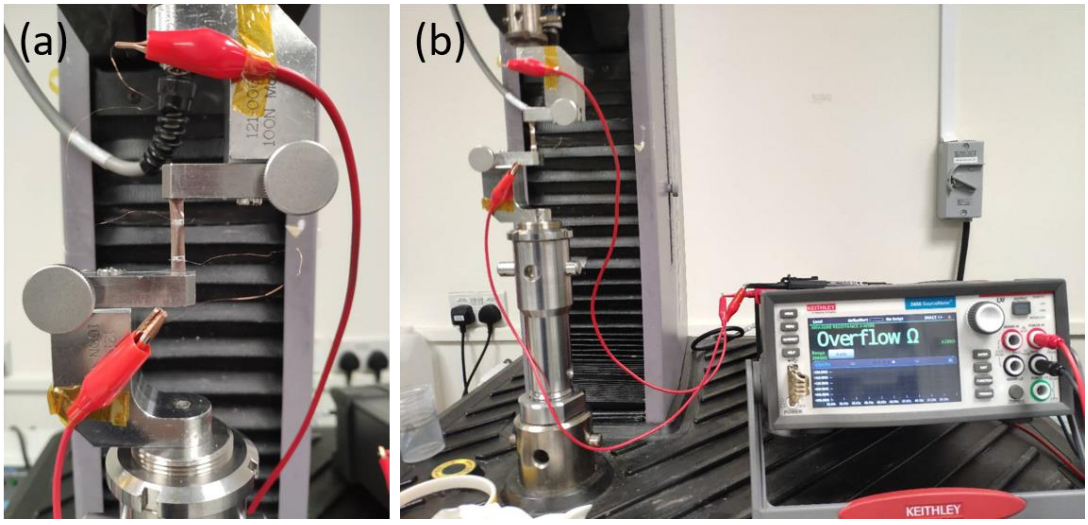

Figure 37. Stretchability test set-up. (a) The sample was clamped and liquid metal was applied on it. (b) Full set-up of the test.

3.3.6 Interfacial Impedance Measurements of Plant Conformable Electrodes

Electrical impedance spectroscopy (EIS) is a nondestructive characterization technique that quantifies the resistance of a material. Measurements are done through small alternating currents at known frequencies to the samples and the voltage and the phase difference of the voltage and current are recorded using digital technique, which later are used to calculate the capacitance and conductance values at corresponding frequency. The relationship between the conductance and capacitance with the changes in frequency reveals the electrical properties of the material.

The interfacial impedance between electronic films and hydrogel was measured by an electrochemical workstation. A hydrogel film (1 cm x 1 cm) was sandwiched by two conformable films (2 cm x 1 cm), with Au in contacting with two sides of the hydrogel film (Fig.38a). The impedance of Au-hydrogel-Au was measured from 1 Hz to 10^6 Hz.

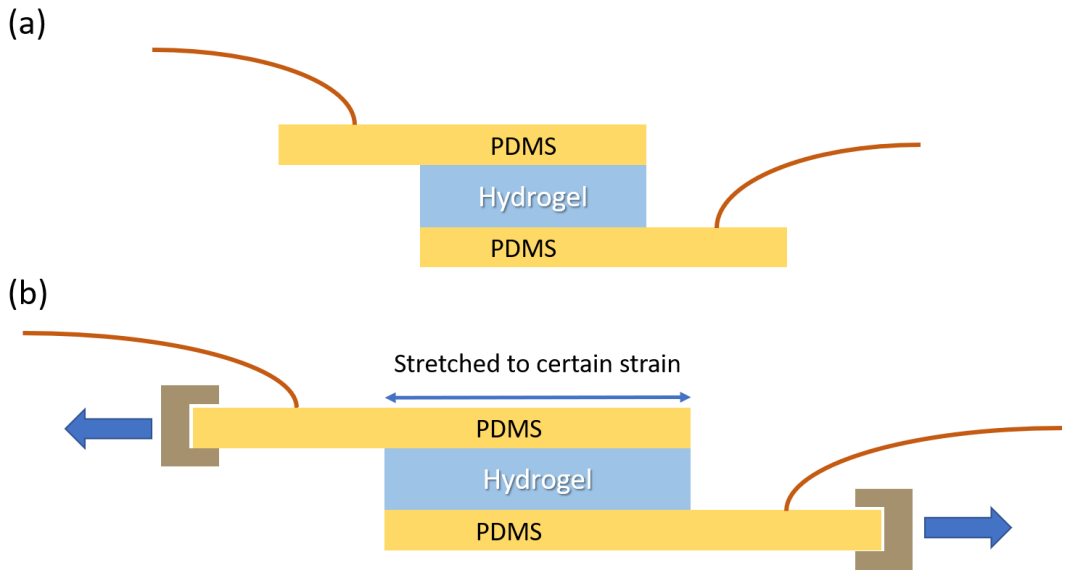

Figure 38. Impedance measurement set-up. Hydrogel was sandwiched between the Au deposited PDMS electrodes with two copper wires connecting to the electrochemical workstation. (a) the static impedance measurement set-up. (b) the dynamic impedance measurement set-up. The stacked electrodes were being stretched by a tensile workstation.

In addition, since the electrodes could undergo certain strain during the signal measurements, we would also test the impedance at various strains. The electrodes were pulled to a designated strain and conducted the impedance measurement.

3.4 *Mimosa Pudica* Electrical Signal Measurements

In the section, two different experiments were conducted. The first part was the mechanical stimulation of the petiole of mimosa and using three recording electrodes to detect the generation of APs. The second experiment was to use a 3.0V battery to apply a voltage across different locations on the mimosa and to observe the bending of petiole.

3.4.1 Mechanical Stimulation of *Mimosa Pudica*

Three electrodes (0.3cm x 1.0cm) were warped onto the petiole of *mimosa*, with 1cm spacings from one another. Another electrode was warped onto the stem of *Mimosa* as reference electrode (RE). The three recording electrodes (marked as CH, CH2, CH3) were wired with copper wires through liquid metal sealed in Ecoflex. The schematic illustration of mechanical stimulation of mimosa is shown in Figure 39.

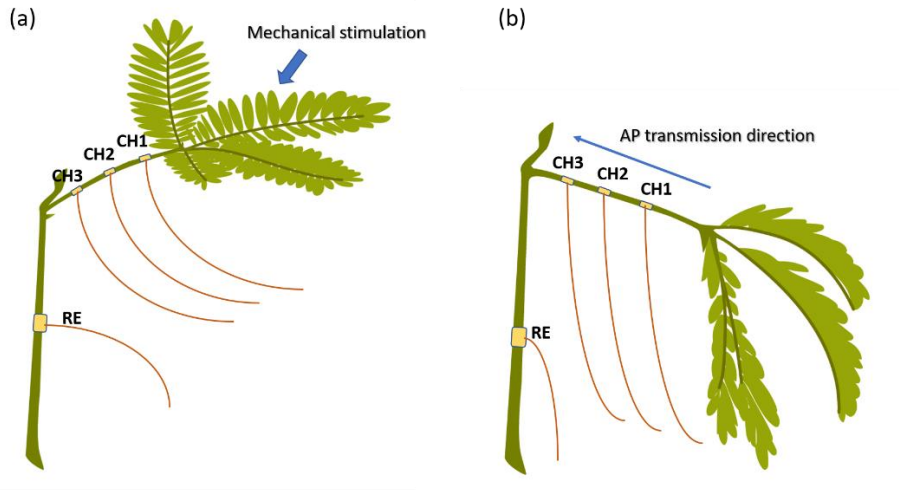

Figure 39. Schematics of mechanical stimulation set-up. (a) Before stimulation; (b) after stimulation.

The pinnules of mimosa was touched to stimulate the electrical signals that propagated along the petiole and eventually led to the bending of petiole. Electrical signals were recorded by data acquisition system (USB-2610 Series DAQ, Smacq Technologies) at 100 Hz sampling rate. Distances between every CH would be measured and used to calculate the AP transmission speed.

3.4.2 Electrical Stimulation of *Mimosa Pudica*

Two electrodes (0.3cm x 1.0cm) were warped onto the petiole of *mimosa*, with a rough 2 cm spacing from each other. Two electrodes were warped onto the stem of *mimosa*, with one above the testing petiole and another below. These three electrodes

were later used as the electrical stimulation electrodes (marked as ES1, ES2 and ES3) using a 3.0V battery. The reference electrode was warped onto another stem of *mimosa*.

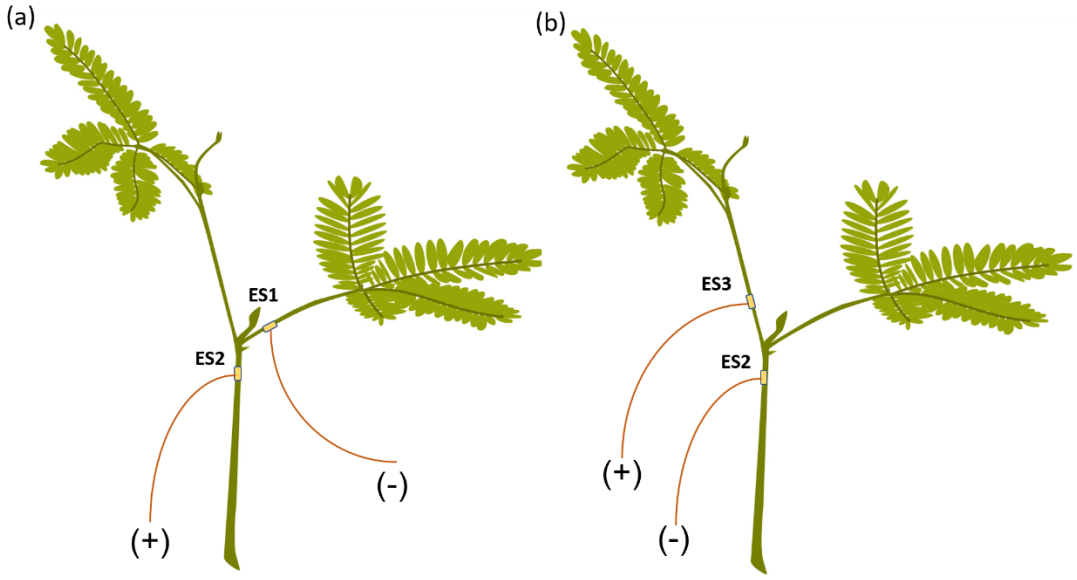

Figure 40. Schematics of electrical stimulation set-ups. (a) APs induced by voltage applied across ES1 and ES2; (b) Control experiment to observe if APs were induced when voltage was applied across ES2 and ES3.

The experiment was divided into two different parts. For the first part of experiment, the ES1 and ES2 were connected to the negative and positive terminals of a 3.0V battery. The second part of experiment was a control experiment, where ES2 and ES3 were connected to the negative and positive terminals of the 3.0V battery. The objective of these two parts of experiment was to detect the presence of action potential in the petiole and to observe the bending of petiole upon excitation.

3.4.3 Smartphone-controllable Platform for *Mimosa* Movements Manipulation

The previous electrical stimulation on *mimosa* was done by manual connecting the electrodes with a 3.0V battery. Hereby, a smartphone-controllable platform is designed to enable triggering physical movements at specific locations on *mimosa* plant. As the electrostimulation on mimosa only requires a voltage output of 3.0V, any

miniaturized electronic systems (such as Wi-Fi module with output voltage of 3.3 V) could be used to electrically stimulate the *mimosa* movements.

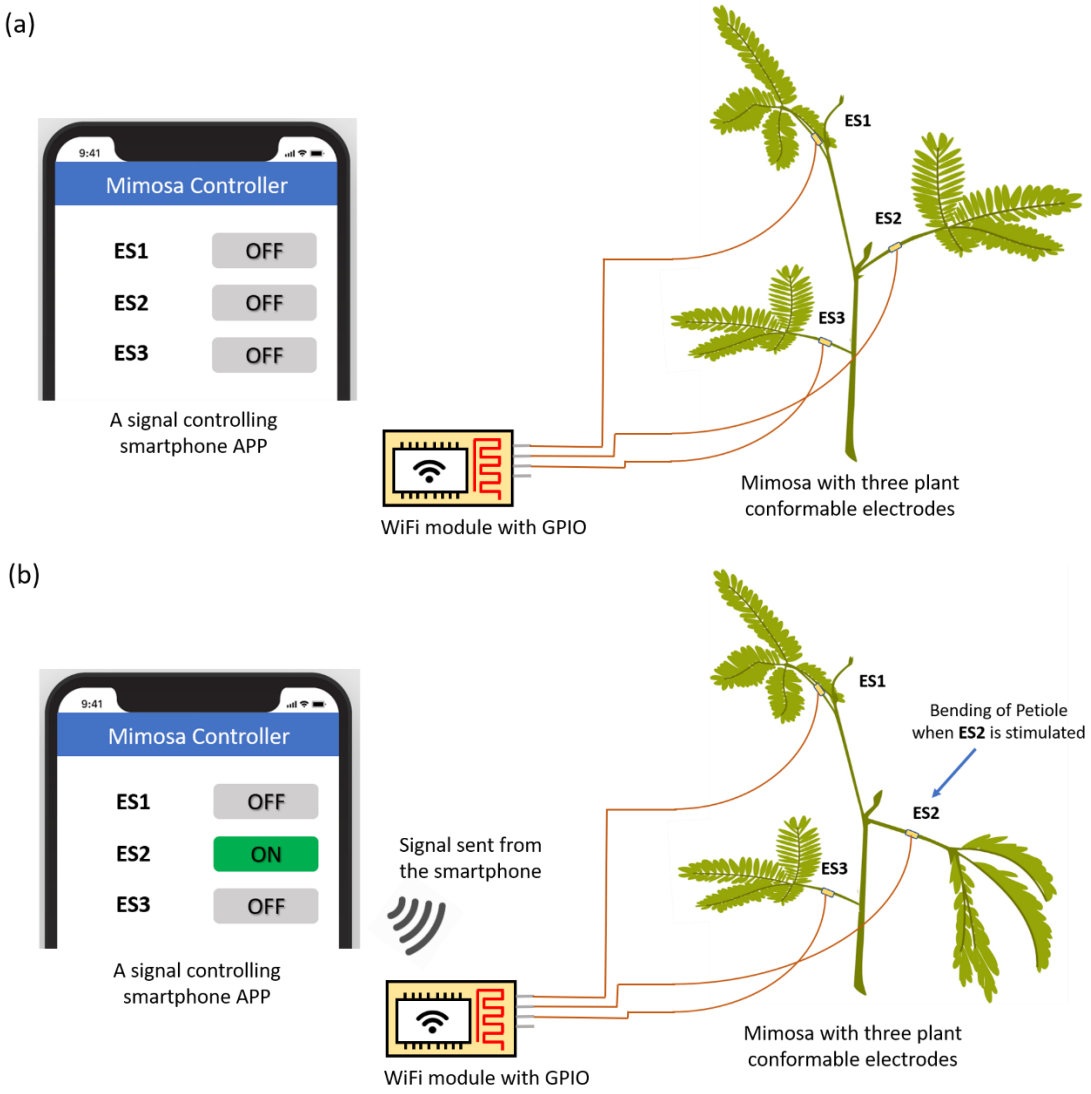

Figure 41. Schematic of the smartphone-controllable platform that enables inducing physical movements of *mimosa* at designated locations. The platform consists of a smartphone application that could send the command via internet, a Wi-Fi module with General Purpose Input Output (GPIO) that could deliver a 3.3V electrical output to the plant conformable electrodes warped onto the petioles of *mimosa*. (a) The initial set-up. (b) When a "on" command for ES2 is sent from the application via internet, and Wi-Fi module then impose a 3.3V voltage onto the ES2, leading the dropping of the petiole.

From Fig.41, we will be able to control the dropping of the petioles by simply tapping the designated electrostimulation electrode (ES) warping on the petiole, and the command will be sent from the smartphone and received by the Wi-Fi module, which in

this case, applies a 3.3 V voltage to the ES2, causing the petiole that ES2 is warped onto to bend.

References

[1] M. Liu, J. Sun, Y. Sun, C. Bock, Q. Chen, Journal of Micromechanics and Microengineering 2009, 19, 035028.
[2] M. Pei, L. Huo, K. Zhang, H. Zhou, P. Liu, Colloids and Surfaces A: Physicochemical and Engineering Aspects 2020, 585, 123984.
[3] X. Zhao, Soft Matter 2014, 10, 672.
[4] S. Bhattacharya, A. Datta, J. M. Berg, S. Gangopadhyay, Journal of Microelectromechanical Systems 2005, 14, 590.
[5] H. Hillborg, U. W. Gedde, Polymer 1998, 39, 1991.
[6] M. L. Chabinyc, D. T. Chiu, J. C. McDonald, A. D. Stroock, J. F. Christian, A. M. Karger, G. M. Whitesides, Analytical Chemistry 2001, 73, 4491.
[7] C. Decker, A. D. Jenkins, Macromolecules 1985, 18, 1241.
[8] A. K. O'Brien, C. N. Bowman, Macromolecules 2006, 39, 2501.
[9] P. Trinder, Annals of Clinical Biochemistry 1969, 6, 24.
[10] J. R. Davis, Tensile Testing, 2nd Edition, ASM International, 2004.
[11] P. May, University of Bristol.
[12] S. Kubis, R. Patel, J. Combe, J. Bédard, S. Kovacheva, K. Lilley, A. Biehl, D. Leister, G. Roís, C. Koncz, P. Jarvis, Plant Cell 2004, 16, 2059.
[13] B. Capon, Botany for Gardeners, Timber Press, 2010.

Chapter 4 Results and Discussion

In this chapter, the experiment results and discussion are included. Firstly, morphologies of the fabricated electrodes under optical microscopes and the scanning electron microscopes are shown. The physical performance of the electrodes obtained from various tensile testing and electrical properties measured via an electrochemical workstation are also presented. Lastly, the electrical signals resulted from the mechanical stimulation and electrical stimulation of Mimosa pudica are recorded.

4.1 Introduction

Over the last decade, remarkable breakthroughs in flexible electronics have been achieved and will certainly bring about revolutionary improvements in quality of lives in the future. As compared to the rigid electronic devices, these flexible devices have the advantages of conformability and compliance, which are very important for healthcare, digital display and energy storage applications[17]. Hence, it is essential to design and fabricate materials with mechanical characteristics that can withstand geometrical deformations and yet, maintaining a good electrical conductivity.

In the previous section, we fabricated a plant conformable electrode based on PDMS substrate that consists of a layer of conductive Au thin film formed by thermal evaporation and a layer of hydrogel formed by photopolymerization as the adhesion layer between the electrode to the *Mimosa Pudica* surface. Hydrogels are water-rich polymeric materials with a distinct three-dimensional structure. Despite its versatile applications in biomedicine, adaptive and responsive materials and soft electronics, most hydrogels have weak mechanical properties such as low stretchability[18] and weak bonding between hydrogels and solid materials[19]. Therefore, PDMS provides most of the stretchability for the entire electrode to compensate the weak mechanical properties of hydrogel. Since the Au thin film cannot be directly attached to the plant surface, hydrogel is added as the adhesion. As compared to the previous plant electrical signal measurements, which were invasive and damaging, the plant conformable electrodes are non-damaging, and easily reusable.

4.2 Results and Discussions

In this section, the results from the experimental methodology would be shown and discussed to see if the hypothesis proposed was valid.

4.2.1 Surface Morphology Characterization

Since the generation of APs from mimosa would definitely accomplish with visible movements, it is therefore vital to ensure good electrical signal transmission and to maintain good interfacial adhesion between the plant and the electrodes at the same time.

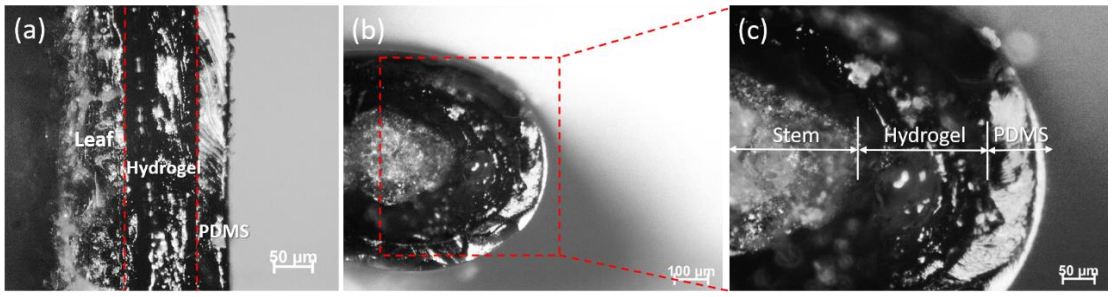

Figure 42. Cross-sections of plant conformable electrodes under optical microscope: (a) plant conformable electrodes stuck tightly on leaf; (b) & (c) plant conformable electrodes warped around the *mimosa* stem.

From the optical microscopes, we could observe the clear distinctions among the leaf, the hydrogel, and the PDMS layers (Fig.42a). A cross-section picture of the electrode warping tightly. around the mimosa stem was also shown (Fig.42b&c). It could be seen that close adhesion with no void spacings at the interfaces between the hydrogel and stem.

4.2.2 Adhesion Strength of Conformable Plant Electrodes on Leaves

Good adhesiveness of the plant conformable electrodes is essential for steady signal measurements on *mimosa pudica*. As mentioned previously, the generation of electrical signals in *mimosa* involves physical movements such as pinnules folding and petiole bending. Hence, the electrodes synthesized should processed the ability to stay adhered onto the surface. From the previous section, the adhesion could be visually seen, and the exact amount of adhesive strength would be quantified here.

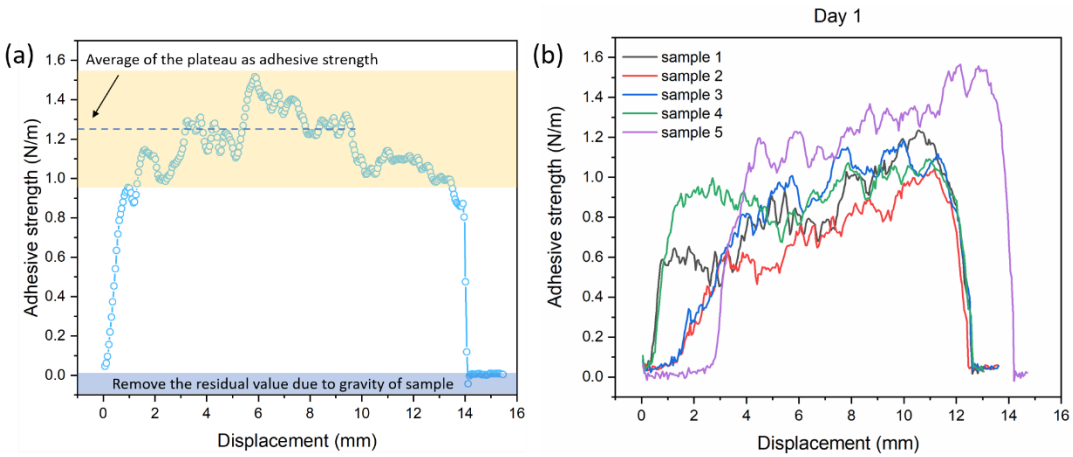

Figure 43. (a) Illustration of the adhesive strength versus displacement diagram; (b) The adhesive strength versus displacement diagram in day 1.

From the Fig.43a, the adhesive strength increased rapid in the first few millimeters and reached a plateau as the electrodes were lifted at a constant speed. And the adhesive strength dropped rapidly as the electrodes were completely peeled off from the leaves. The adhesive strength was obtained from the average of the plateau, minus away the residual value due to sample's gravity, which in this case was negligible. By applying this principle, the average adhesive strength of 5 samples was calculated to be around 1.2 N/m (Fig.42b).

Due to the invasive nature of measurement in the previous works, a resting period ranging from 3 to 25 hours was required for the mimosa to recover from the wounding state. Our electrodes did not cause any damage to the mimosa and the signal detection could be started immediately after the warping onto the petioles and stems. In addition to that, we would also like to test the variation of the adhesive strength in ambient conditions over time, to show the reusability of the conformable electrodes. Briefly, to test the reusability, the same peeling tests were carried out every 48 hours in ambient condition (25℃，~60% humidity).

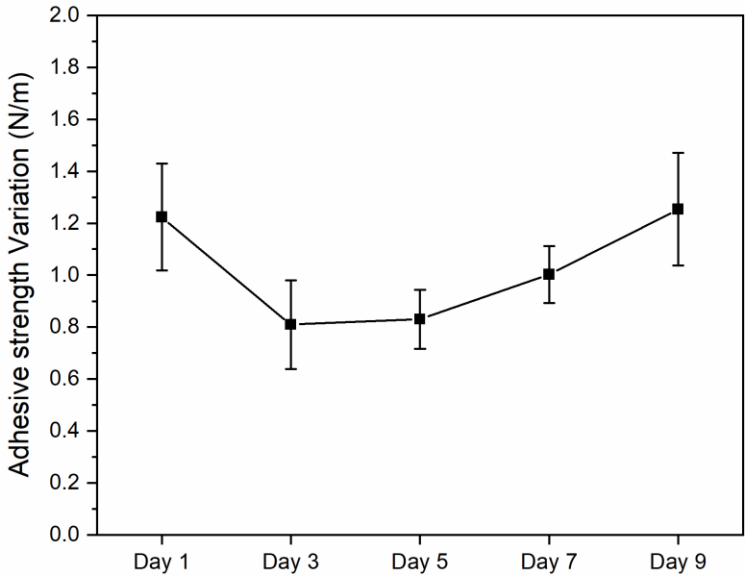

Figure 44. Changes in average adhesive strength of the plant conformable electrodes every 48 hours in ambient conditions.

From Figure 44, the average adhesive strength of the conformable electrodes underwent a one-third fall from day 1 values after 48 hours, and then gradually increased from day 3 onwards, and eventually returned back to the initial value in day 9. The ability to restore the adhesive strength might to be contributed by the hygroscopicity of lithium chloride salt inside the hydrogel, which absorb moisture from the surrounding to maintain the 3D structure of hydrogel. This result shows that the plant conformable electrodes could be reusable for multiple tests.

4.2.3 Adhesion Strength between Hydrogel and PDMS Substrates

While the good attachment between the plant conformable electrodes and the plant is required, strong interfacial adhesion between the hydrogel and PDMS substrates prevents disintegration of the electrodes during movements of the *mimosa*. If the adhesion of hydrogel on the PDMS substrates is weak, the PDMS substrates could fall off from the petiole and resulting in breaking of the conducting pathways. Hence, two pieces of electrode were placed face-to-face, with hydrogel attaching tightly, a gradually pulled away in one direction to observe if any structural disintegration occurred.

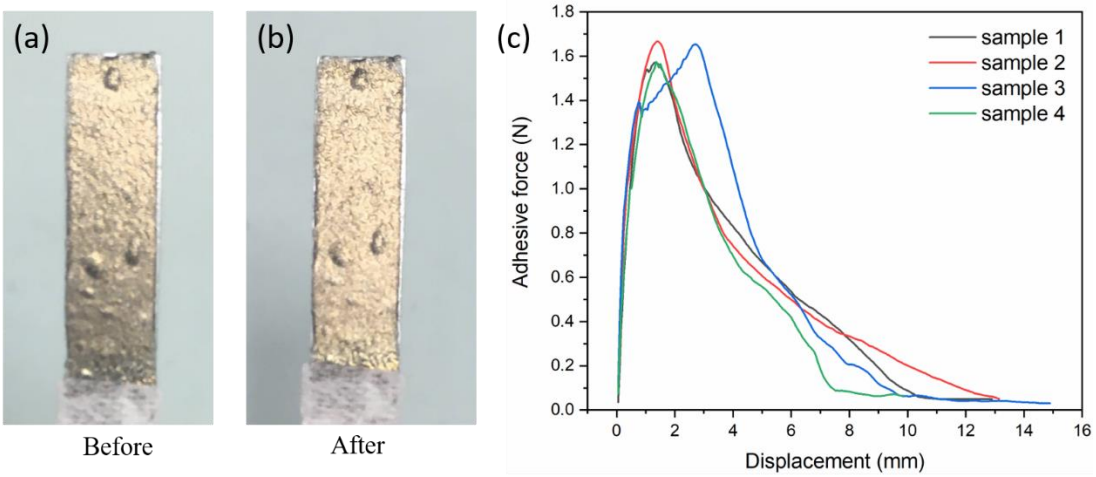

Figure 45. (a) & (b) The surfaces of the electrodes before and after the test. (c) The adhesive force versus displacement diagram of 4 samples.

From Fig.45a and 45b, we could see that the hydrogel layer was not detached from the PDMS substrates after the test, which proved that the plant conformable electrode had a decent interfacial stability. The average adhesive force of the samples was around 1.5 N (Fig.44c).

4.2.4 Effect of Plant Conformable Electrodes on Plant Leaves

As mentioned previously, the nitrogen and chlorophylls content on leaf are two direct indicators of the photosynthesis function of the plant, or simply, the ability to convert energy for own usage. Ideally, the synthesized plant conformable electrodes should not have any impact on the nitrogen content and the chlorophylls on leaves.

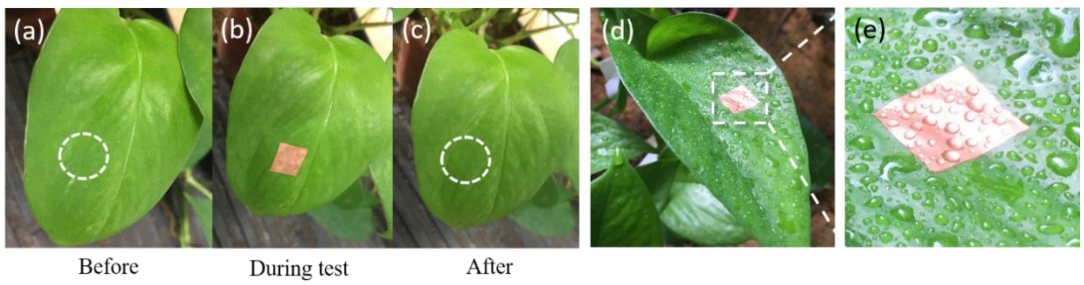

Figure 46. Photos of devil's ivy leaf: (a) before the test, (b) during the test and (c) right after the test. (d) & (e) Photos of the electrode on leaf after rains.

From Figure 46a-c, there was no observable change of color or leaf texture in the covered region. During the experiment, a photo shot of the leaf was captured after rains (Fig.46d&e). It could be seen that the electrode remined conformable on the leaf even after raining, demonstrating excellent adhesive ability.

To further quantify the effects of electrodes on leaf, the variation of chlorophylls and nitrogen contents of the tested leaves measured by a chlorophyll meter were plotted.

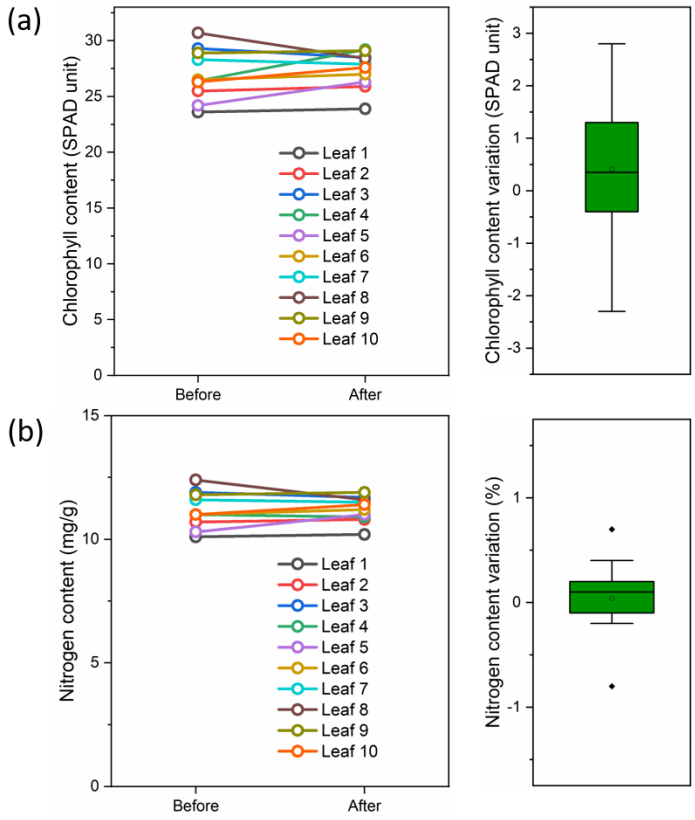

Figure 47. (a) Variations of chlorophyll content and (b) nitrogen content.

From Fig.47, we could tell that the chlorophyll and nitrogen content of the affected regions vary in both direction to a similar extent. Hence, we could conclude that the plant conformable electrodes do not cause a negative impact on plant.

4.2.5 Stretchability of Plant Conformable Electrodes

Since physical movements of the *mimosa* plant are expected, the good adhesion is required. On top of that, it is important for electrodes to remain conductive while being stretched to a certain extent.

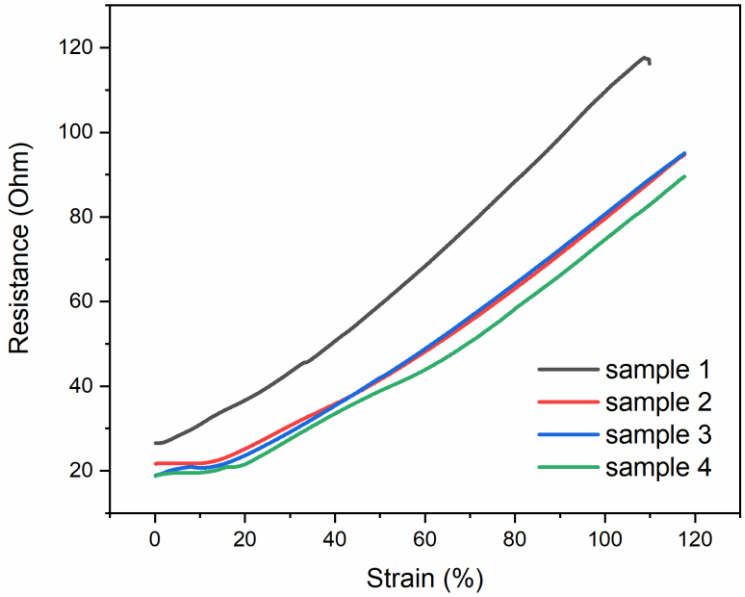

Figure 48. A plot of resistance variations versus strain for plant conformable electrodes.

From Figure 48, we could see that all samples underwent around 100% strains, and the resistances increased around 4 times. Yet the resistance of all samples still lied within the conductive range. Thus, the as-synthesized electrodes could qualify for the electrical signal measurements for *mimosa pudica*.

4.2.6 Impedance Measurements of Conformable Plant Electrodes

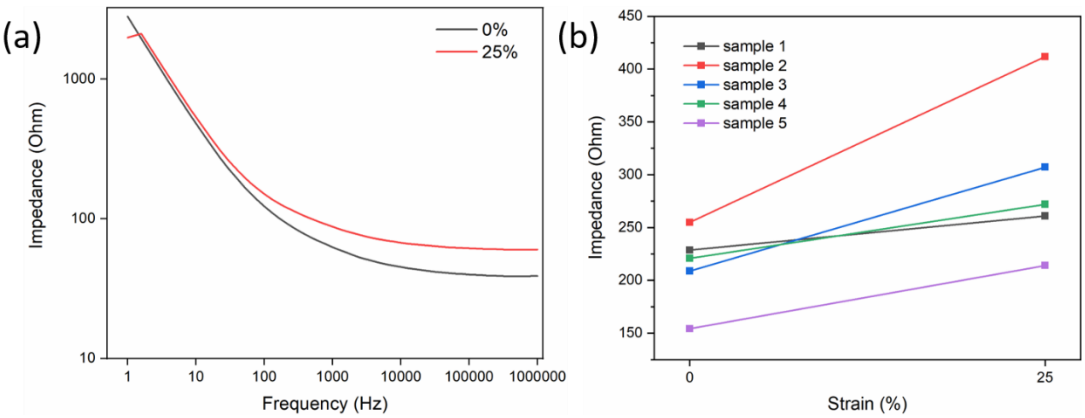

Figure 49. (a) Impedance of conformable plant electrodes at 0% and 25% strain conditions. (b) Variations of impedance versus strain at 30Hz for 5 samples.

The electrical benefit of conformable plant electrode was demonstrated by a sandwiched Au-hydrogel-Au impedance measurement (Fig.49a), with electrodes showing impedance of ~2000Ω at low frequencies (1-10Hz), indicating a low contacting impedance of the conformable plant electrodes. Even the electrode was stretched to 25% strain, the impedance did not vary too much, which showed good stretchability. At 30Hz, the variation of the impedance from 0 to 25% strain was less than 65% (Fig.49b), showing a good potential for signal measurements. The reason why we only obtained two strain levels was because at strain of 50%, the sandwiched electrodes were slowly sliding apart until separation. The impedance measurement requires the electrodes to stay stationary as the stacked area should remain unchanged during the change.

4.2.7 Mechanical Stimulation of *Mimosa Pudica*

Using the conformable plant electrodes, we first verified if the generation of AP signals for *mimosa* via mechanical stimulation. Physical touch of the secondary pulvinus led to the bending of petiole, and an AP signal was evoked, transmitting basipetally to the main stem. Three AP spikes were detected upon mechanical stimulation by three recording electrodes (Fig.50a).

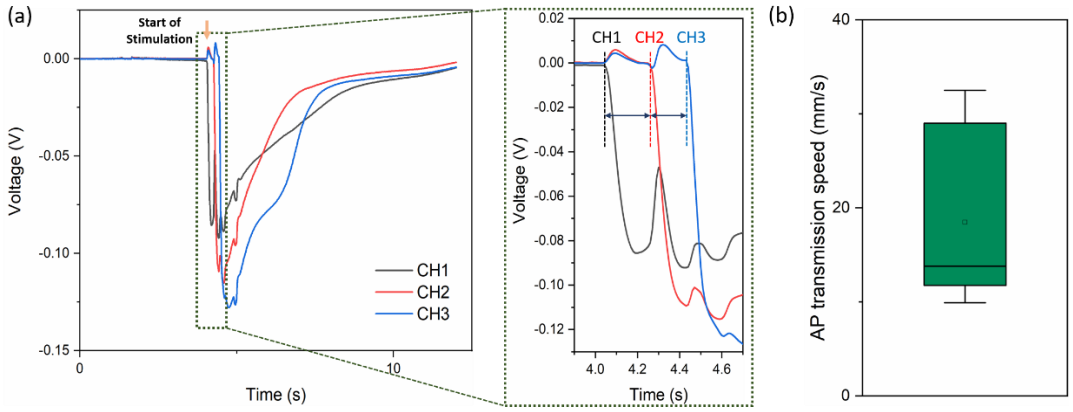

Figure 50. Mechanical stimulation of *Mimosa pudica*. (a) Upon stimulation, three spikes were detected by the three electrodes, shown as three successive troughs. By zooming in, the time intervals between each AP could be measured, and subsequently, the AP transmission speed was calculated in (b).

The sudden decline of the voltage upon stimulation was due to the depolarization of membrane in the petiole, and an AP was evoked and transmitted along the petiole to the primary pulvinus. The time interval between two signals could be measured and the transmission speed of APs was then calculated shown in Fig.50b.

$$\text{AP transmission speed} = \frac{\text{Distance between neighbouring electrodes}}{Time\ intervals}$$

From the box chart, the average transmission speed of AP is around 18.5 mm/s, which is close to the value (~20mm/s) in the previous studies.

4.2.8 Electrical Stimulation of *Mimosa Pudica*

Conversely, we could manually apply a voltage in the mimosa that induces an AP to trigger the physical movements. In order to prevent generation of VP, which is excited when damages such as cutting or burning the plant, a safe voltage of 3.0V was applied. As mentioned earlier, this electrostimulation experiment was separated into two parts.

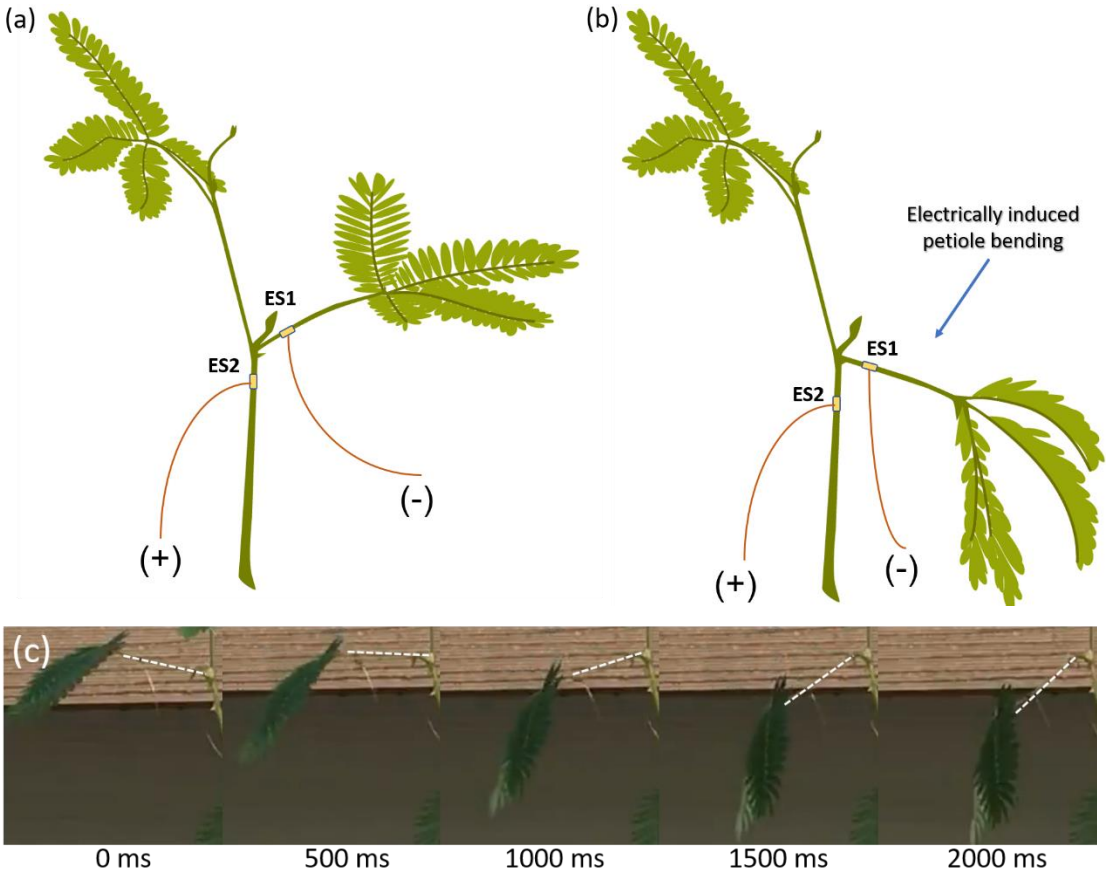

Figure 51. Electrostimulation of *mimosa* pudica. Schematic illustration of (a) mimosa in normal state, and (b) after connecting to the battery. (c) Time series of the bending of petiole upon electrostimulation.

From Fig.51a, by applying a voltage at ES1 and ES2, bending of petiole was observed. The time series of petiole bending is shown in Fig.51c, the bending process took approximately around 2 seconds upon electrostimulation.

The second part of experiment was a control experiment, the only difference was the location (ES2 and ES3) of voltage applied (Fig.52a).

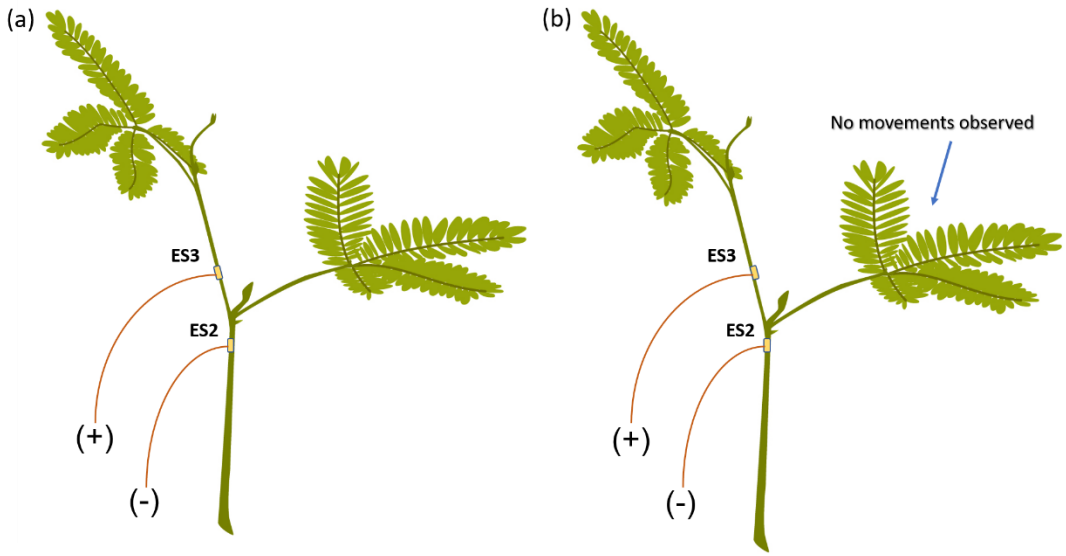

Figure 52. Control experiment on electrostimulation. Schematic illustration of (a) mimosa in normal state, and (b) after connecting to the battery.

When voltage was applied across ES2 and ES3, which was the main stem, no petiole bending observed (Fig.52b). From literature, APs cannot be transmitted in the stem[20], and hence, no physical movements should happen. The experiment results matched the conclusions from literature.

4.2.9 Smartphone-controllable Platform for *Mimosa* Movements Manipulation

A smartphone-controllable platform was designed to enable triggering physical movements at specific locations on *mimosa* plant. We used a Wi-Fi router (Mini Mi WIFI Router 11AC Wi-Fi Roteador 2.4G/5G) to electrically stimulate the *mimosa* movements. Two comfortable electrodes were warped onto the mimosa petiole (Fig. 53a) and connected with a circuit board. From the “mimosa controller” application, tapped the on button and a voltage was applied onto the two electrodes, causing the petiole to bend down within two seconds (Fig.53c).

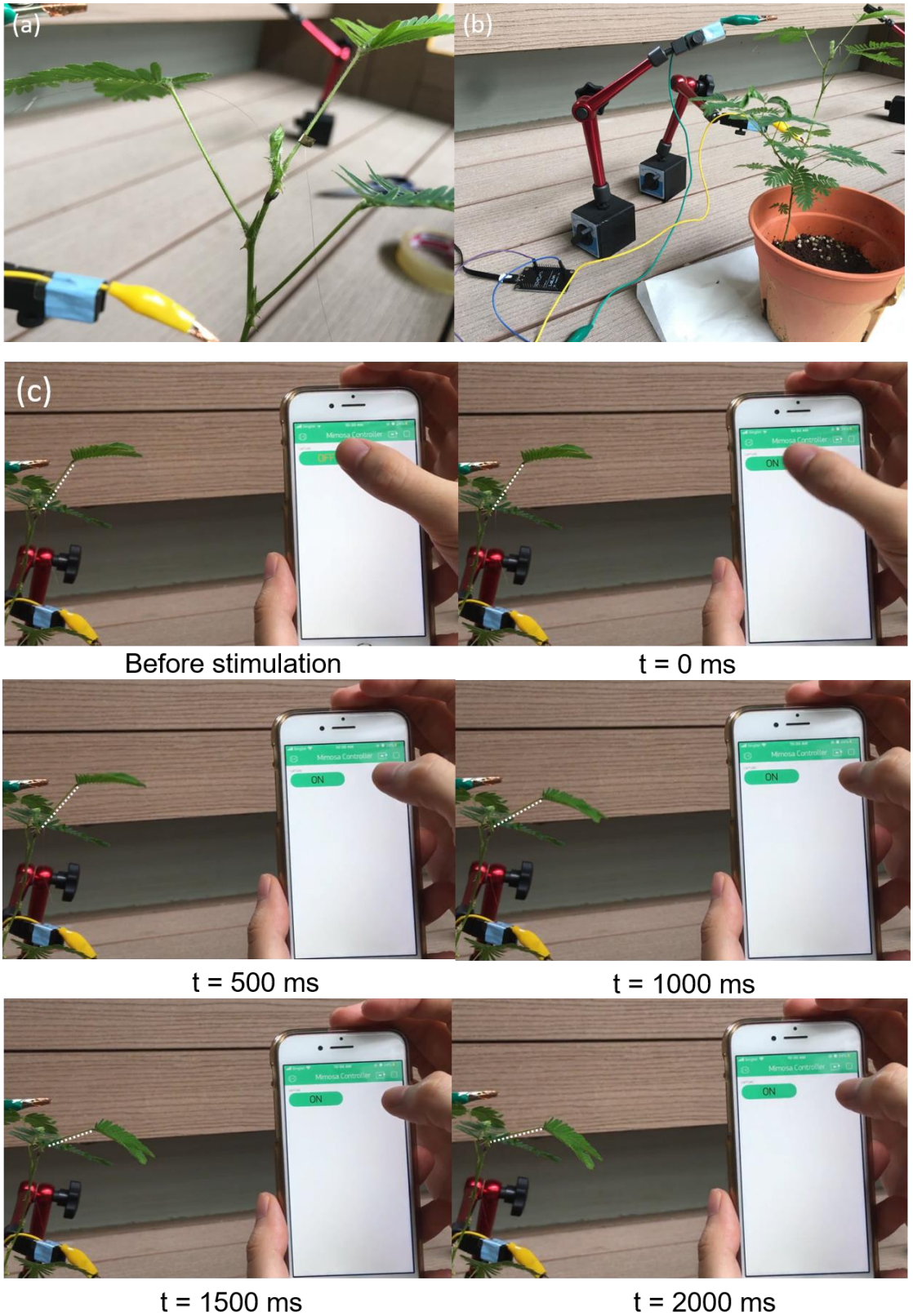

Figure 53. (a)-(b) Setup of the mimosa controlling platform. (c) Time series of petiole bending controlled by the "mimosa controller" app.

References

[1] M. Liu, J. Sun, Y. Sun, C. Bock, Q. Chen, Journal of Micromechanics and Microengineering 2009, 19, 035028.
[2] M. Pei, L. Huo, K. Zhang, H. Zhou, P. Liu, Colloids and Surfaces A: Physicochemical and Engineering Aspects 2020, 585, 123984.
[3] H. Guo, J. Tang, M. Zhao, W. Zhang, J. Yang, B. Zhang, X. Chou, J. Liu, C. Xue, W. Zhang, Nanoscale Research Letters 2016, 11, 112.
[4] C. F. Guo, Y. Chen, L. Tang, F. Wang, Z. Ren, Nano Letters 2016, 16, 594.
[5] T. Li, Z. Suo, International Journal of Solids and Structures 2007, 44, 1696.
[6] X. Zhao, Soft Matter 2014, 10, 672.
[7] S. Bhattacharya, A. Datta, J. M. Berg, S. Gangopadhyay, Journal of Microelectromechanical Systems 2005, 14, 590.
[8] H. Hillborg, U. W. Gedde, Polymer 1998, 39, 1991.
[9] M. L. Chabinyc, D. T. Chiu, J. C. McDonald, A. D. Stroock, J. F. Christian, A. M. Karger, G. M. Whitesides, Analytical Chemistry 2001, 73, 4491.
[10] C. Decker, A. D. Jenkins, Macromolecules 1985, 18, 1241.
[11] A. K. O'Brien, C. N. Bowman, Macromolecules 2006, 39, 2501.
[12] P. Trinder, Annals of Clinical Biochemistry 1969, 6, 24.
[13] J. R. Davis, *Tensile Testing, 2nd Edition*, ASM International, 2004.
[14] P. May, University of Bristol.
[15] S. Kubis, R. Patel, J. Combe, J. Bédard, S. Kovacheva, K. Lilley, A. Biehl, D. Leister, G. Ríos, C. Koncz, P. Jarvis, Plant Cell 2004, 16, 2059.
[16] B. Capon, *Botany for Gardeners*, Timber Press, 2010.
[17] D. Lipomi, Advanced materials (Deerfield Beach, Fla.) 2015, 28.
[18] J.-Y. Sun, X. Zhao, W. R. K. Illeperuma, O. Chaudhuri, K. H. Oh, D. J. Mooney, J. J. Vlassak, Z. Suo, Nature 2012, 489, 133.
[19] H. Yuk, T. Zhang, S. Lin, G. A. Parada, X. Zhao, Nature Materials 2016, 15, 190.
[20] J. FROMM, S. LAUTNER, Plant, Cell & Environment 2007, 30, 249.

Chapter 5 Future Work

In this chapter, conclusion of this thesis is present, summarizing the design, fabrication and characterization of the conformable plant electrodes, as well as the signals measurement experiment of on Mimosa pudica. Future work plan is also discussed.

5.1 Conclusions

We have successfully fabricated a stretchable conformable plant electrode consisting three functional layer: (1) PDMS as elastic substrate to accommodate any strain resulted from the *mimosa* movements; (2) vacuum-deposited Au layer as the conductive network for electrical signal transmission; (3) toughened hydrogel as the adhesion for the electrodes and the plants.

From the optical microscopes, the electrodes demonstrated good conformability on leaf surfaces and *mimosa* stem. The adhesion strength was verified by the peeling test on leaf surface and the pulling test on hydrogel. Meanwhile, the adhesive strength of the electrodes could be maintained up to 9 days, indicating a promising reusability. The stretchability of the electrodes was also good enough (~100 Ohm at ~100% strain). The impact of electrodes on leaves was also examined by sticking onto the leaves for 48 hours and the test results showed no negative effects for leaves. The electrical benefits of the electrodes could also be verified by the impedance test at rest and at 25% strain.

During the plant signal testing, we successfully measured APs generated by physical movements of *mimosa pudica* plant, and the calculated AP transmission speeds in *mimosa* were comparable to those reported in literatures. Furthermore, we also electrically stimulated the *mimosa* via the as-synthesized electrodes to trigger the petiole bending. The control experiment showed that no AP signal could be generated by applying a voltage across the stem, and this experiment result matched the conclusion from the previous works.

To summarize, the plant conformable electrodes proposed by us are advantageous to the previous invasive thin metal wire electrodes, because once the plant conformable electrodes were warped onto the *mimosa* plant, the signal detection and electrostimulation could be instantly performed. In addition, the electrodes could be removed

easily at any time and left no damages to the plant. Therefore, by using this convenient electrode, any plants electrical signals could be easily detected and/or stimulated. The ultimate goal of this work is to provide an easy tool to study the mechanism for plant movements and use the knowledge to inspire new design for soft robots in the future.

5.2 Future Work

5.2.1 Hydrogel Patterning via Photolithography

During the photopolymerization of hydrogel, there was no pattern or design. The electrodes were manually cut into desired size, where smaller size (<2mm for width) was very difficult to achieve by manual cutting. Using photolithography in chip design as an example, many studies have applied photolithography into precise patterning in hydrogel (Fig.54)[1, 2].

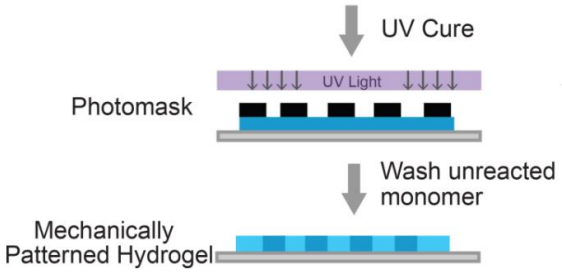

Figure 54. Schematic of patterning process of hydrogel. The UV light would only shine on the unmasked region. The covered regions would not crosslink and subsequently washed away. The patterned hydrogel would replicate the details from the photomask[1], © 2017 by The American Society for Cell Biology.

Hence, by designing a suitable mask with fine details, miniaturization of electrodes could be achieved.

5.2.2 Electrically-induced Pinnules Folding Movements in *Mimosa*

Besides petiole bending, APs can also make the pinnules of *mimosa* to close. However, the distance between the base of pinnules is very small (<1mm), it is very difficult to make electrodes with width that is smaller than that. Hence, by achieving miniaturization of electrodes via proper masks, the AP signals caused by pinnules closing could be detected. Furthermore, we could also control the closing of the pinnules via electrical stimulation.

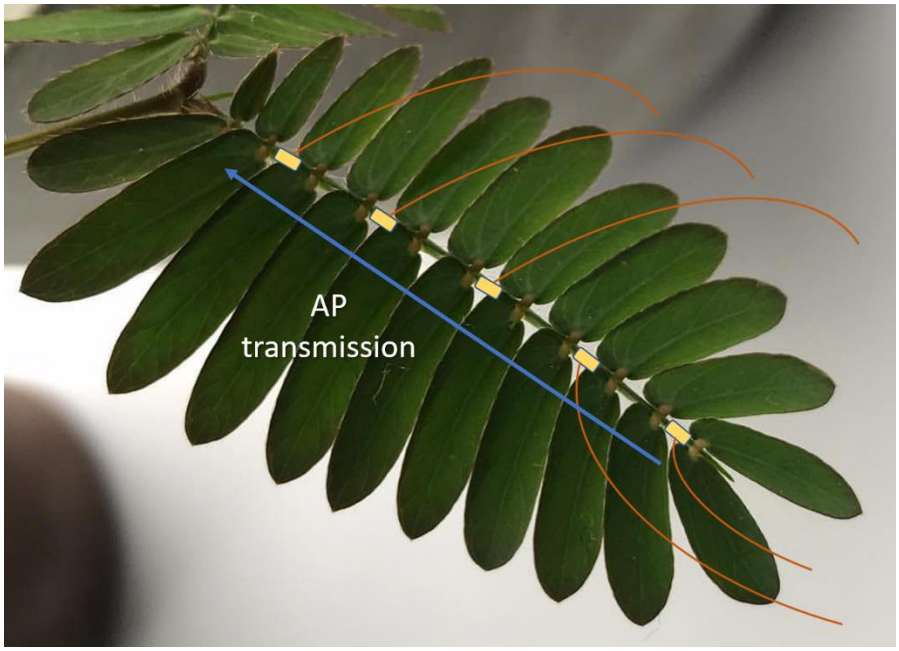

Figure 55. Illustration of AP detection and stimulation in rachis. The electrodes were wrapped between the tertiary pulvinus (bases of pinnules).

A simple illustration for the pinnule folding test was shown in Fig.55. Once an AP is induced at the tip of rachis, it will lead to the sequential closing of pinnules as the AP transmits. Successive AP spikes would be recorded by these electrodes. On the other hand, we could also apply voltage at various electrode locations to close the pinnules.

5.2.3 Increase the Transparency of Electrode using PEDOT: PSS

The as-synthesized plant conformable electrode was gold in color due to the presence of vacuum deposited gold layer. For long term application on plants, it is important to increase the transparency of the electrodes to allow light to pass through, maintaining its ability to photosynthesize. Therefore, poly(2,3-dihydrothieno-1,4-dioxin)–poly(styrenesulfonate) or PEDOT: PSS, is a promising candidate for stretchable electrodes fabrication, due to very high conductivity[3]. However, PEDOT and PSS are intrinsically semi-crystalline, a plasticizer is required to improve the intrinsically low stretchability[4]. Blending with other soft polymers is another method to increase stretchability in PEDOT: PSS. Strain-induced electrical properties are introduced by microphase separation of the elastomer and PEDOT: PSS.

As such, we could test a range of different plasticizer or mixing with soft polymers to obtain a desired stretchability and transparency, while achieving high conductivity. Fig.56 demonstrates the schematic illustration of the new structure for plant conformable electrode. This new fabrication method could also reduce the cost of the electrode as expansive gold is now replaced with PEDOT: PSS.

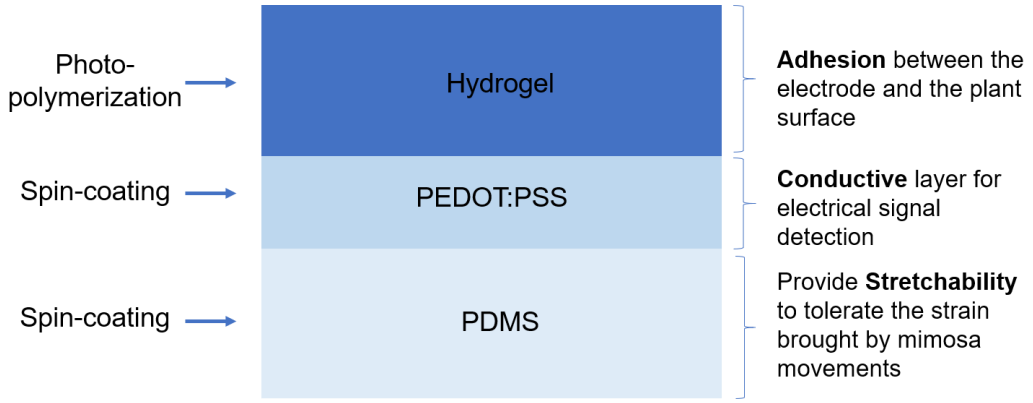

Figure 56. Schematic illustration of three functional layers of new plant conformable electrode. High transparency is achieved by replacing the vacuum deposited gold layer to spin-coated PEDOT: PSS layer.

5.2.4 Isolation of *Mimosa Pudica* for Portable Experiment

All the previous experiments on *mimosa* were carried out in flowerpot filled with soil, which was not convenient to conduct the experiments. In the future, we would find a way to isolate the mimosa using some kind of water-rich material to maintain its life and make it portable for experiments (Fig.57).

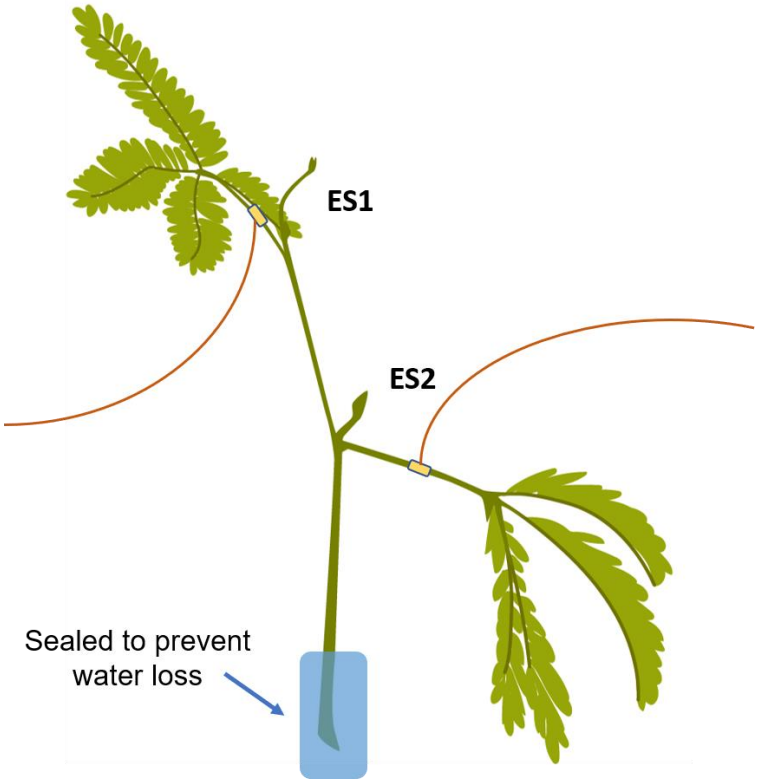

Figure 57. Schematics of a portable mimosa soft robot with its root soaked in water-rich material to maintain its life form.

References

[1] C. L. Happe, K. P. Tenerelli, A. K. Gromova, F. Kolb, A. J. Engler, Mol Biol Cell 2017, 28, 1950.
[2] S. J. Bryant, J. L. Cuy, K. D. Hauch, B. D. Ratner, Biomaterials 2007, 28, 2978.
[3] L. Groenendaal, F. Jonas, D. Freitag, H. Pielartzik, J. R. Reynolds, Advanced Materials 2000, 12, 481.
[4] S. Savagatrup, E. Chan, S. M. Renteria-Garcia, A. D. Printz, A. V. Zaretski, T. F. O'Connor, D. Rodriquez, E. Valle, D. J. Lipomi, Advanced Functional Materials 2015, 25, 427.